CH3D Hydrodynamic Model Validation Draft Report

September 12, 2004

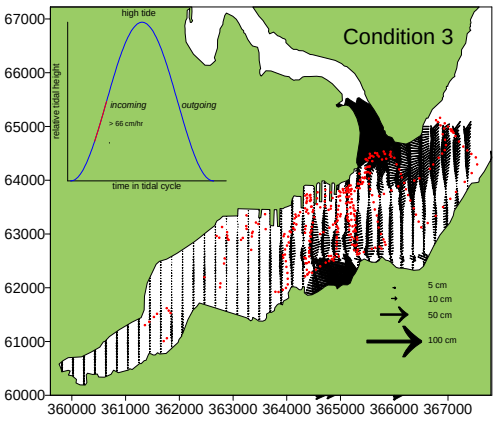

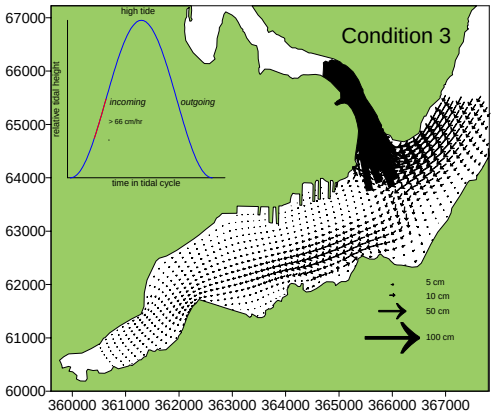

Prepared by

K.E. Richter, Ph.D.
Space and Naval Warfare Systems Center Code 2375
San Diego, CA

For

Puget Sound Naval Shipyard
Project ENVVEST

Introduction

This report estimates the accuracy of hydrodynamic predictions by the model CH3D in Sinclair and Dyes Inlets from measurements made during 1997 and 1998 (Katz et al. 2004). This report is essentially a comparison of measured and predicted water currents. Description of the hydrodynamic model and its implementation in the Inlets can be found in Wang and Richter (1999) and Brown (2001).

Model grids: CH3D was set up in Dyes and Sinclair Inlets at two different resolutions. The first, employing 1345 nodes and designated as the 9183 grid (for 91 by 83 nodes, 1345 of which are in water) was set up and run in 1998 (Fig 1). The second, employing 2481 nodes and designated as grid 9196 was set up and run in 2001 (Fig 2). The second, higher resolution grid was created to address model inaccuracies at the confluence of Sinclair Inlet and Washington Narrows, a region where water velocity changes abruptly over a short distance. Field measurements of water velocity are compared to model predictions for both model grids.

Figure 1: 9183 CH3D grid, 1345 nodes

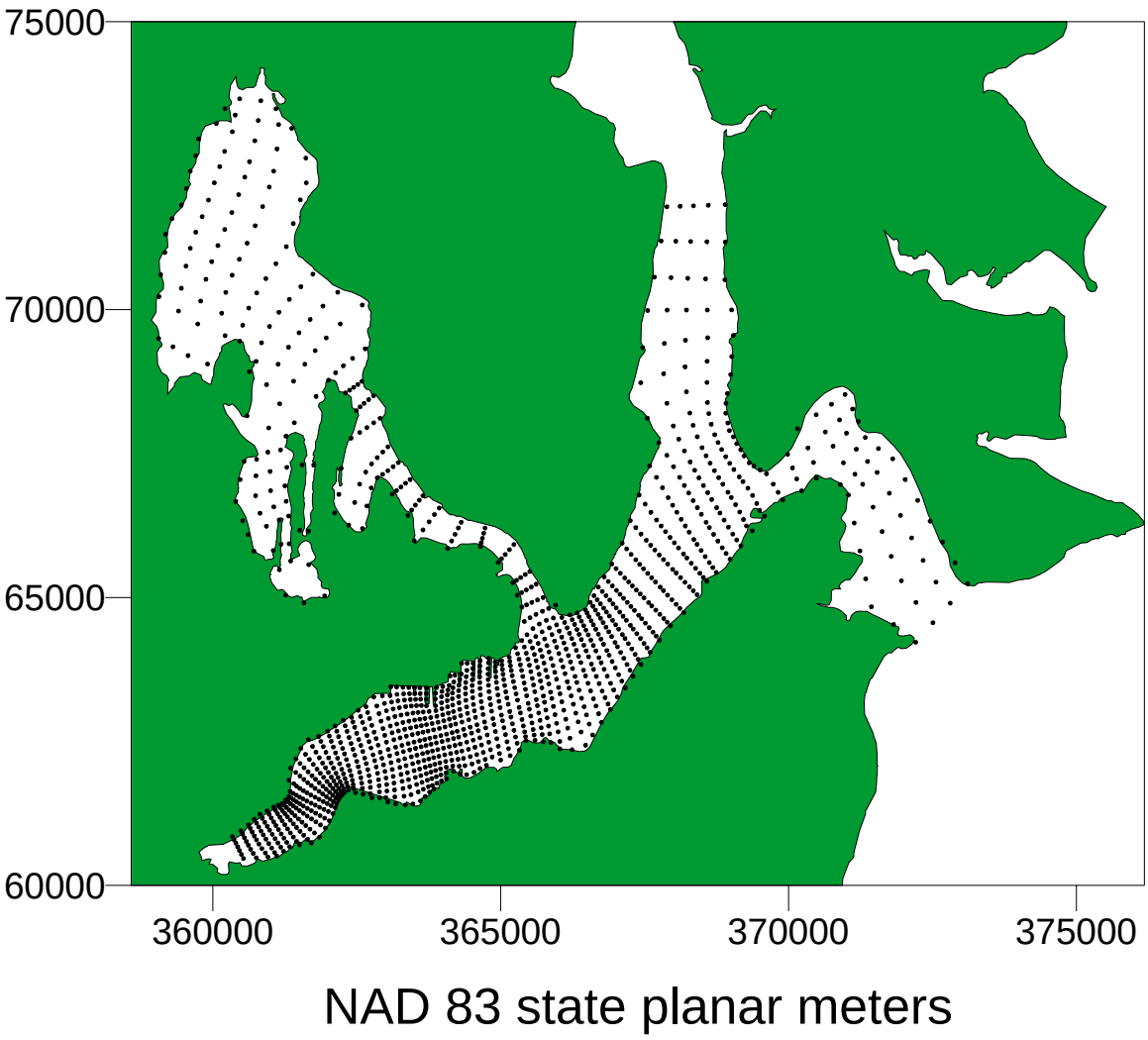

Figure 2: 9196 CH3D grid, 2821 nodes

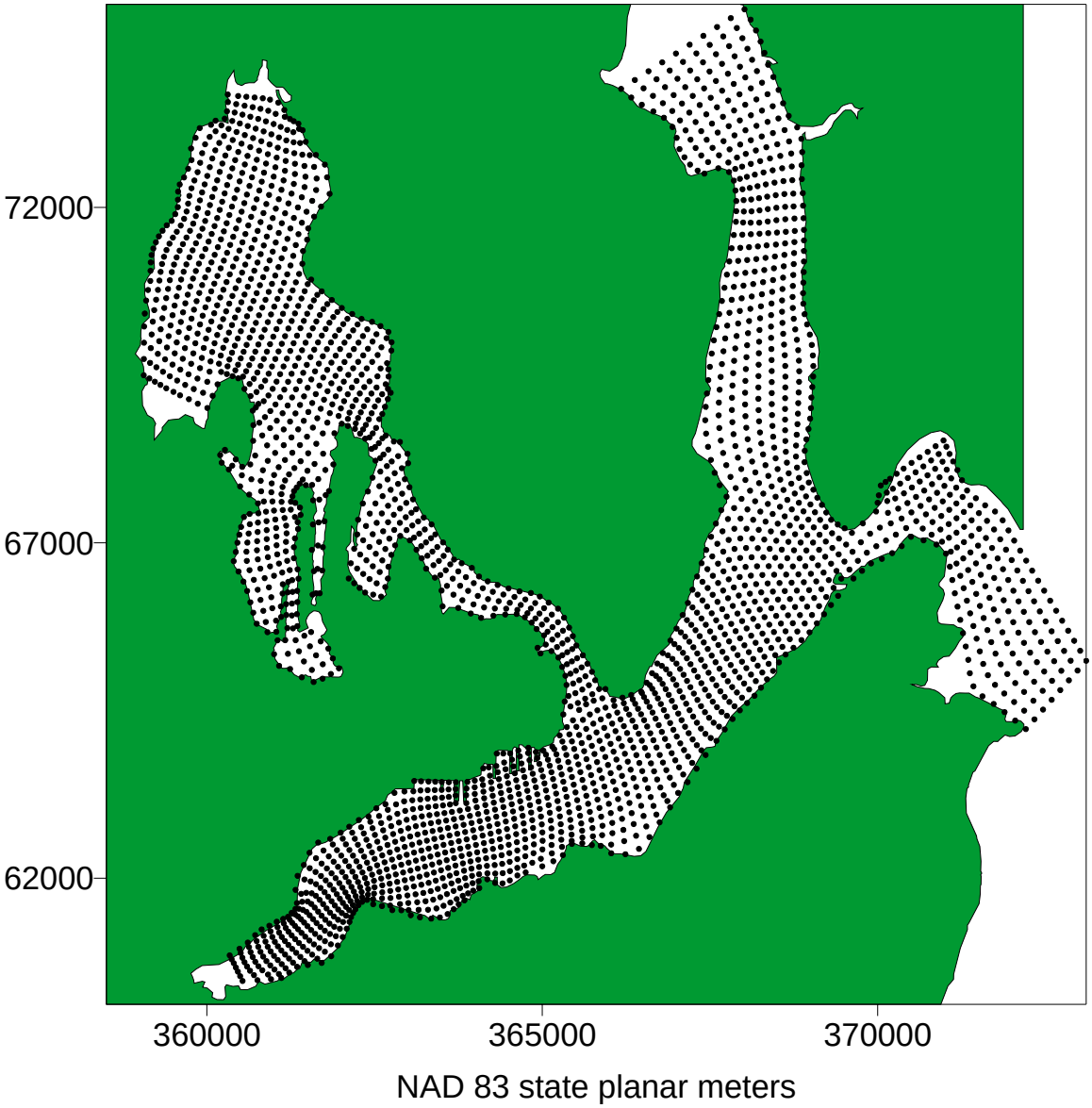

Field measurements: Water velocity data were collected from a variety of sources from 1997 to 1998, primarily in Sinclair Inlet (Katz et al. 2004). Data were collected from a vessel-mounted acoustic current meter (RD Instrument 1200 KHz narrow band acoustic Doppler current profiler) that measures water velocity relative to the bottom (RDI, 1989). The vessel mounted ADCP was programmed to collect water column velocities at 1m vertical resolution to the bottom five times per second. Data were averaged over 10

seconds, yielding a velocity precision of approximately 1.8 cm/sec (RDI, 1989). The vessel typically steamed at 1 m/sec (2 knots), yielding a horizontal resolution of approximately 10 m. On 3 cruises in September, 1997; March, 1998; and July, 1998; a total of 632,424 vertical profiles were collected (Fig 3). Vessel position was determined via differential GPS, recorded simultaneously with the ADCP data.

Figure 3: ADCP velocity data, 632424 profiles

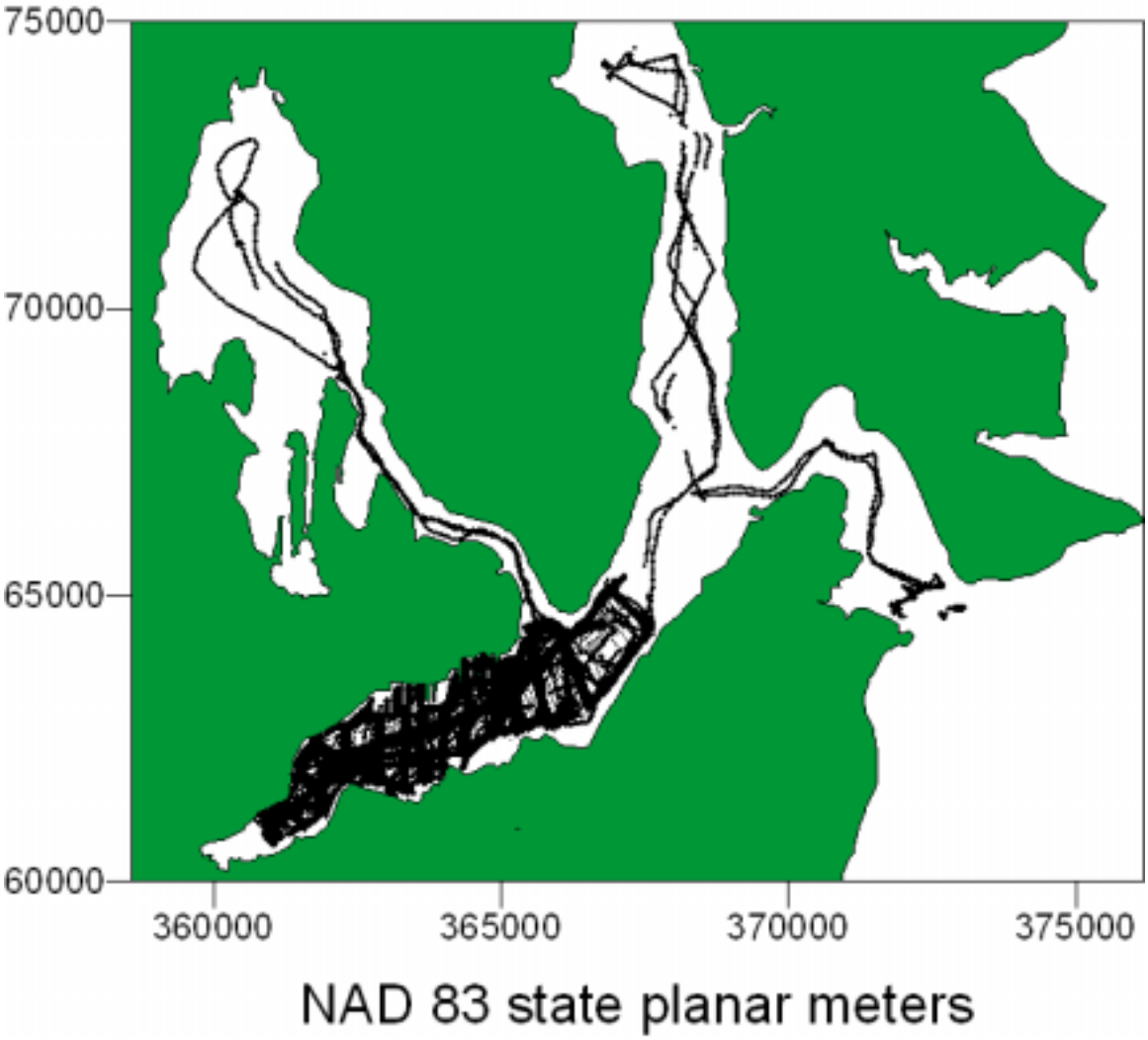

Data were also collected from a wide band 1200 KHz ADCP (RDI, 1996) anchored on the bottom and looking up at 3 different locations from 1997 to 1998, averaging 2 months deployment at each location (Fig 4). Water column velocities were collected at 0.5 m vertical resolution to the surface 3 times per minute. Data were averaged over 5 minutes, yielding a velocity precision again of approximately 1.8 cm/sec (RDI, 1996). A total of 51,480 vertical profiles were collected in this manner.

Figure 4: Locations of moored, upward-looking ADCPs

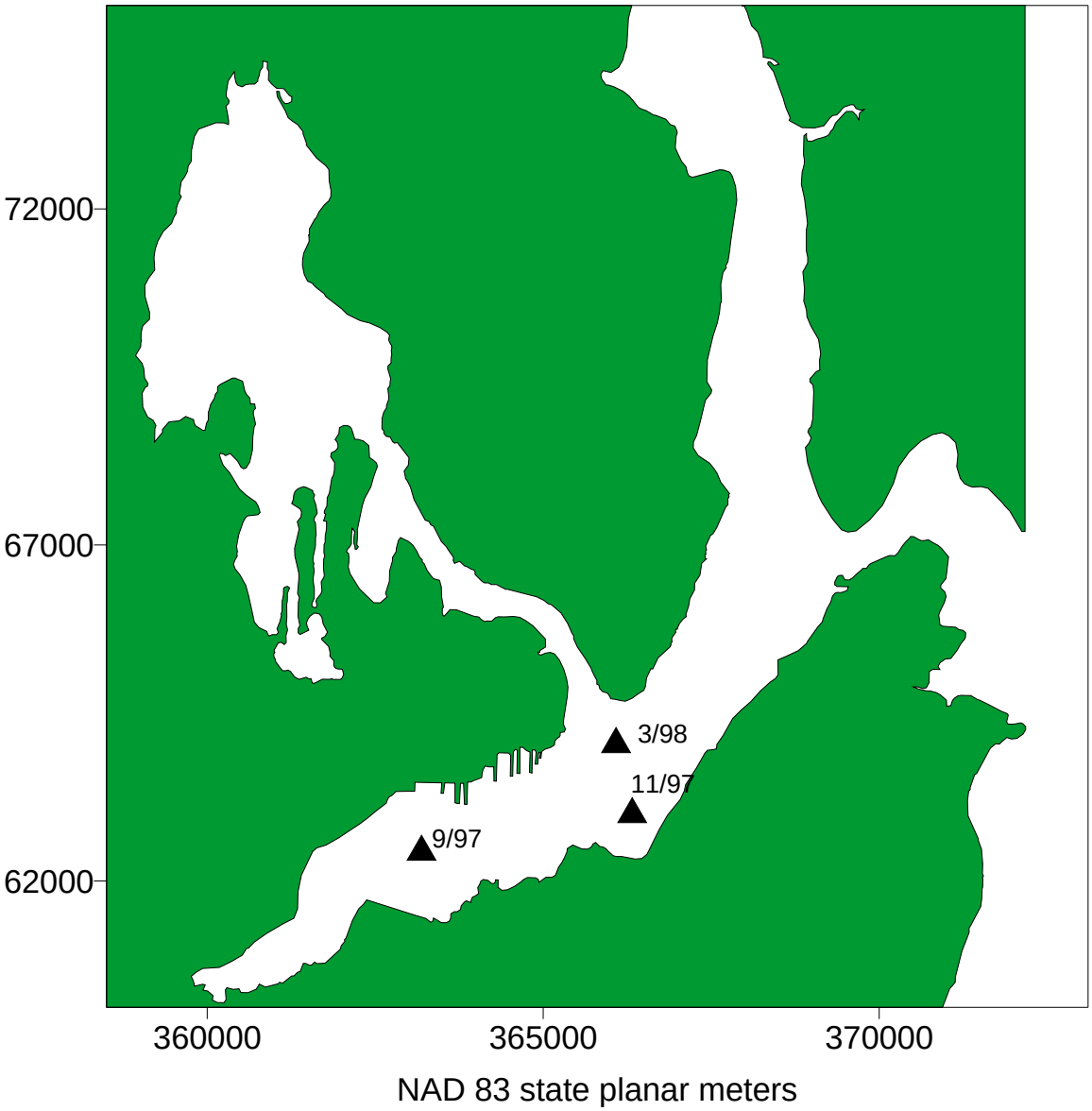

Processing field data: Comparison of field measurements with model predictions were only made in Sinclair Inlet (northing<=65,500) where the bulk of the measurements were made. Data processing is summarized in the following sequence:

1. ADCP data were corrected for magnetic offset (20 degrees in Sinclair Inlet), yielding currents relative to true north. Coordinates were transformed to North

American Datum 83 state planar meters. The data were checked for unreasonable speeds or coordinates.

2. A tidal program (Micronautics, 1997, 1998) was used to predict tidal height at the Puget Sound Naval Shipyard at 5 minute intervals. These data were merged with the ADCP data by time. A tidal rate of change (slope) was calculated for each interval and added to the database.
3. The closest model node to the location of ADCP data location was identified and merged with the data.
4. The ADCP data were averaged into 3 m depth bins to match the depth resolution output by CH3D. The data were then merged to CH3D output by time, spatial location (nearest model node) and depth. CH3D was run to output data at 3 minute intervals during the September 1997 cruise period; at 10 minute intervals during the March, 1998 cruise; and at 1 hour intervals during July, 1998 cruise periods. The change to a longer model time step in the latter two cases stemmed from observations that predicted currents changed slowly over time and the 1 hour time resolution was sufficient. Data were matched to model predictions for both the 9183 and 9196 model grids.
5. Model predictions were compared to current measurements per 3 m depth interval and as water column means. Comparisons were sorted by tidal stage as well: the tidal cycle was divided into 12 stages based on tidal slope, ranging from slack low water, incoming tide, slack high water, outgoing tide, and a second low slack water (Fig 5). For example, the largest tidal slopes (> 66 cm/hour) were associated with large spring tides and were assigned tidal conditions 3,4, 9, and 10 in Figure 5. The demarcation between conditions 3 and 4 or conditions 9 and 10 mark the halfway point in time between high and low water. Figure 6 plots the relative frequency of tidal conditions that occurred during current measurements. The tidal slope values that were used to create the 12 tidal conditions were 0 cm/hour to 33 cm/hour, 33 cm/hour to 66 cm/hour, and greater than 66 cm/hour. The number of observations shown in Figure 6 is the number of tidal predictions made by the tide program over the 1997 and 1998 period of measurements, not the number of current measurements themselves. Tidal conditions were fairly well represented during current measurements, as shown in Figure 7, which plots tidal conditions during measurements in red against all tidal conditions predicted in Sinclair Inlet throughout 1997 and 1998.

Figure 5: Tidal condition (slope) referenced in measurement and model comparisons

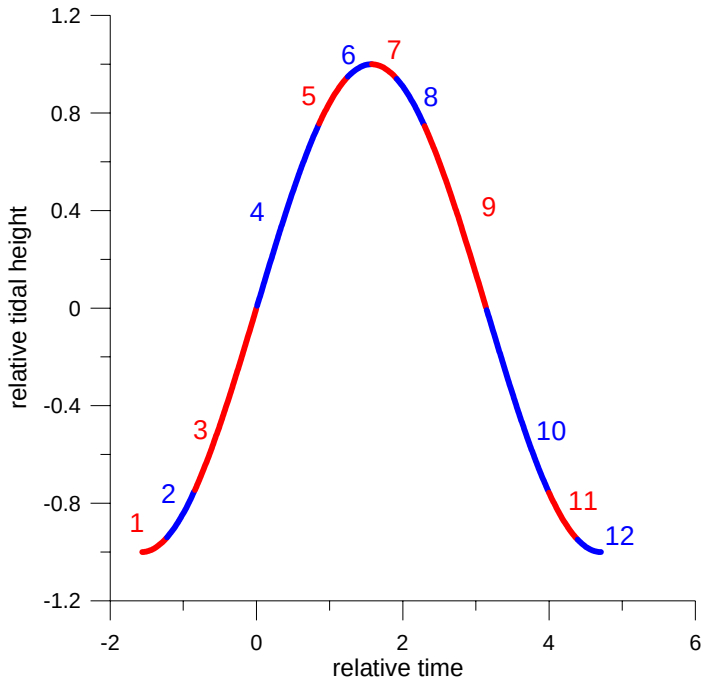

Figure 6: Predicted tidal slopes during ADCP measurements

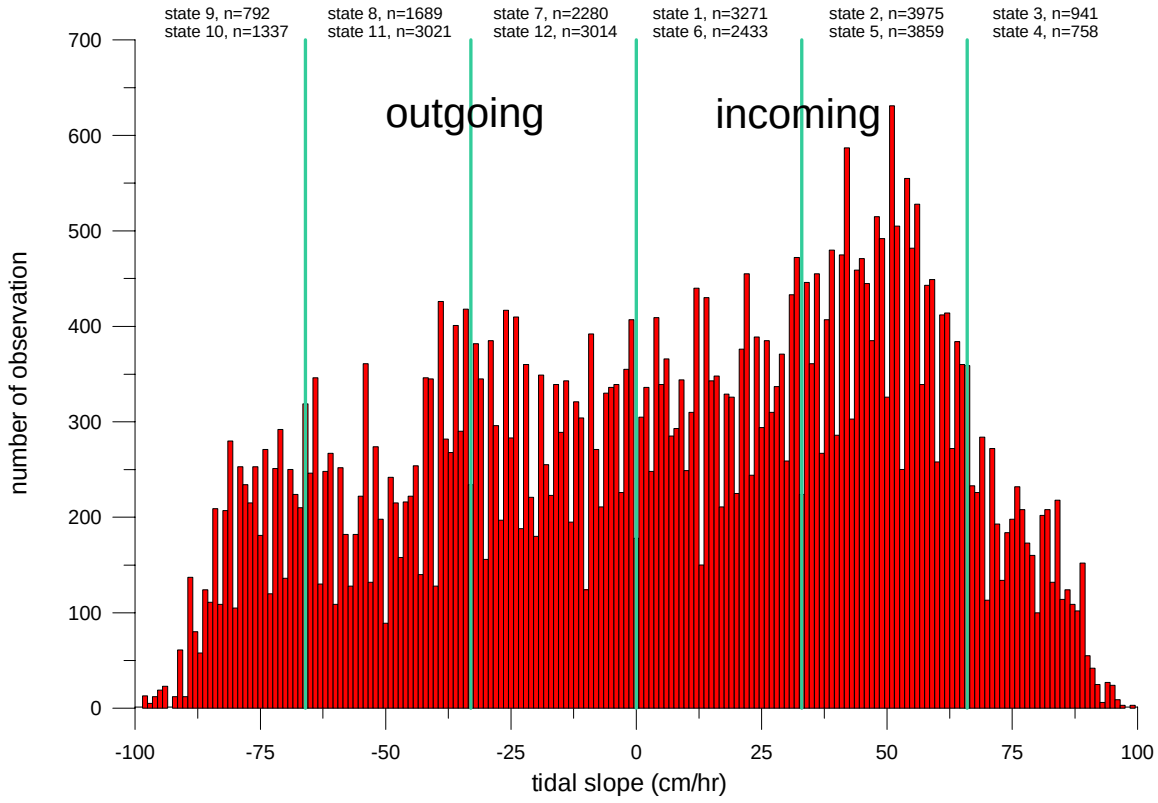

Figure 7: Tidal slopes over the entire 1997-1998 period (blue) and during vessel-mounted ADCP measurements (red)

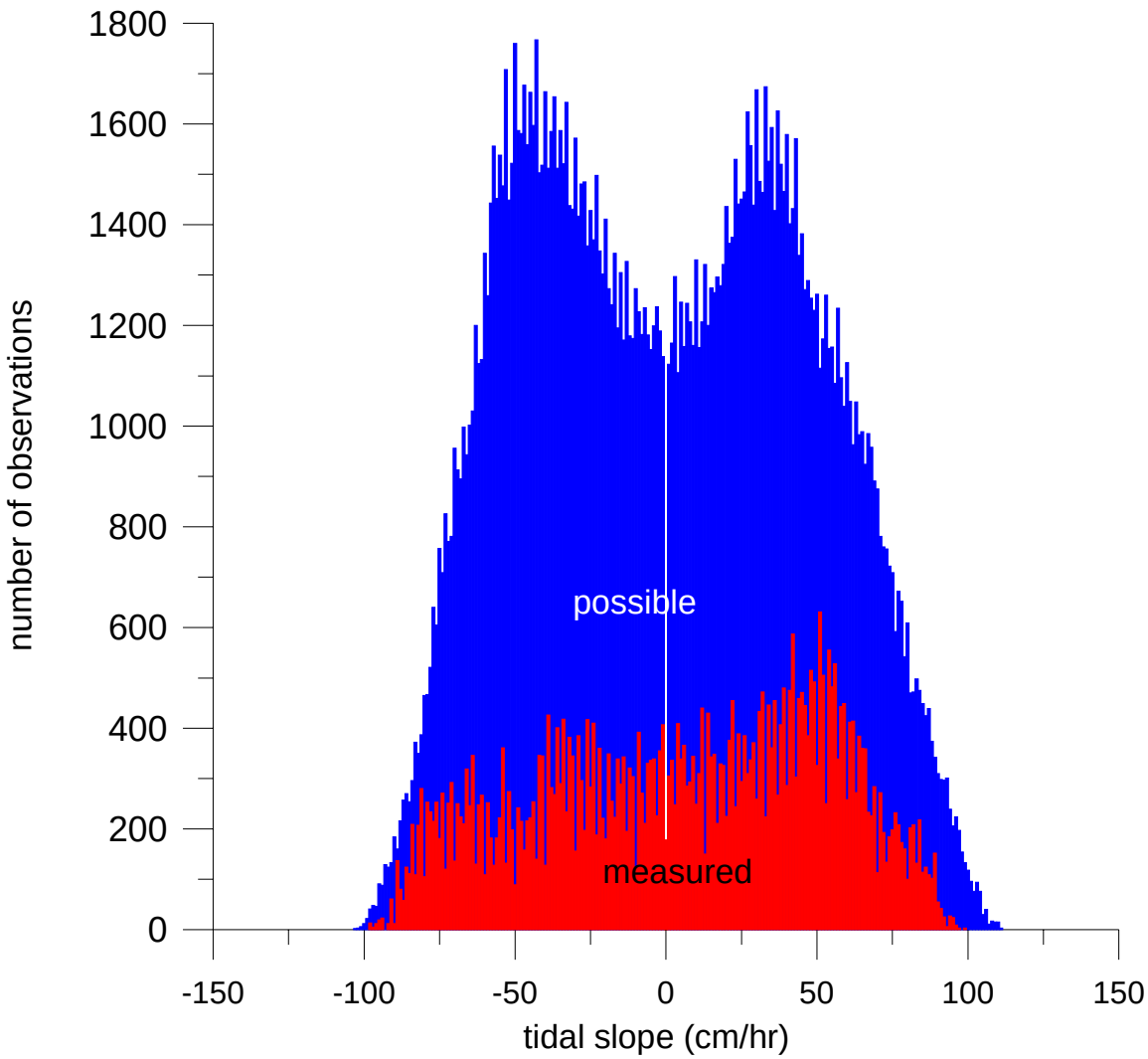

Comparing field data and model predictions: Overall, there was no difference in the accuracy of the 9183 grid compared to the 9196 grid ($p>0.14$, Wilcoxon rank sum test). Figure 8 plots the root mean square difference between mean ADCP results and model predictions by time, node, depth and tidal condition. Time, node, and depth information are pooled in the error bars. The 9196 grid is significantly worse during tidal condition 1 when the tide is just beginning to rise, and significantly better during tidal conditions 4 and 5 when high tide is approaching ($p<0.05$, Wilcoxan rank sum test). In the following figures the results from the 9196 grid are displayed since it offers better spatial resolution with similar accuracy. Subsequent TMDL calculations, not reported here, also are based on the 9196 grid.

Figure 8: RMS error and standard error of Sinclair Inlet current speed predictions

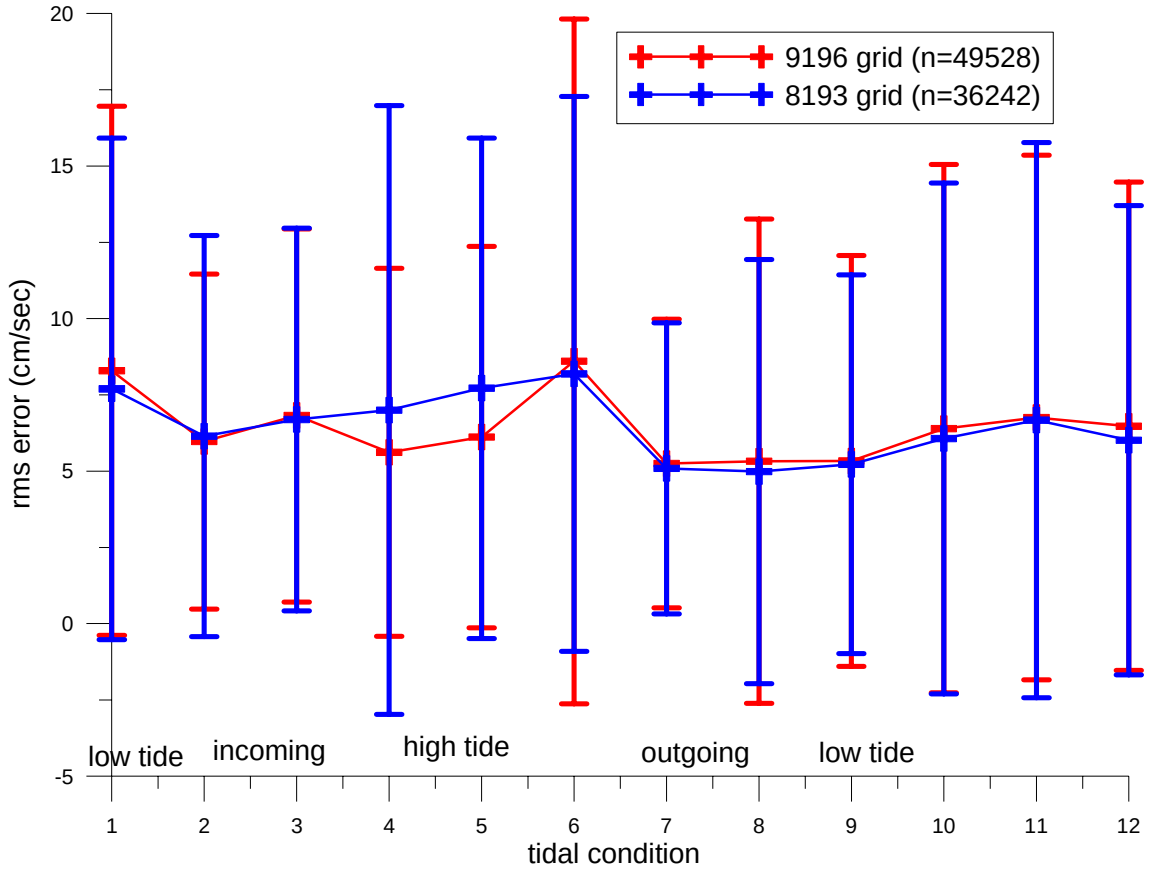

Absolute and relative speed error averaged through the water column: Figures 9-20 plot the absolute difference in current speed between CH3D using the 9196 grid and ADCP current measurements as a function of tidal condition. Also plotted is the speed difference as a percentage of the predicted speed. The black dots in the figures are the model node locations in the 9196 grid where the data was compared and on which the contours are based. While the greatest absolute errors (differences) occur near the mouth of the Washington Narrows, the greatest relative errors occur where the measured and predicted speeds are quite low, in the southern end of Sinclair Inlet. CH3D consistently overpredicts or underpredicts water speed in the same regions and so the model is not out of phase with tidal forcing. Possible phase problems were explored by varying the time at which model predictions and current measurements were merged and compared, then examining rms error. Phase shifts from minutes up to two hours typically resulted in higher rms errors.

Figure 9: Absolute and relative mean water column model error at tide condition 1

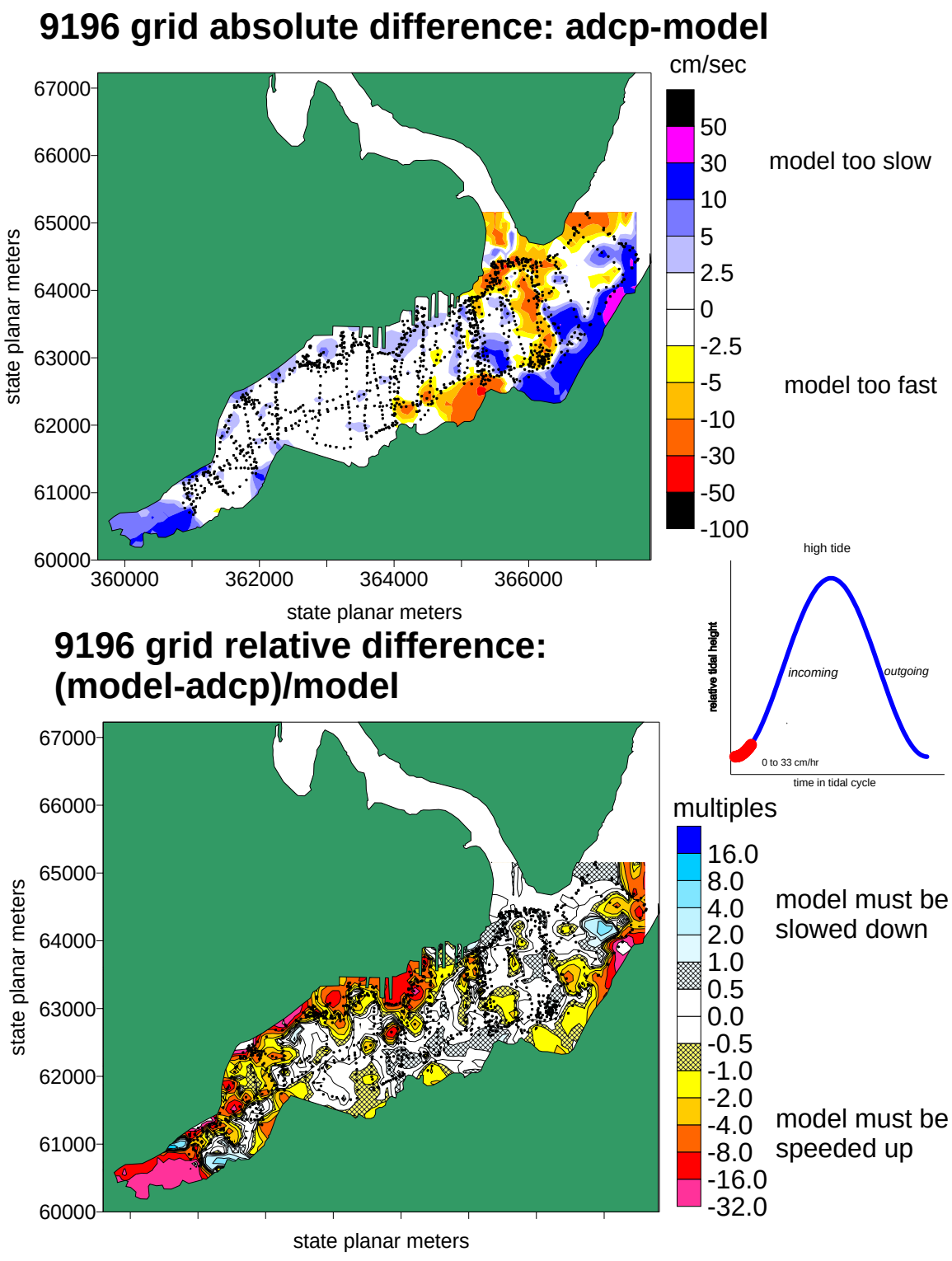

Figure 10: Absolute and relative mean water column model error at tide condition 2

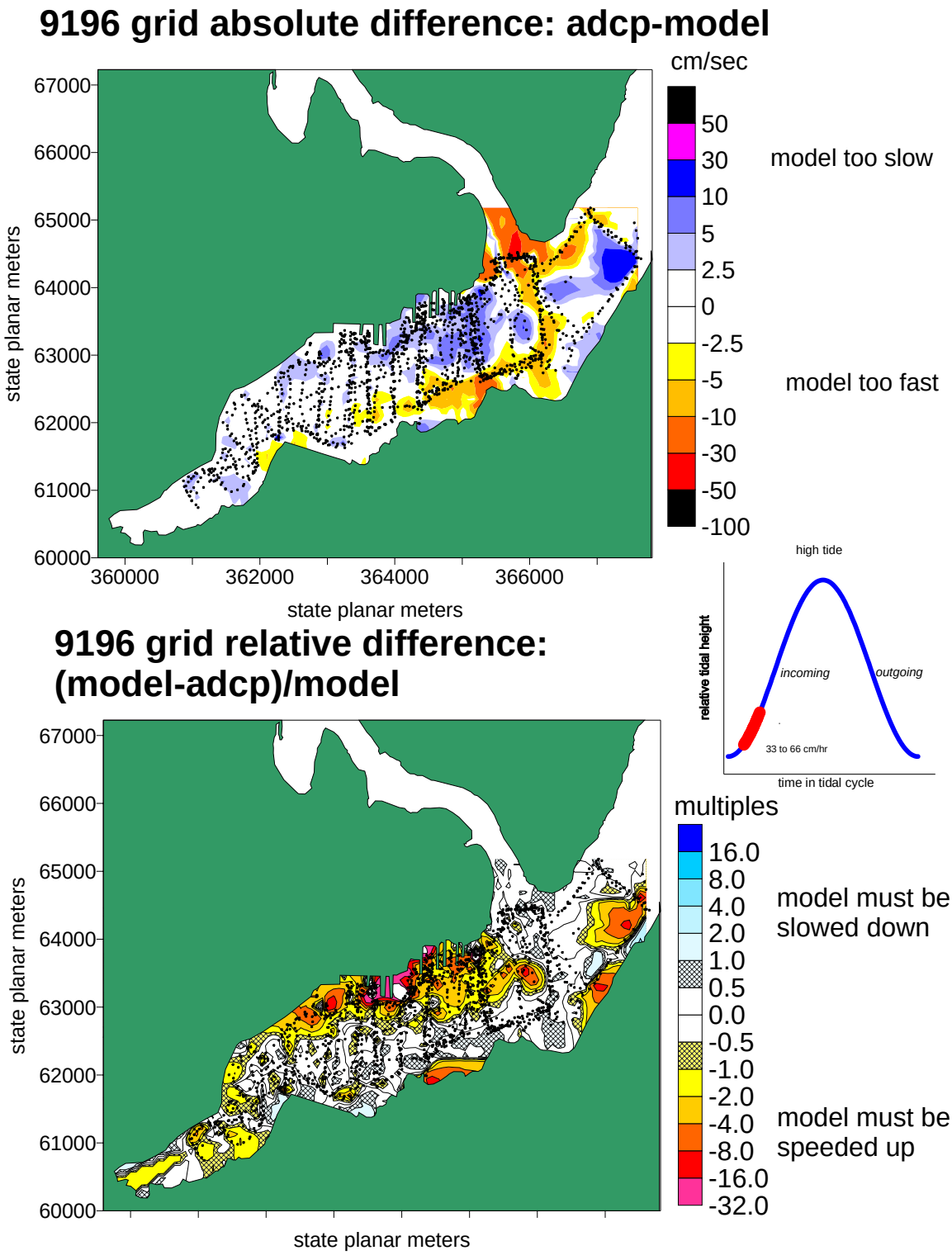

Figure 11: Absolute and relative mean water column model error at tide condition 3

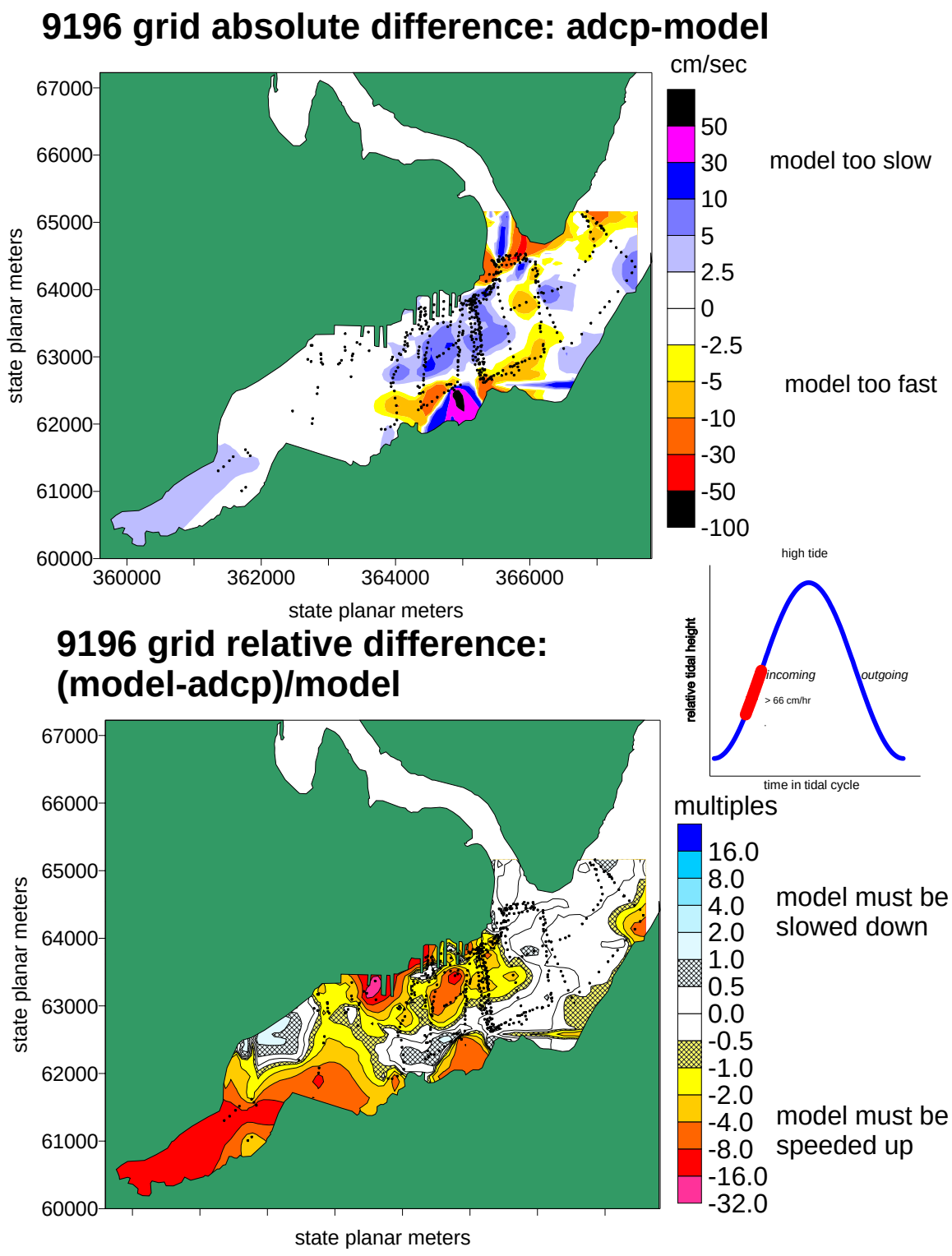

Figure 12: Absolute and relative mean water column model error at tide condition 4

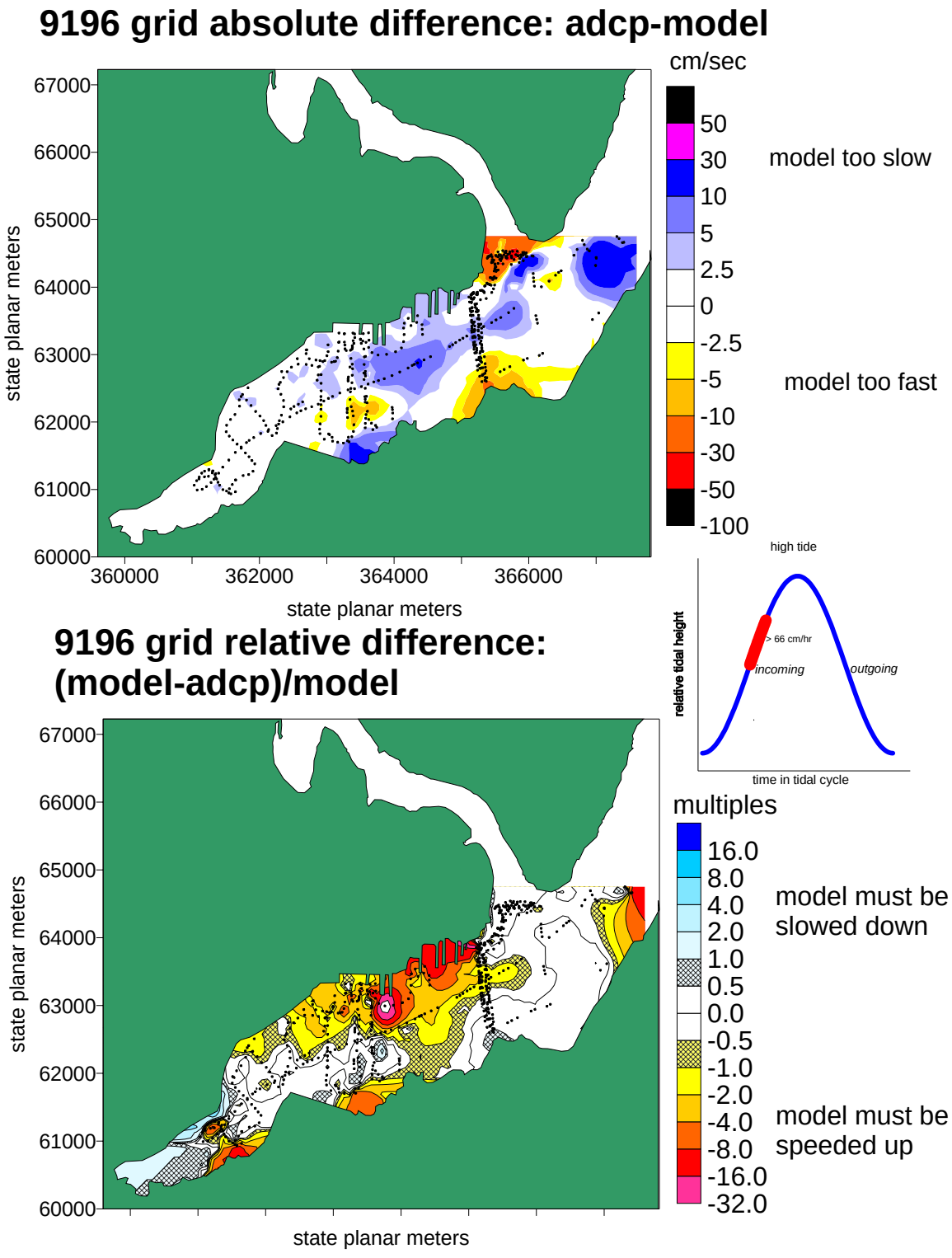

Figure 13: Absolute and relative mean water column model error at tide condition 5

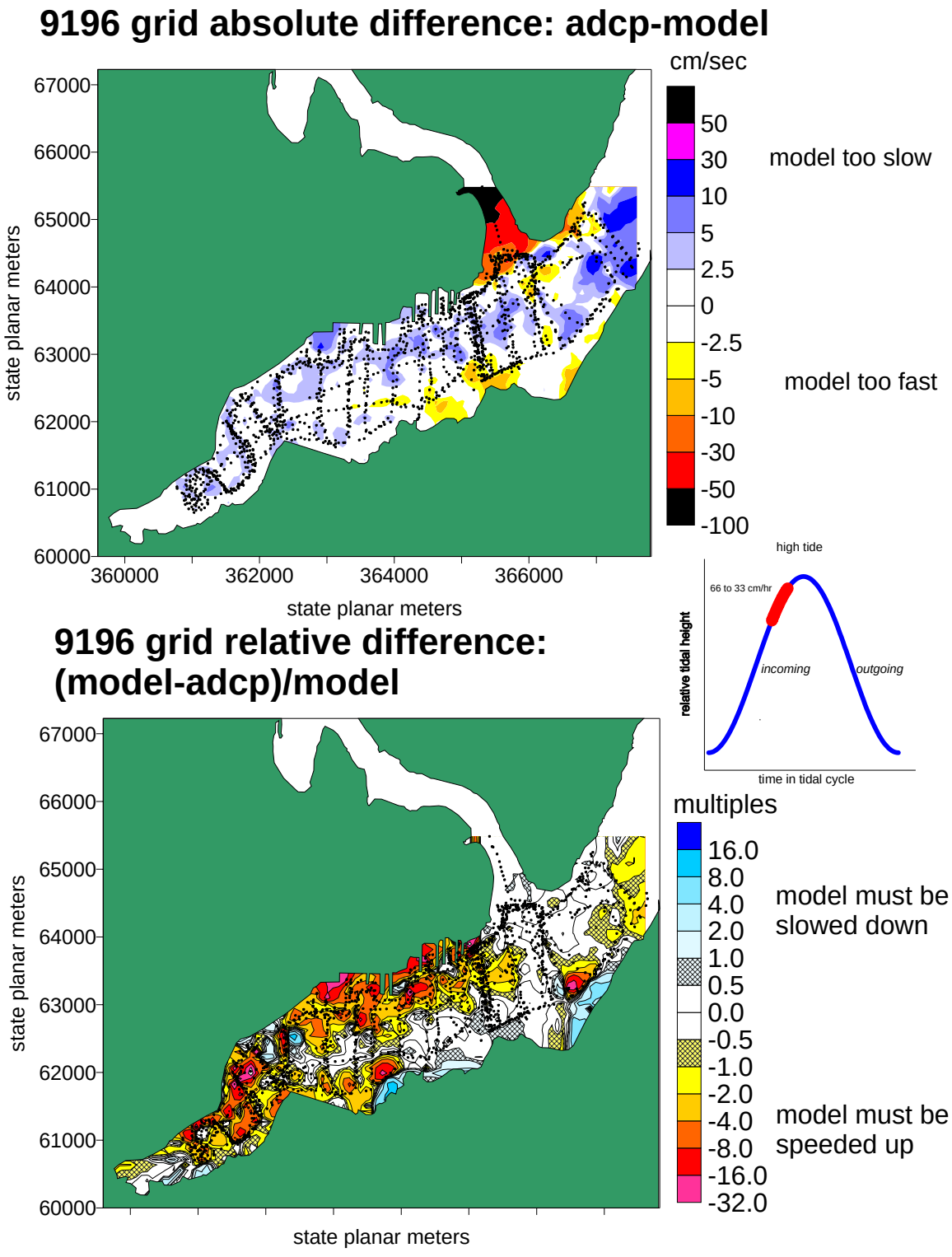

Figure 14: Absolute and relative mean water column model error at tide condition 6

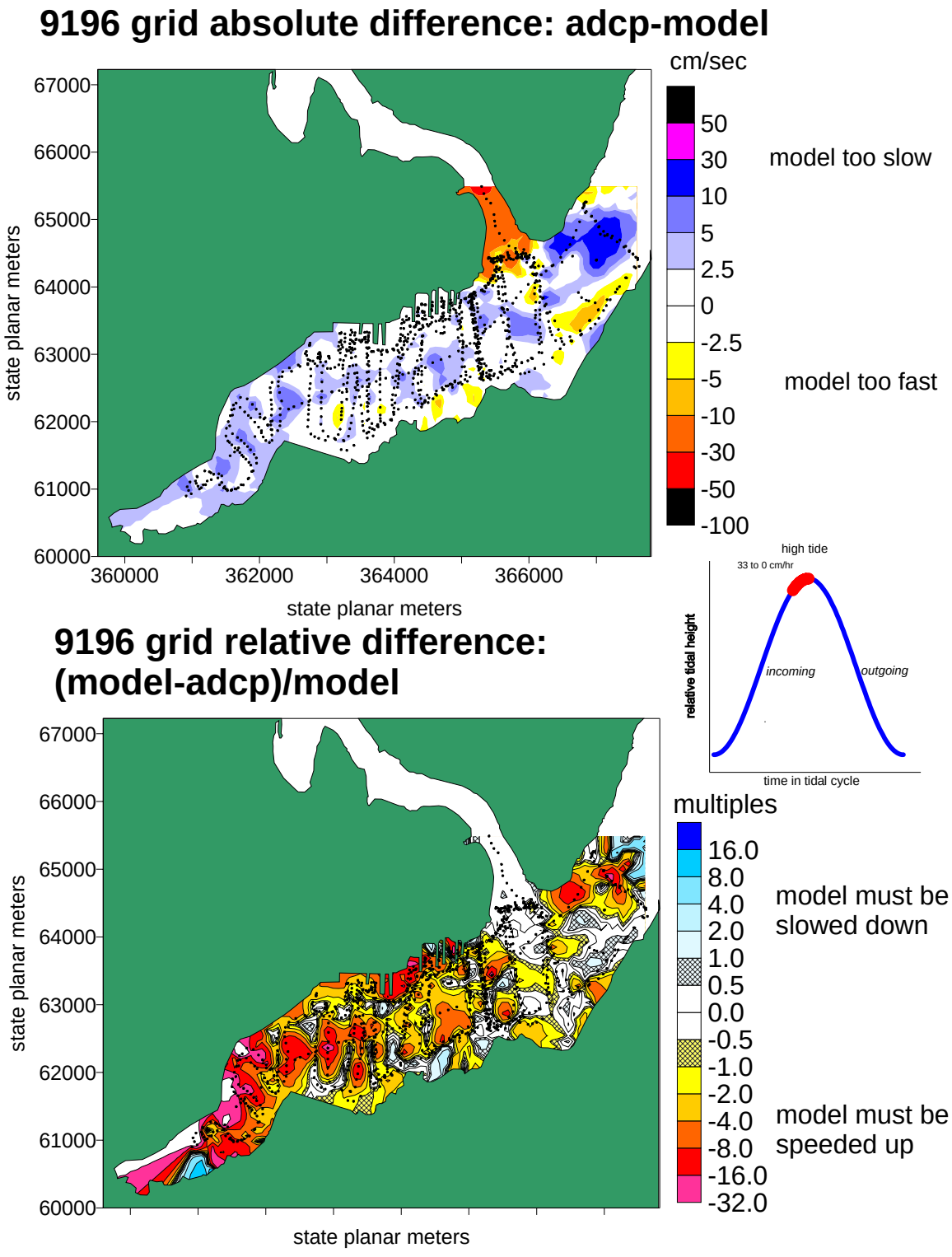

Figure 15: Absolute and relative mean water column model error at tide condition 7

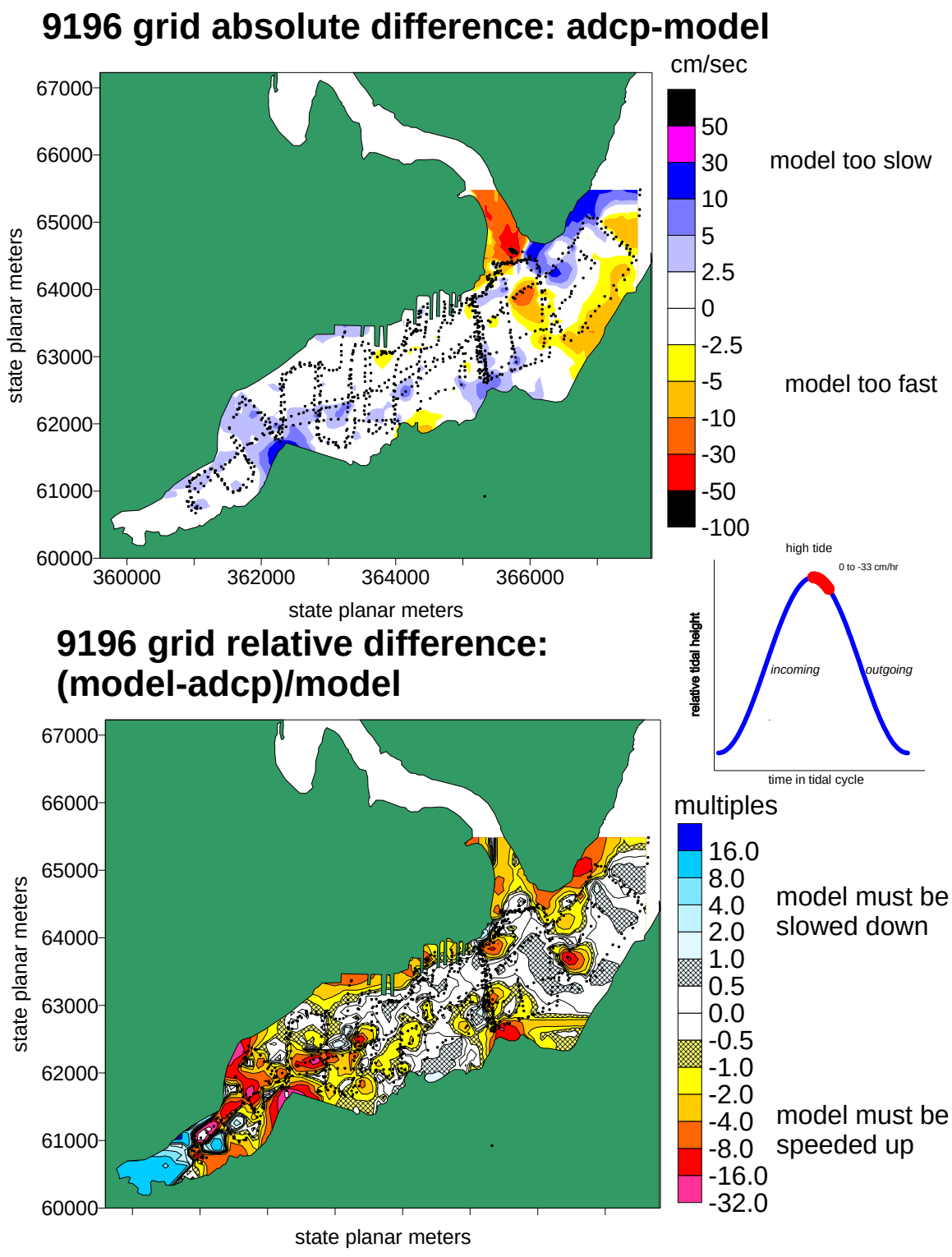

Figure 16: Absolute and relative mean water column model error at tide condition 8

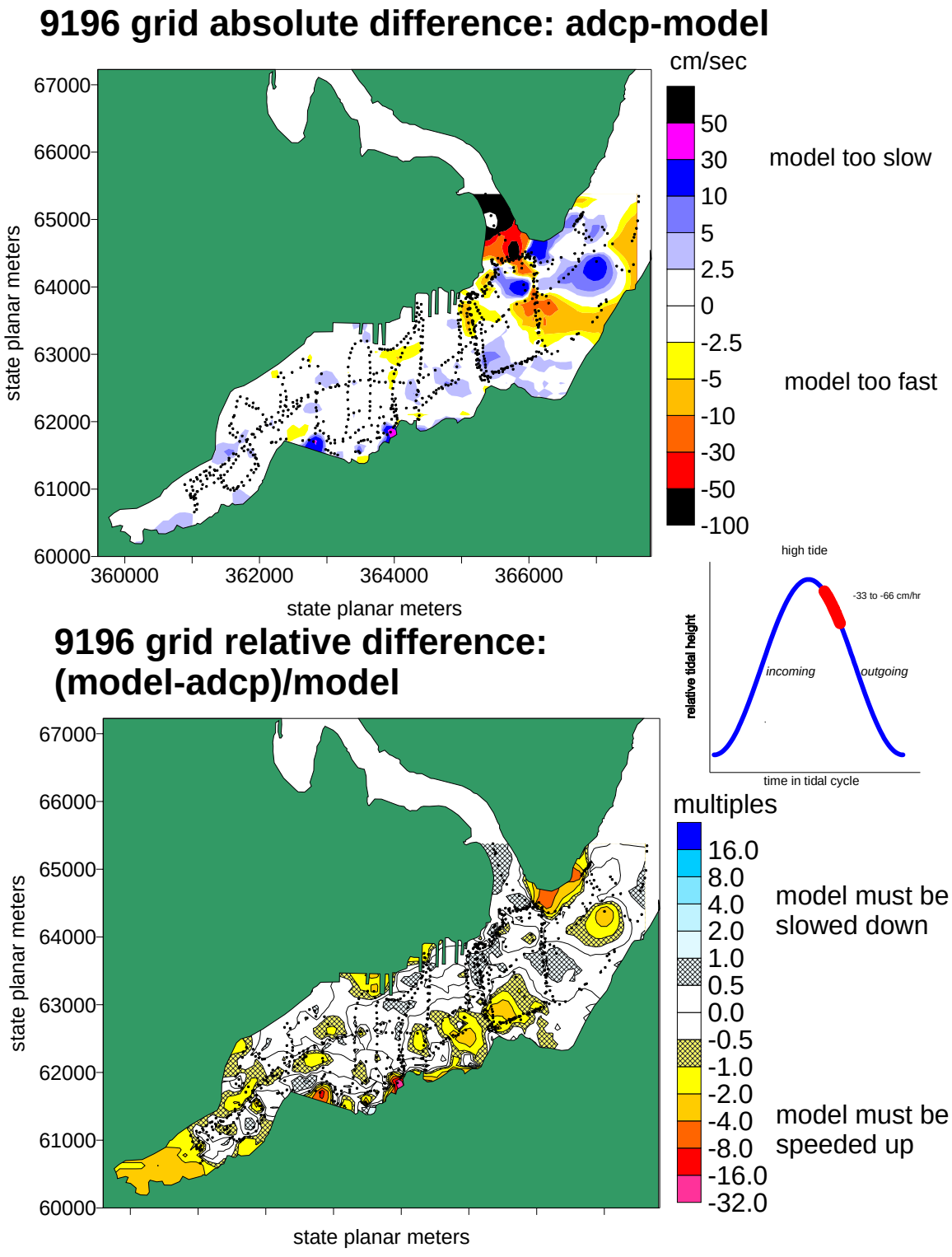

Figure 17: Absolute and relative mean water column model error at tide condition 9

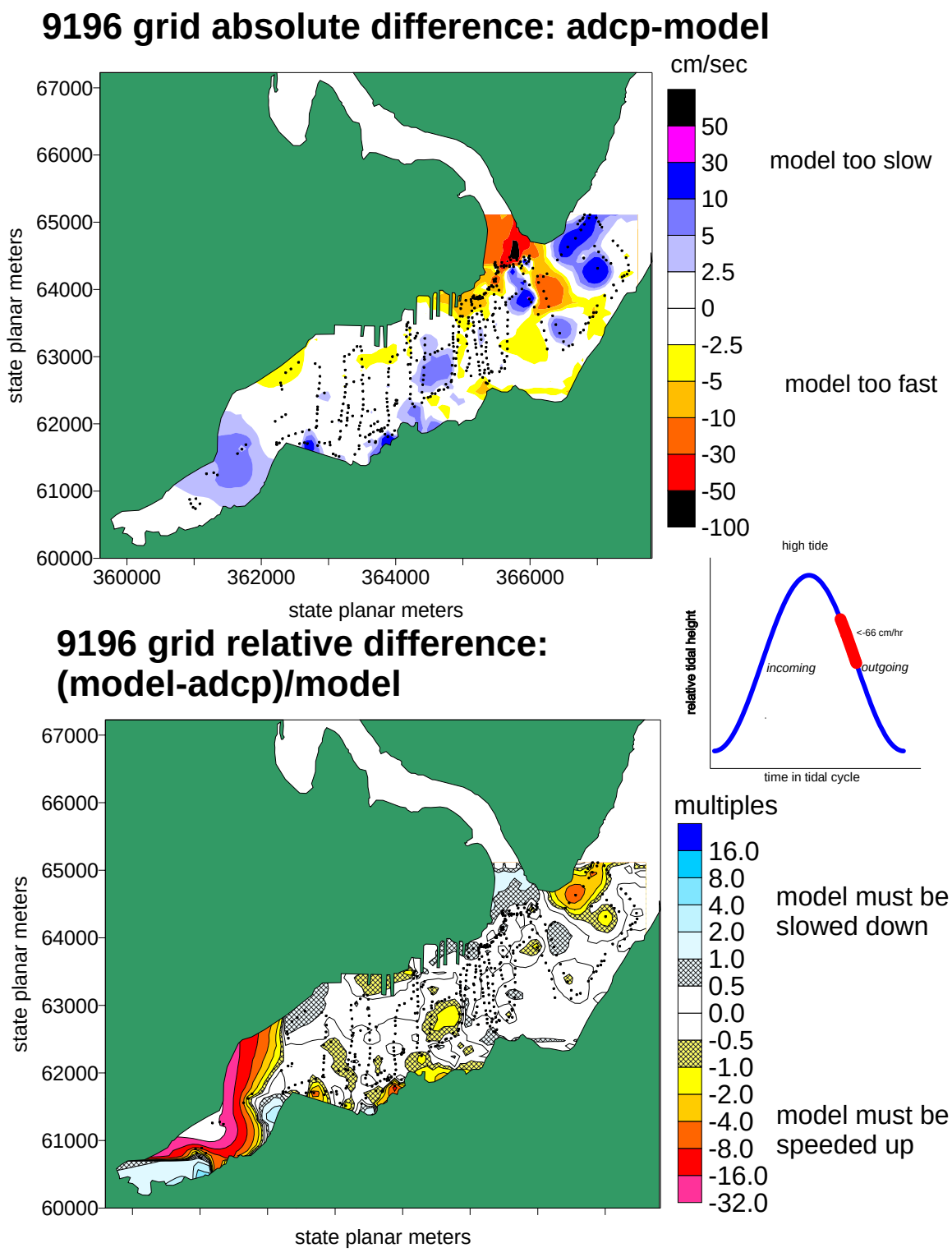

Figure 18: Absolute and relative mean water column model error at tide condition 10

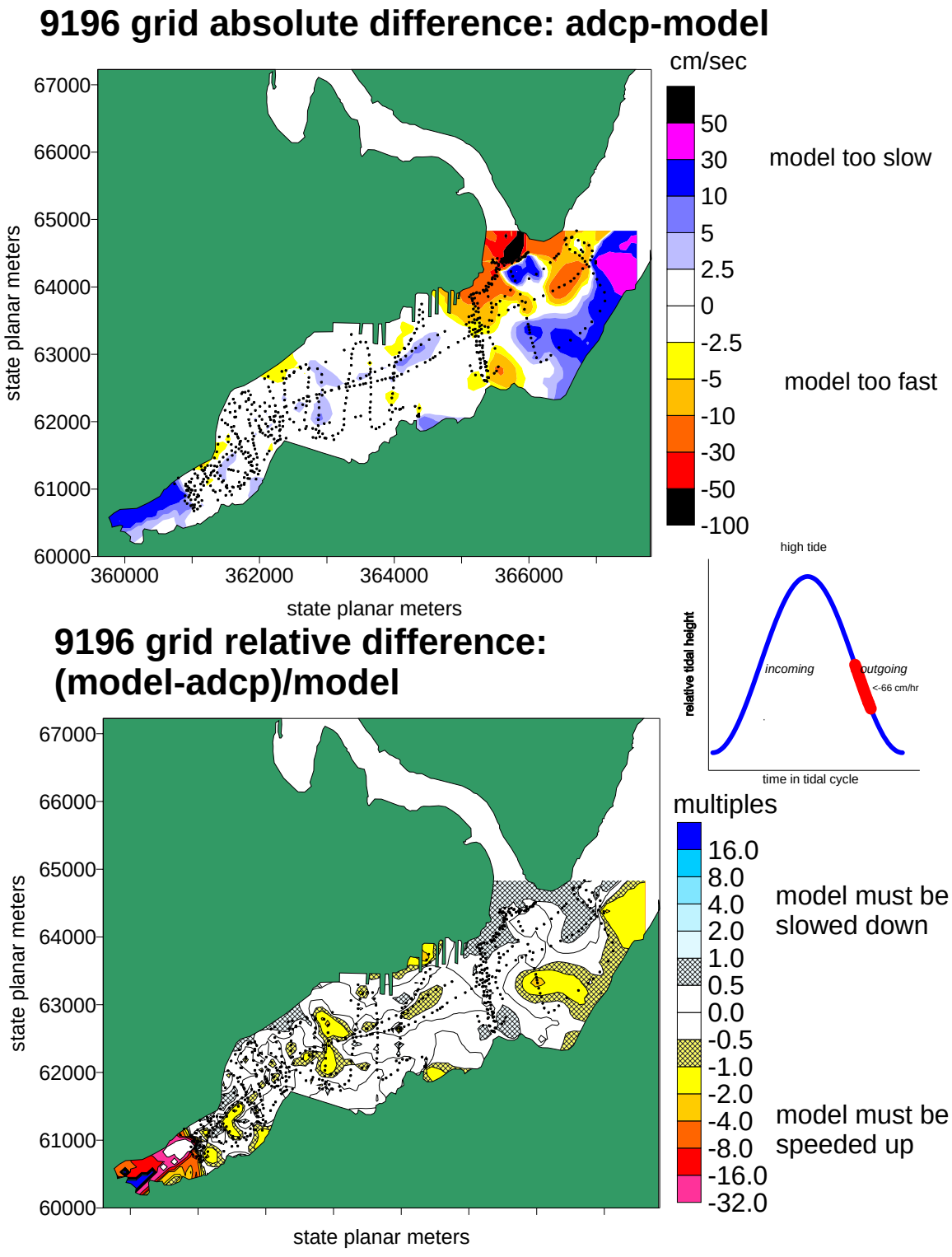

Figure 19: Absolute and relative mean water column model error at tide condition 11

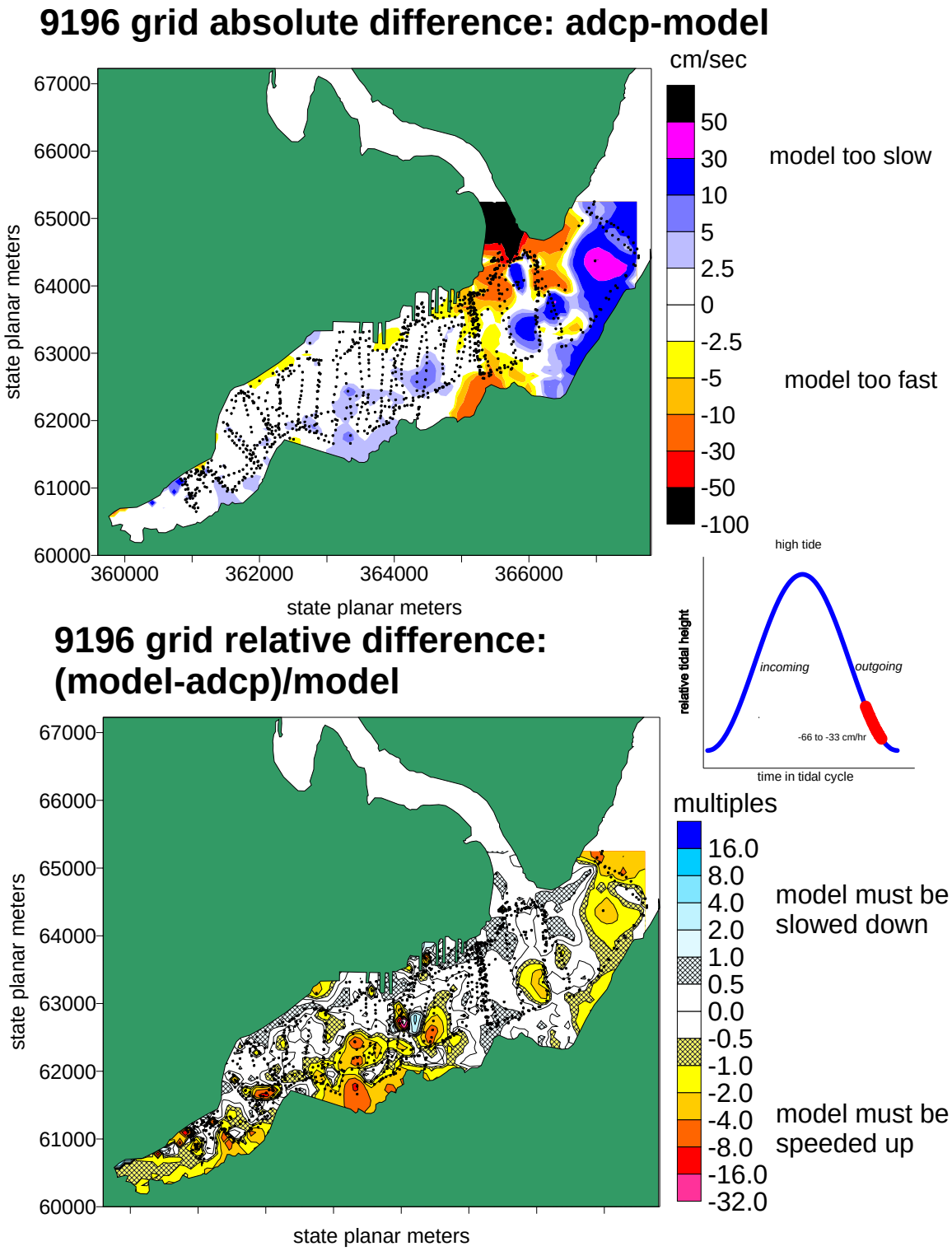

Figure 20: Absolute and relative mean water column model error at tide condition 12

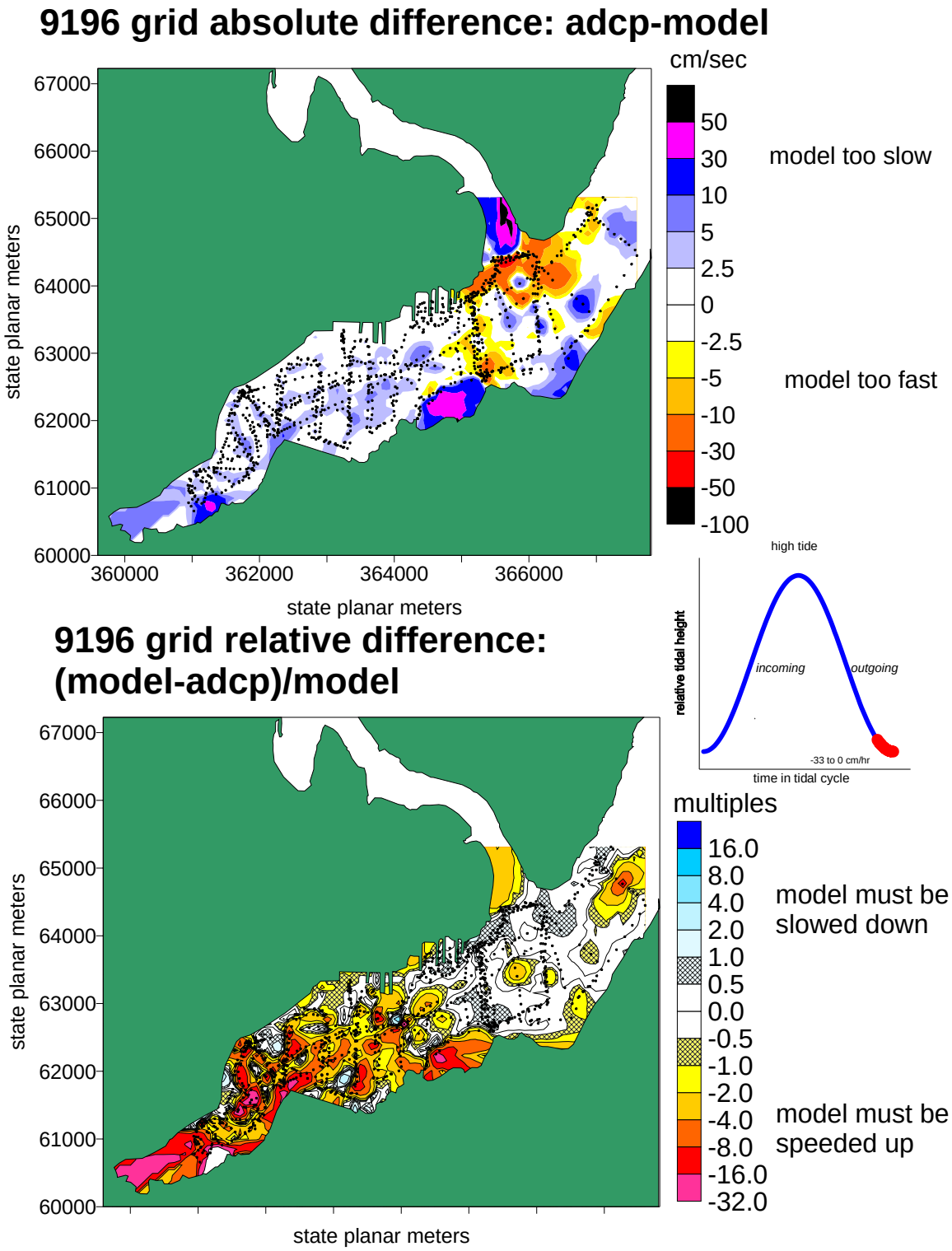

Absolute error by depth: Figures 21-56 plot the absolute difference in current speed between CH3D using the 9196 grid and ADCP current measurements as a function of tidal condition and depth. Three figures are shown for each tidal condition. The first plot is the depth-average difference, similar to the plots above except that value are shown only where data were collected and are not contoured. This plot makes the succeeding two easier to interpret. Note that the direction south is to the top of the page. This orientation makes comparisons in the deep water off Washington Narrows easier to see. The second plot for each tidal condition is the absolute difference plotted in 3 m depth bins – the depth resolution of CH3D. Data are only presented where ADCP measurements were taken. A plot of the outline of Sinclair Inlet at the same aspect is included in order to better estimate spatial location of the displayed data. The third plot shows smoothed contours of absolute error by depth, based on the data presented in the previous plot. The contours make it easier to find areas of model error, but can be misleading since they extrapolate beyond the spatial extent of the collected data. In the following figures, the red portion of the tidal cycle is less distinct, but follows the same sequence as in Figures 9-20.

Figure 21: Absolute difference at all depths during tide condition 1

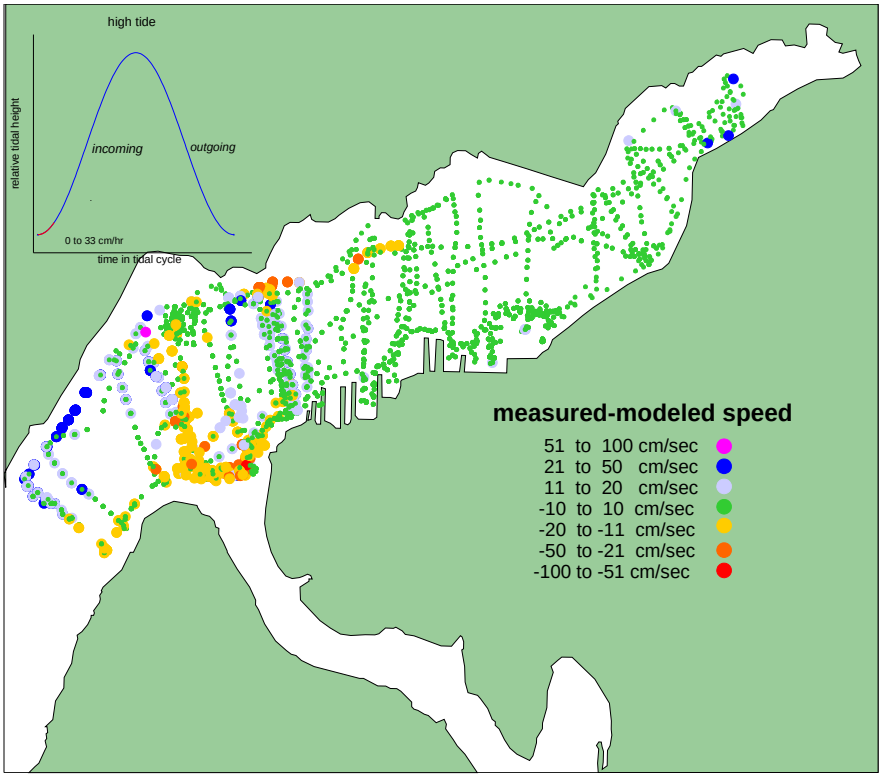

Figure 22: Absolute difference by depth during tide condition 1

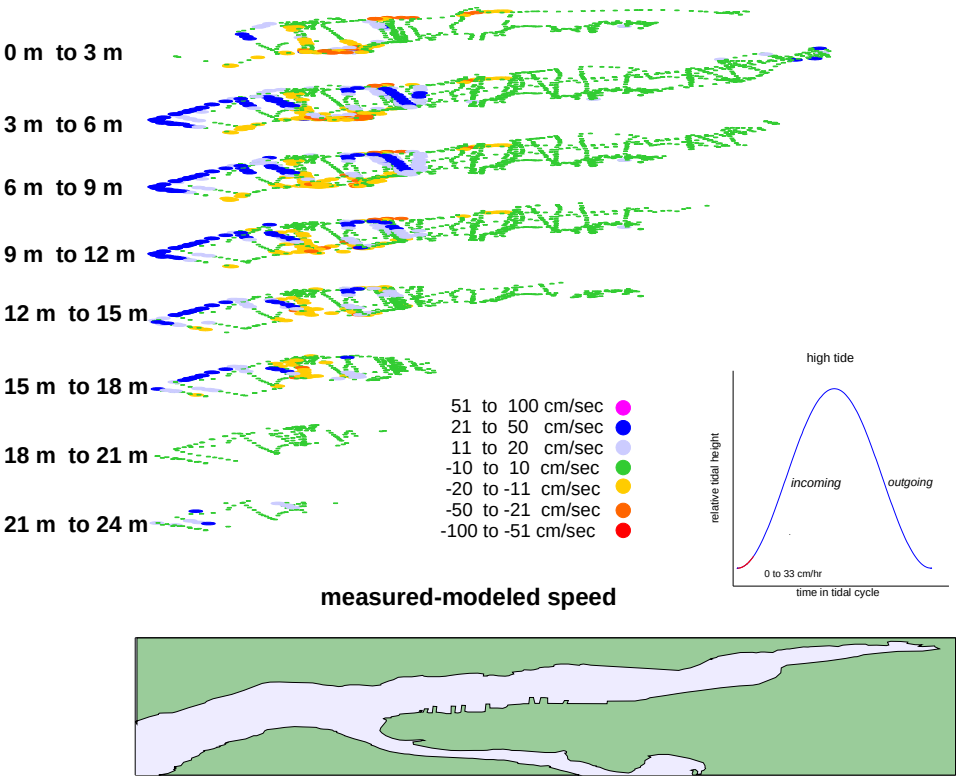

Figure 23: Horizontally smoothed and extrapolated absolute difference by depth during tide condition 1

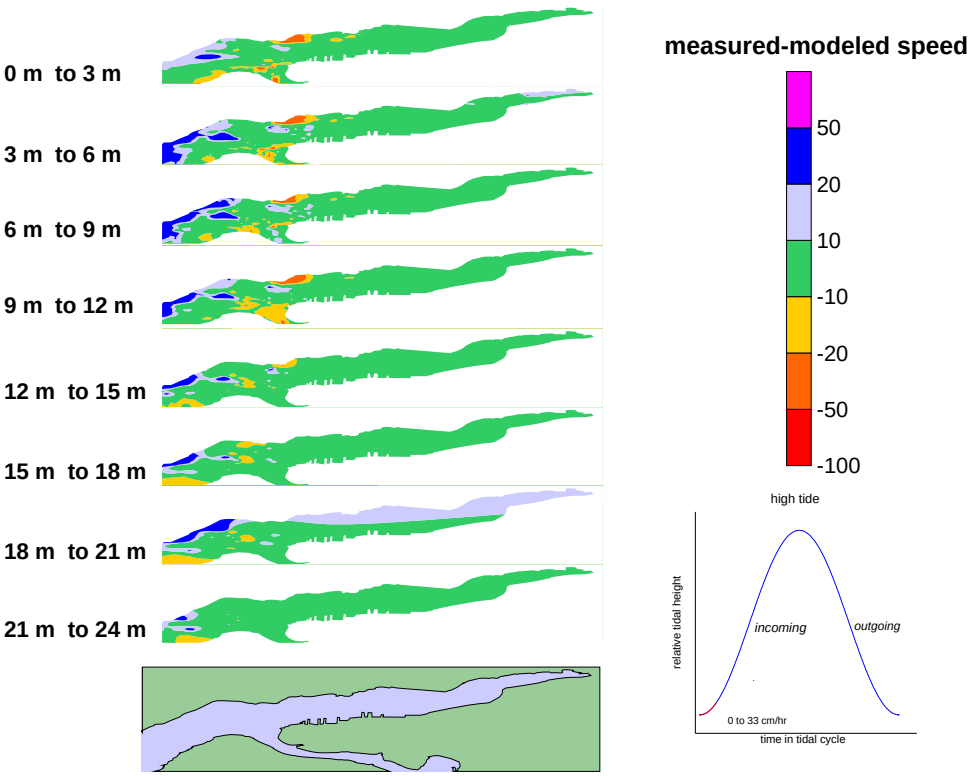

Figure 24: Absolute difference at all depths during tide condition 2

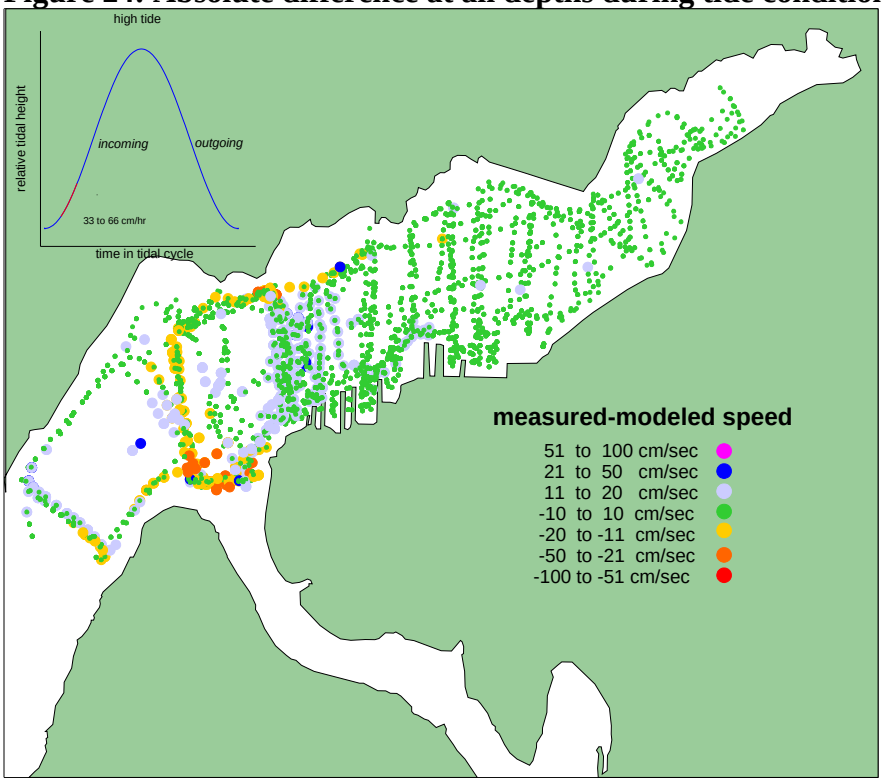

Figure 25: Absolute difference by depth during tide condition 2

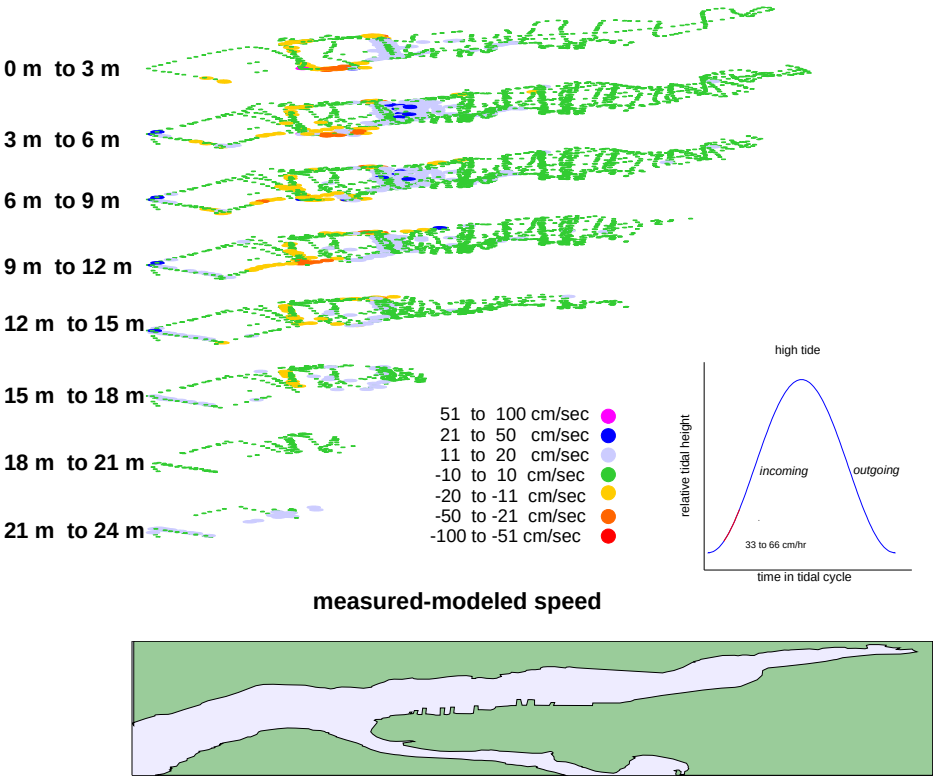

Figure 26: Horizontally smoothed and extrapolated absolute difference by depth during tide condition 2

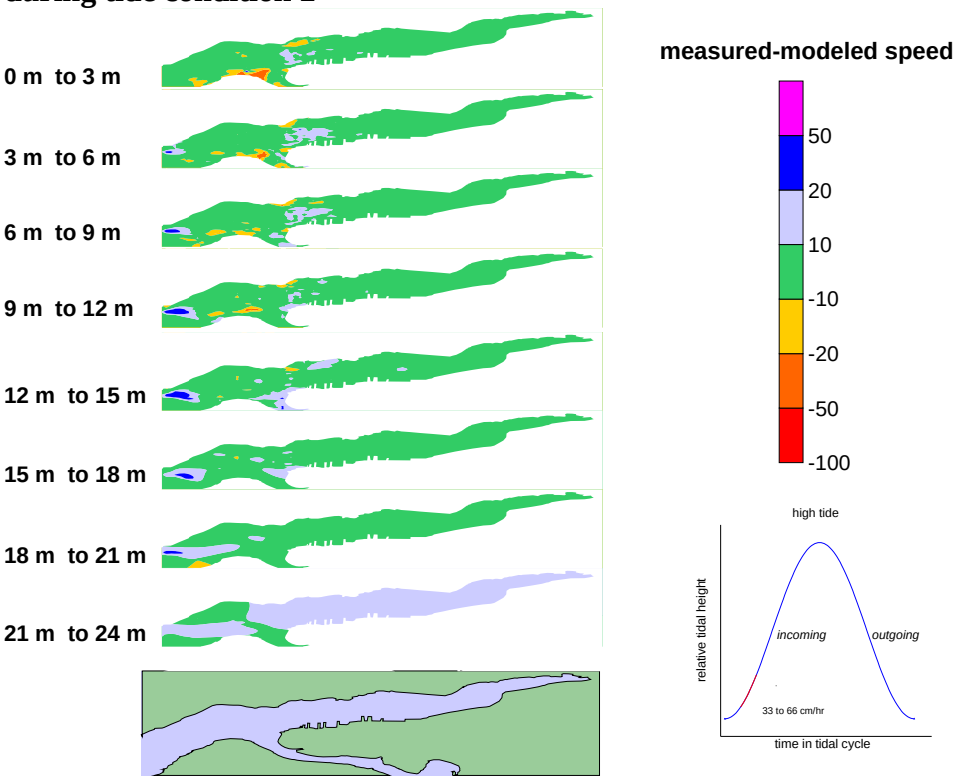

Figure 27: Absolute difference at all depths during tide condition 3

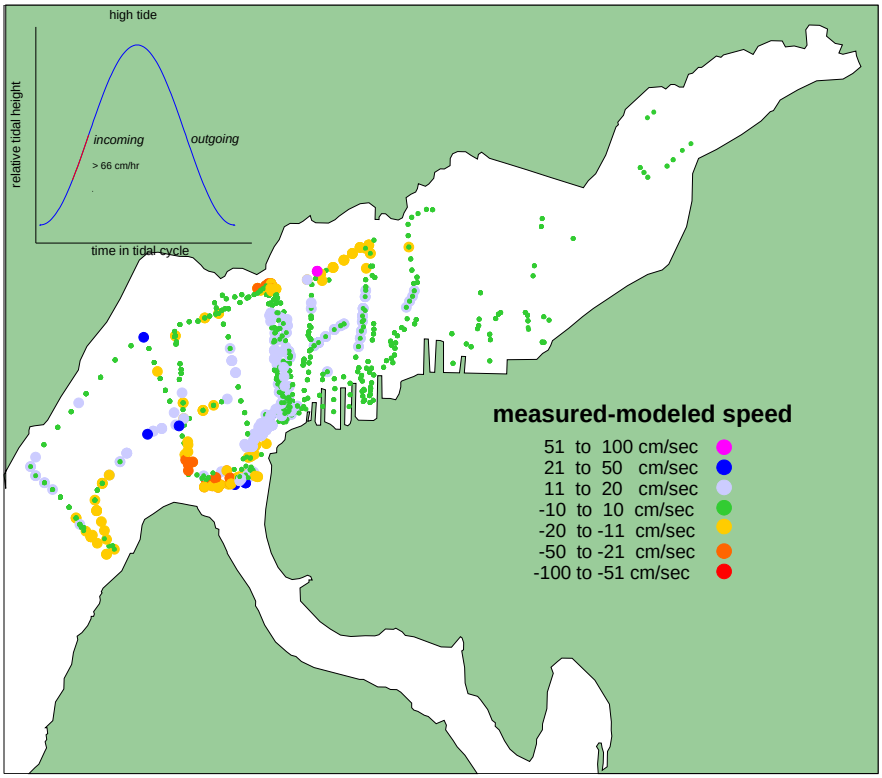

Figure 28: Absolute difference by depth during tide condition 3

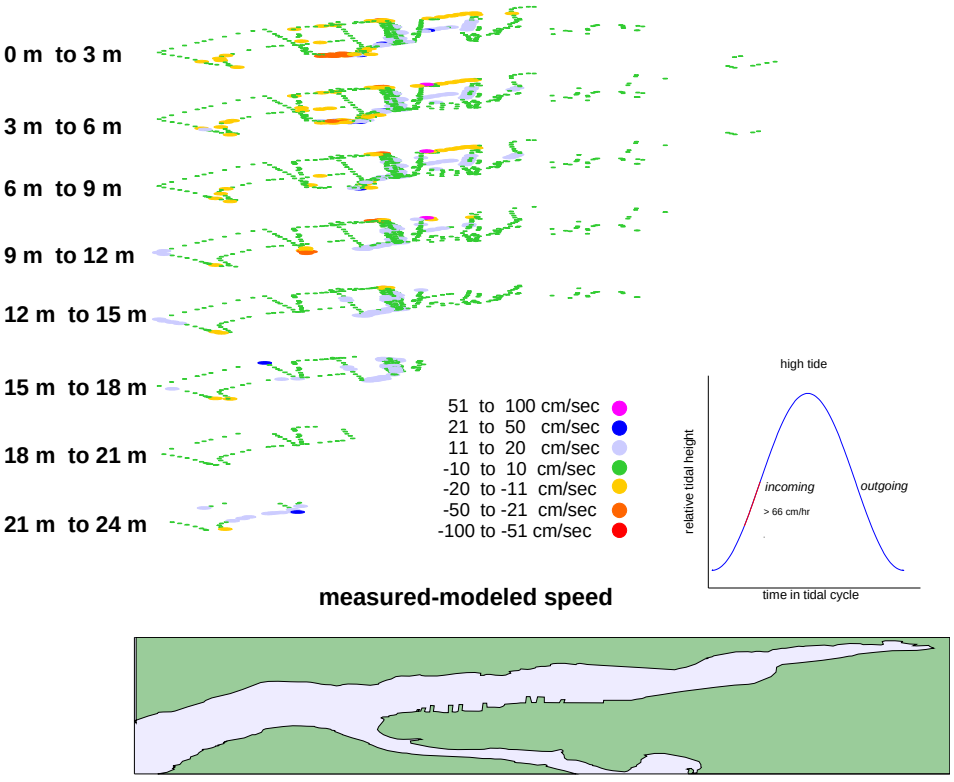

Figure 29: Horizontally smoothed and extrapolated absolute difference by depth during tide condition 3

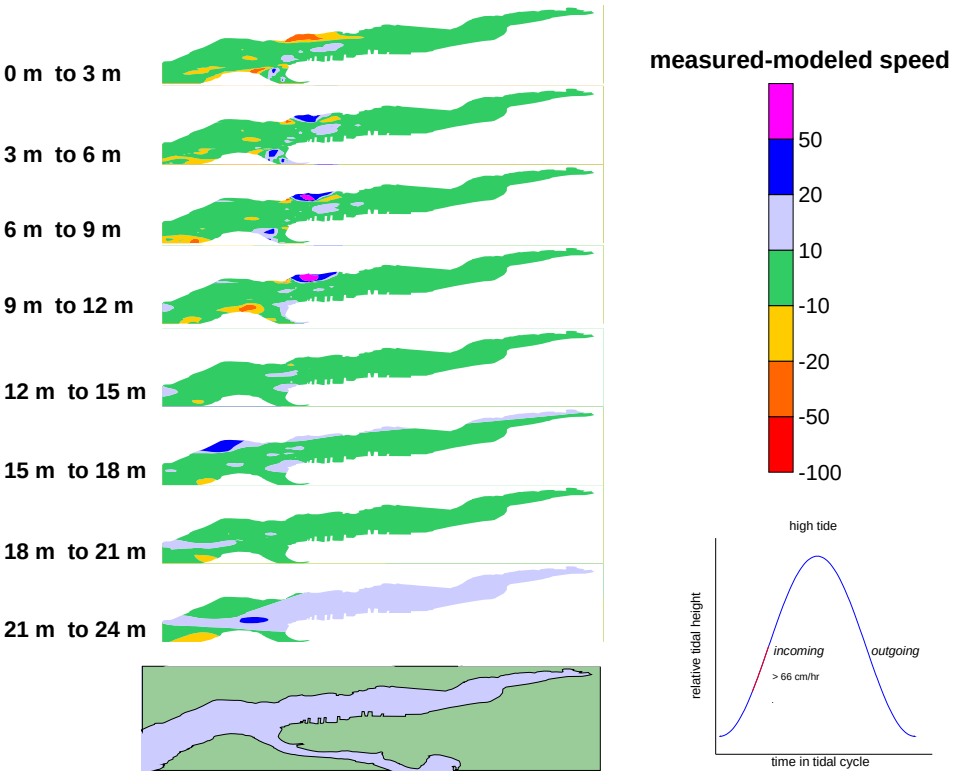

Figure 30: Absolute difference at all depths during tide condition 4

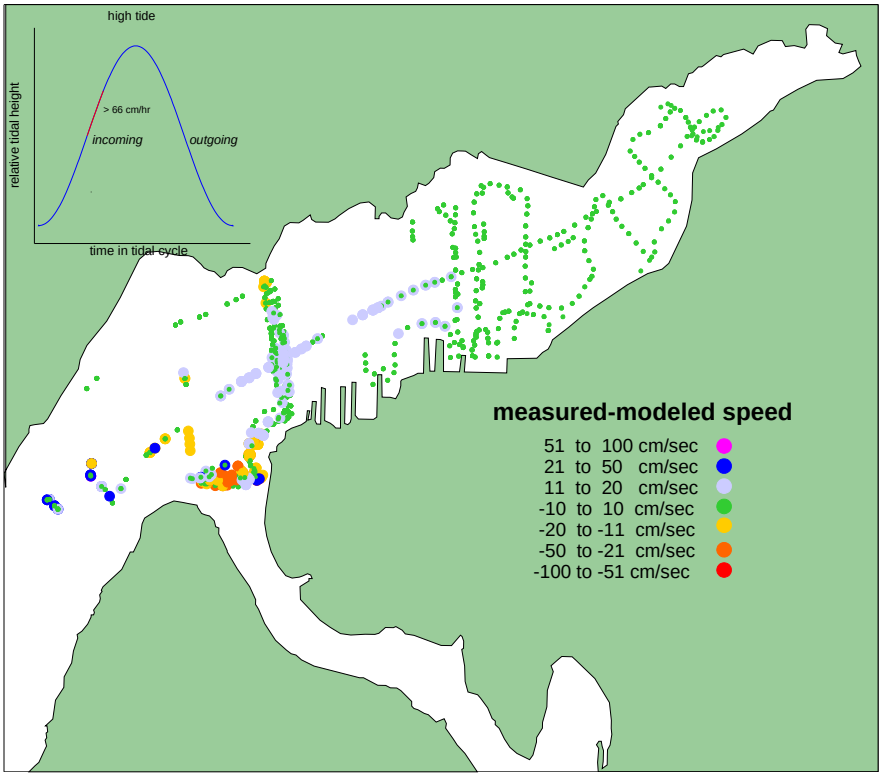

Figure 31: Absolute difference by depth during tide condition 4

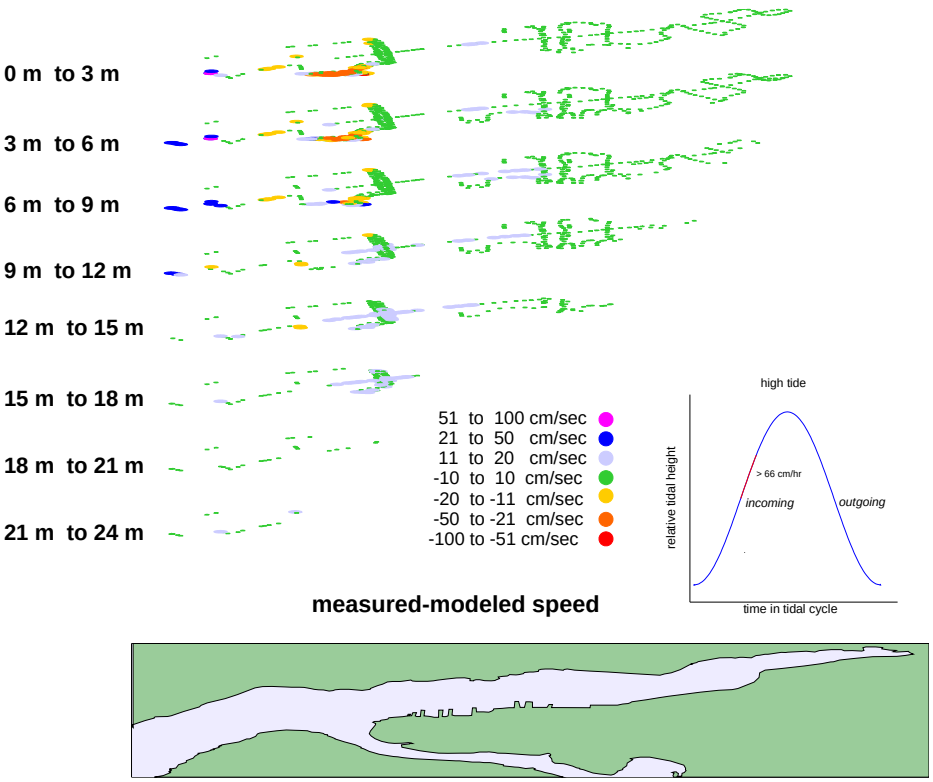

Figure 32: Horizontally smoothed and extrapolated absolute difference by depth during tide condition 4

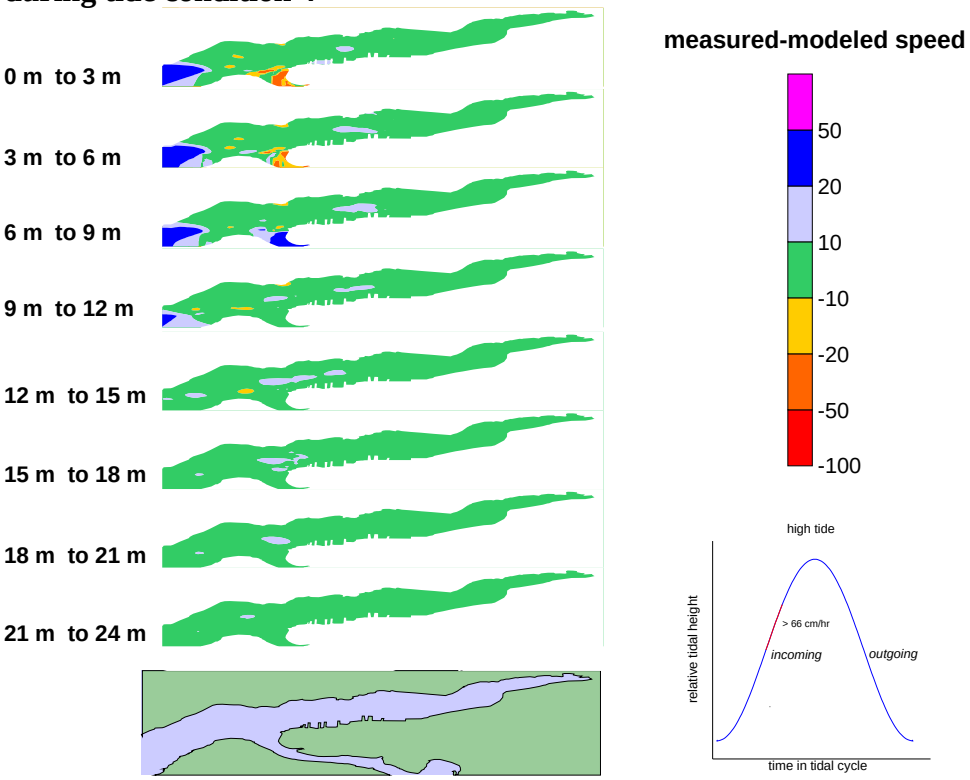

Figure 33: Absolute difference at all depths during tide condition 5

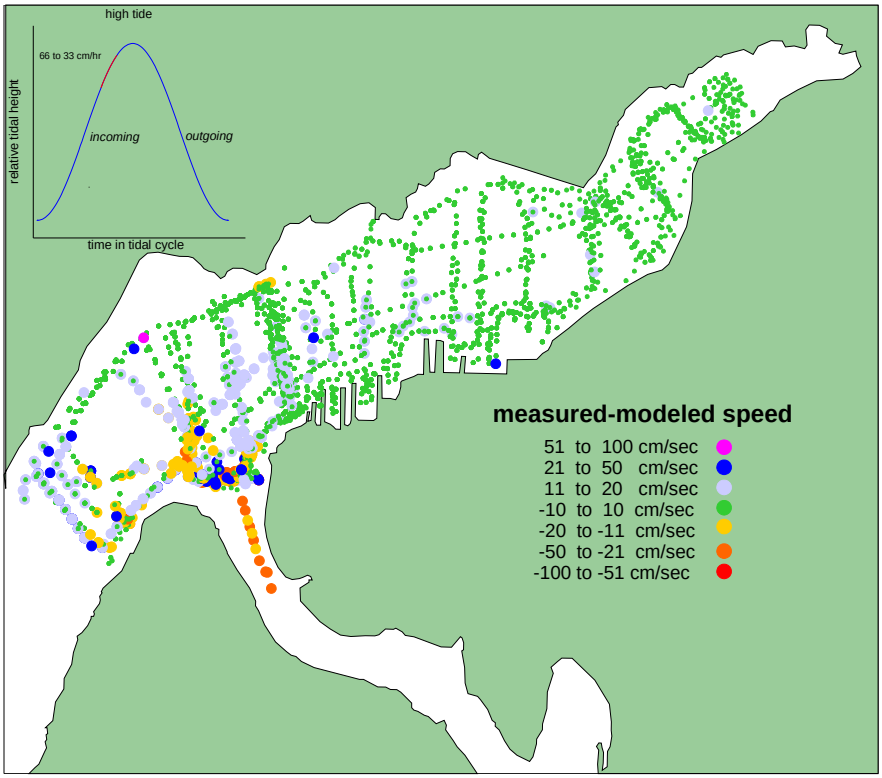

Figure 34: Absolute difference by depth during tide condition 5

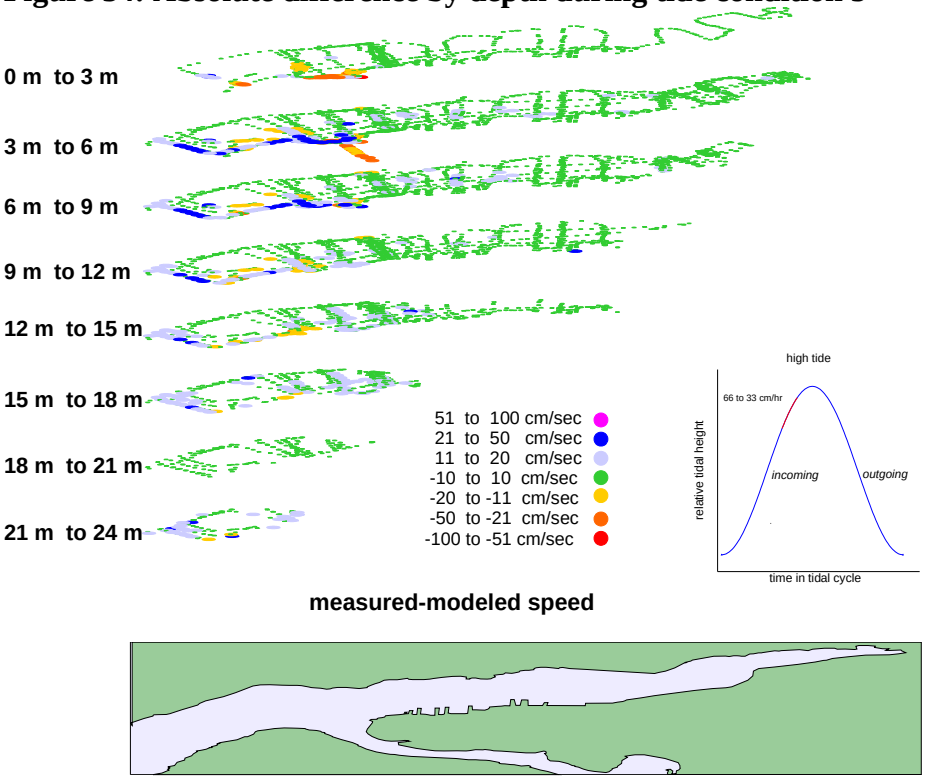

Figure 35: Horizontally smoothed and extrapolated absolute difference by depth during tide condition 5

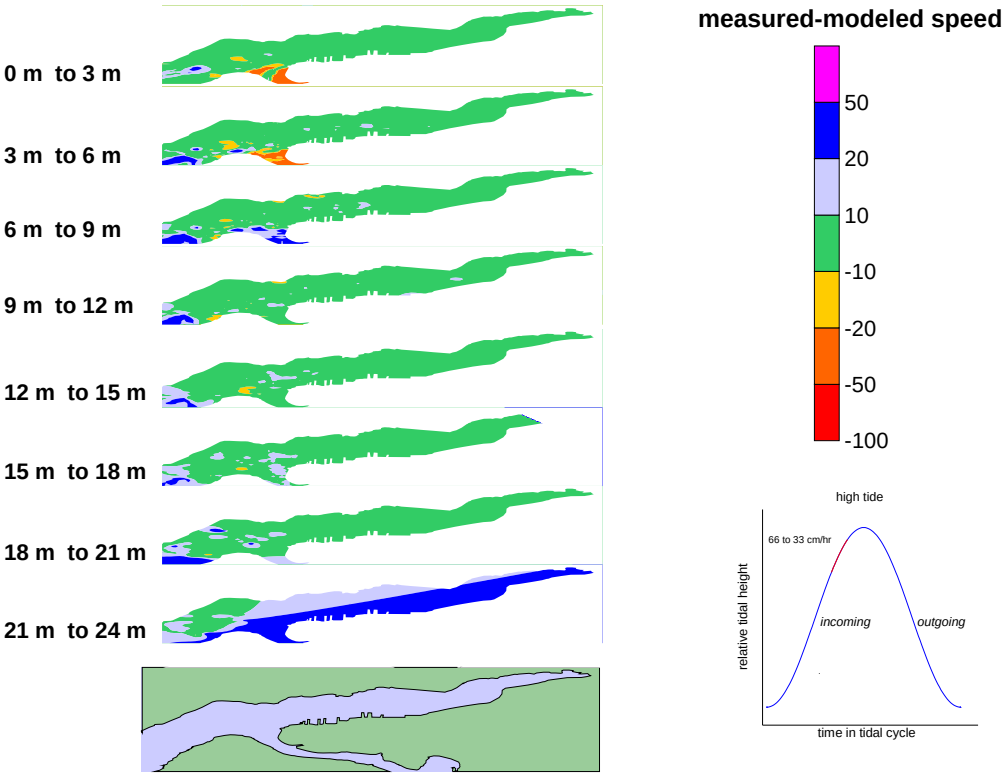

Figure 36: Absolute difference at all depths during tide condition 6

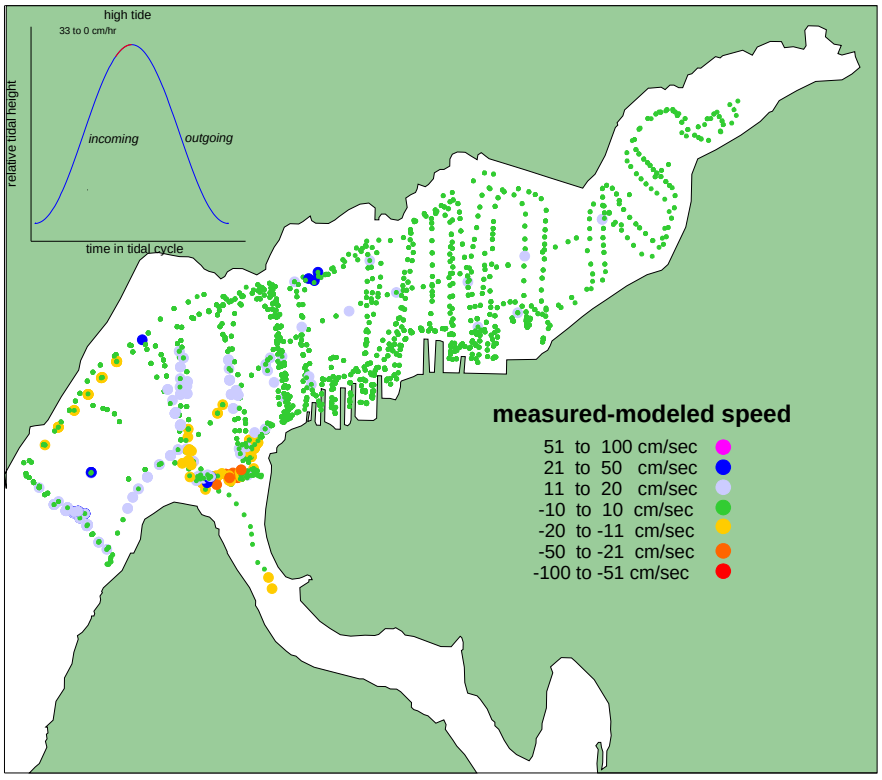

Figure 37: Absolute difference by depth during tide condition 6

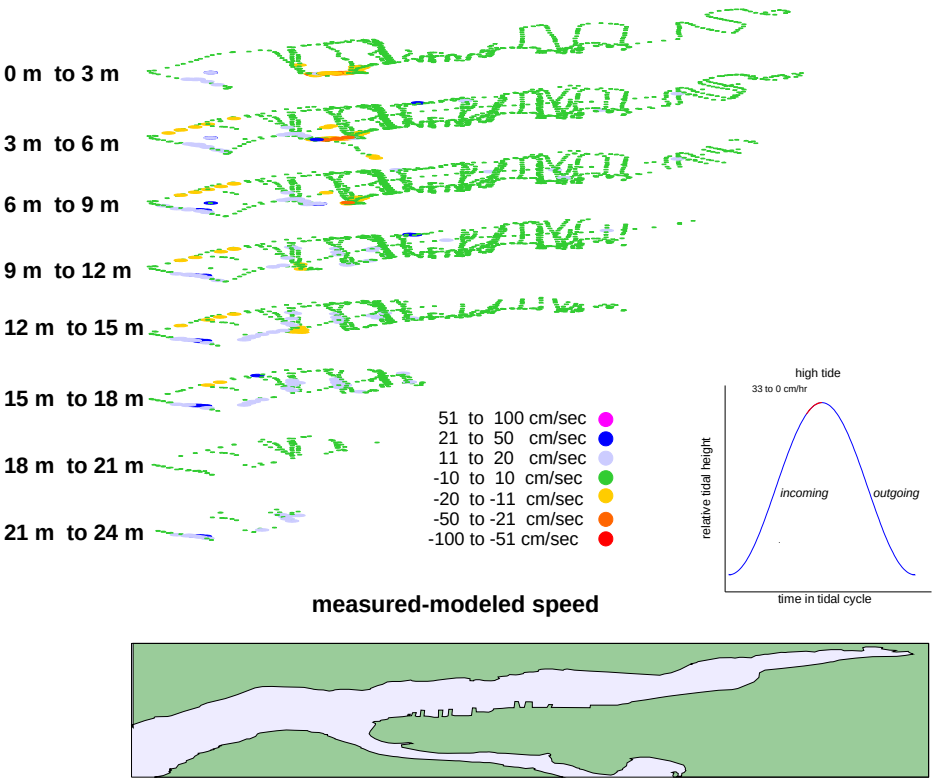

Figure 38: Horizontally smoothed and extrapolated absolute difference by depth during tide condition 6

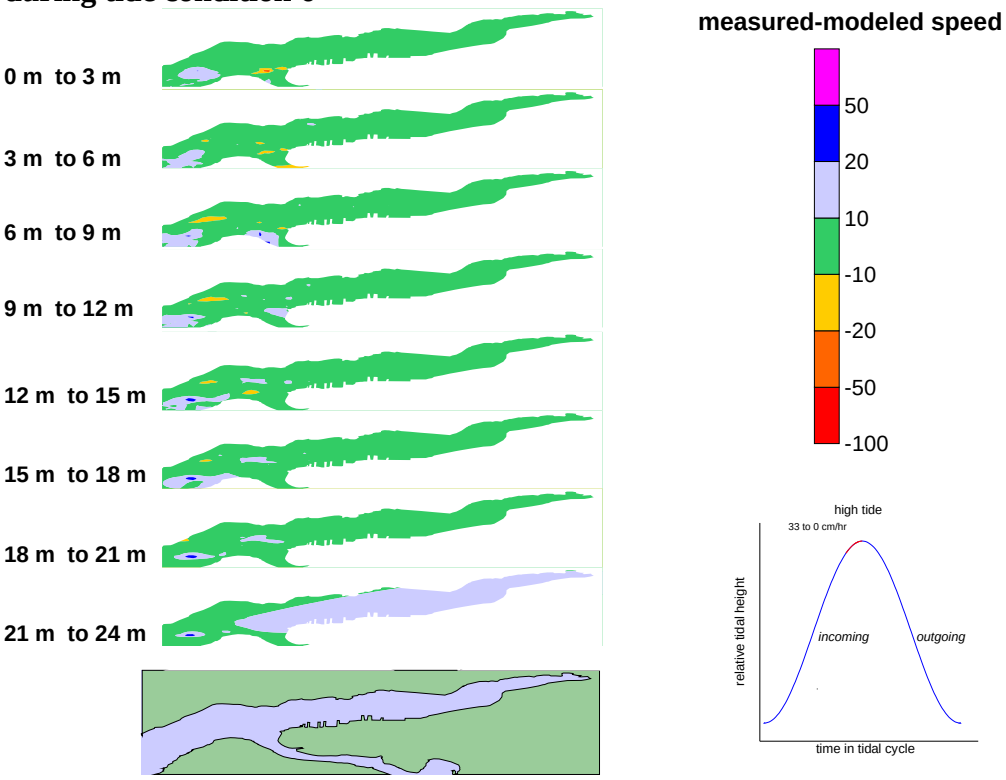

Figure 39: Absolute difference at all depths during tide condition 7

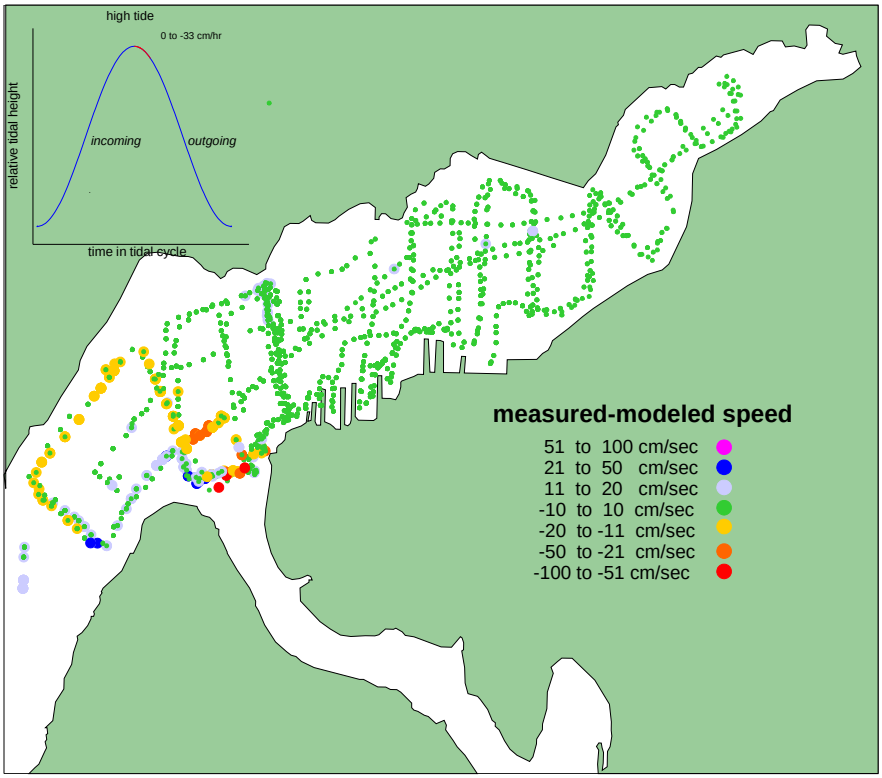

Figure 40: Absolute difference by depth during tide condition 7

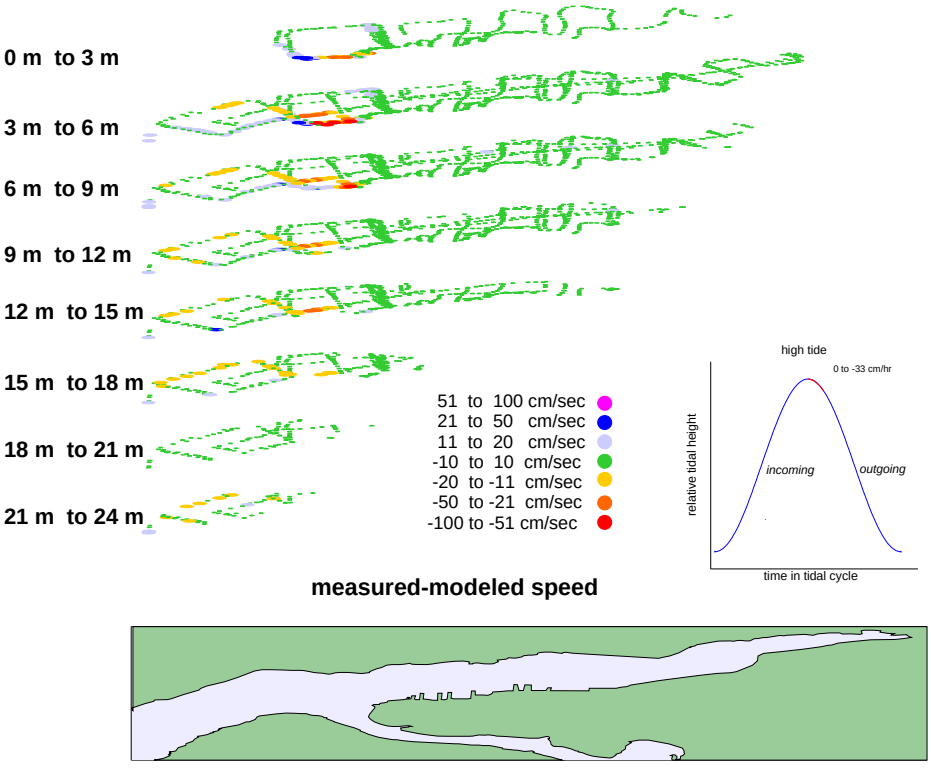

Figure 41: Horizontally smoothed and extrapolated absolute difference by depth during tide condition 7

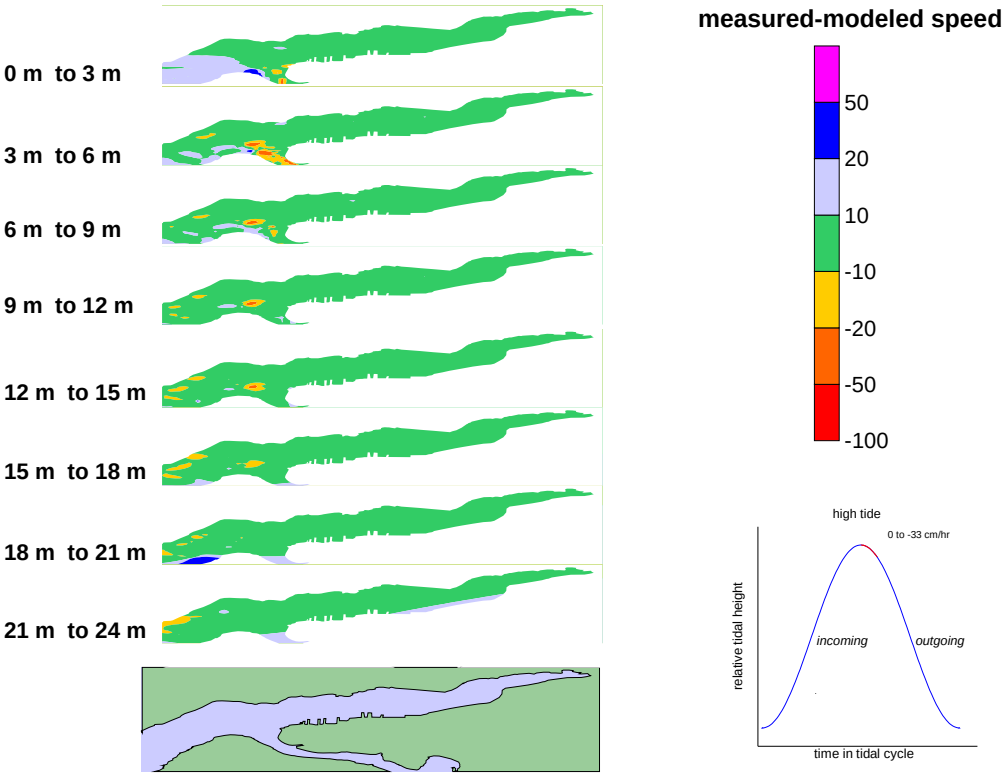

Figure 42: Absolute difference at all depths during tide condition 8

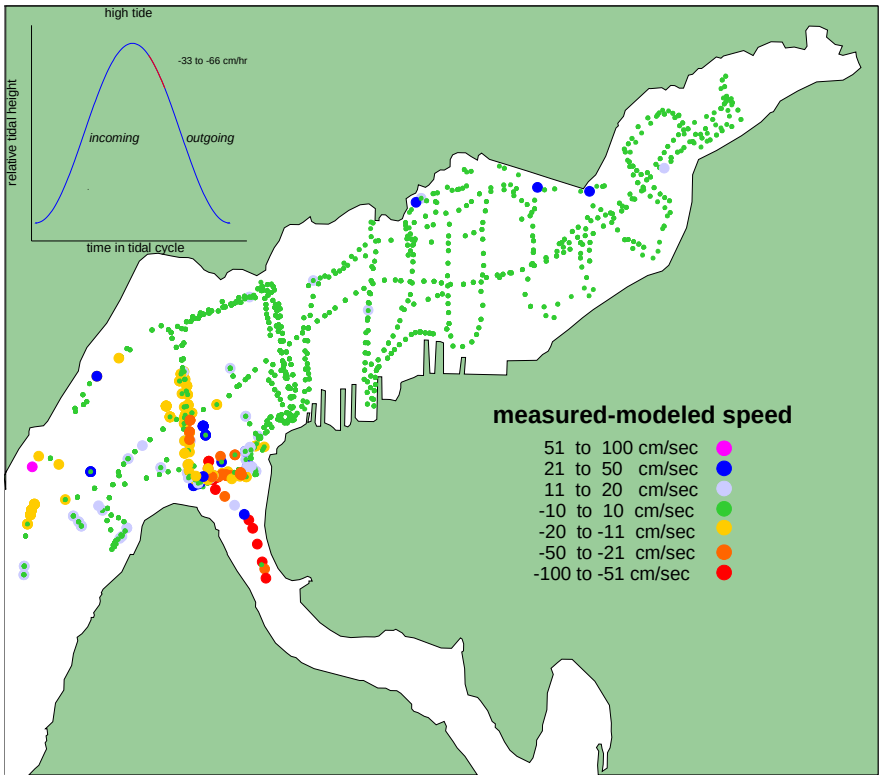

Figure 43: Absolute difference by depth during tide condition 8

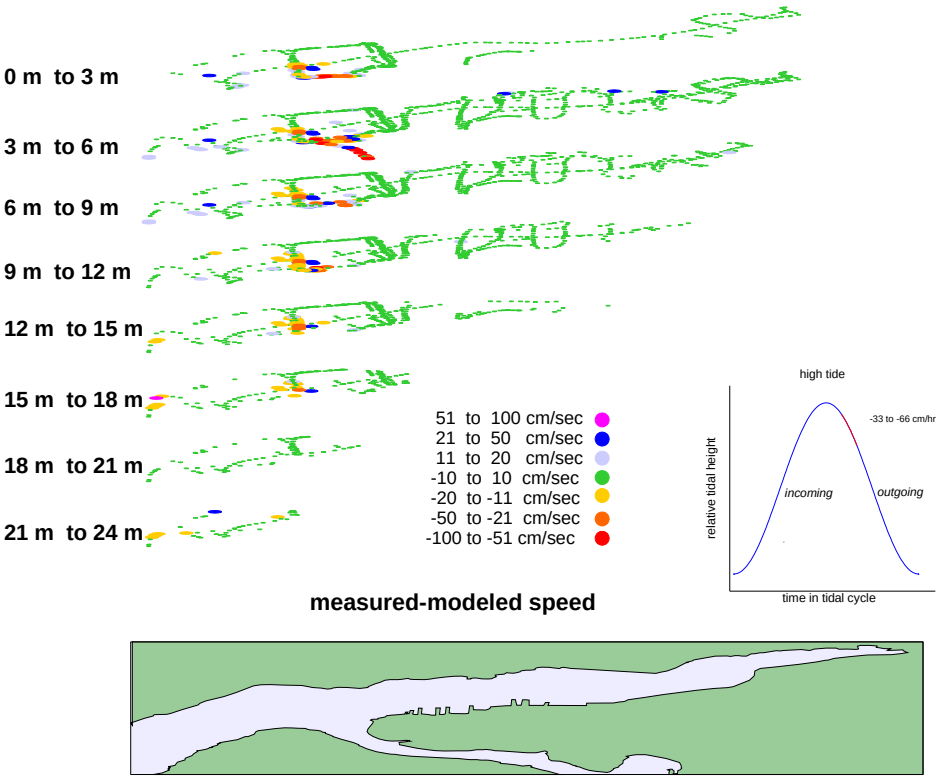

Figure 44: Horizontally smoothed and extrapolated absolute difference by depth during tide condition 8

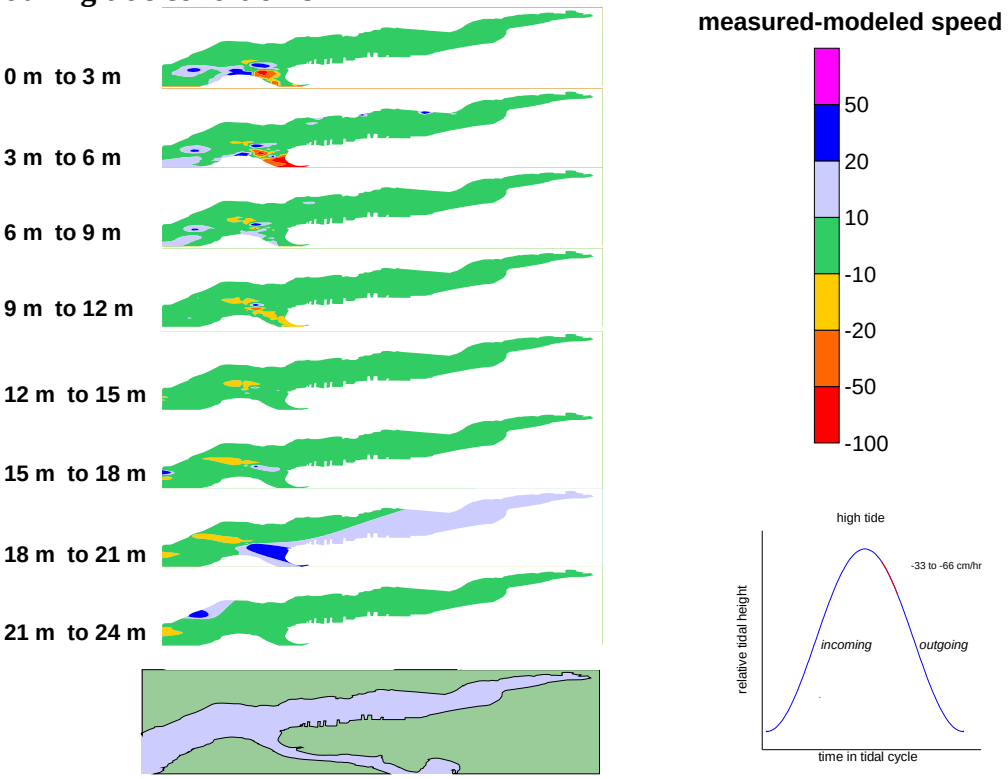

Figure 45: Absolute difference at all depths during tide condition 9

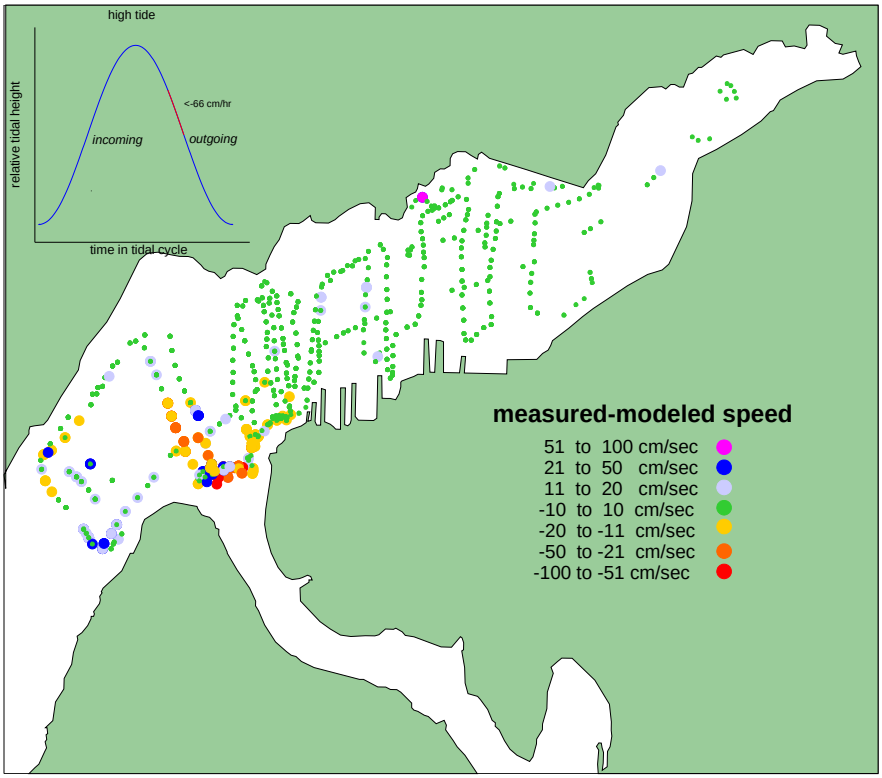

Figure 46: Absolute difference by depth during tide condition 9

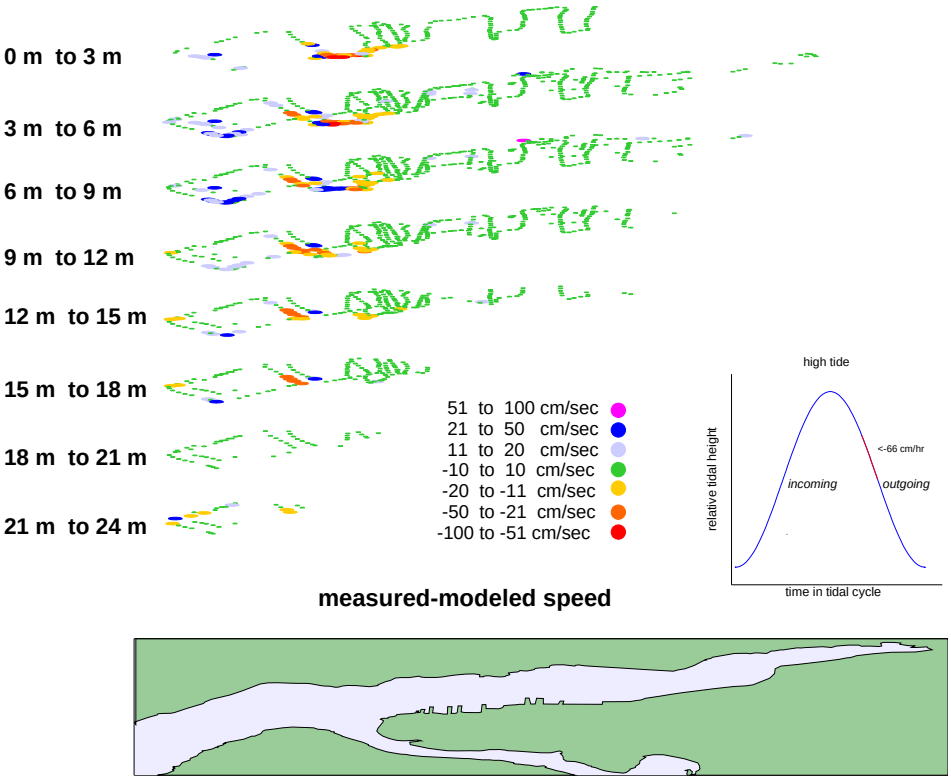

Figure 47: Horizontally smoothed and extrapolated absolute difference by depth during tide condition 9

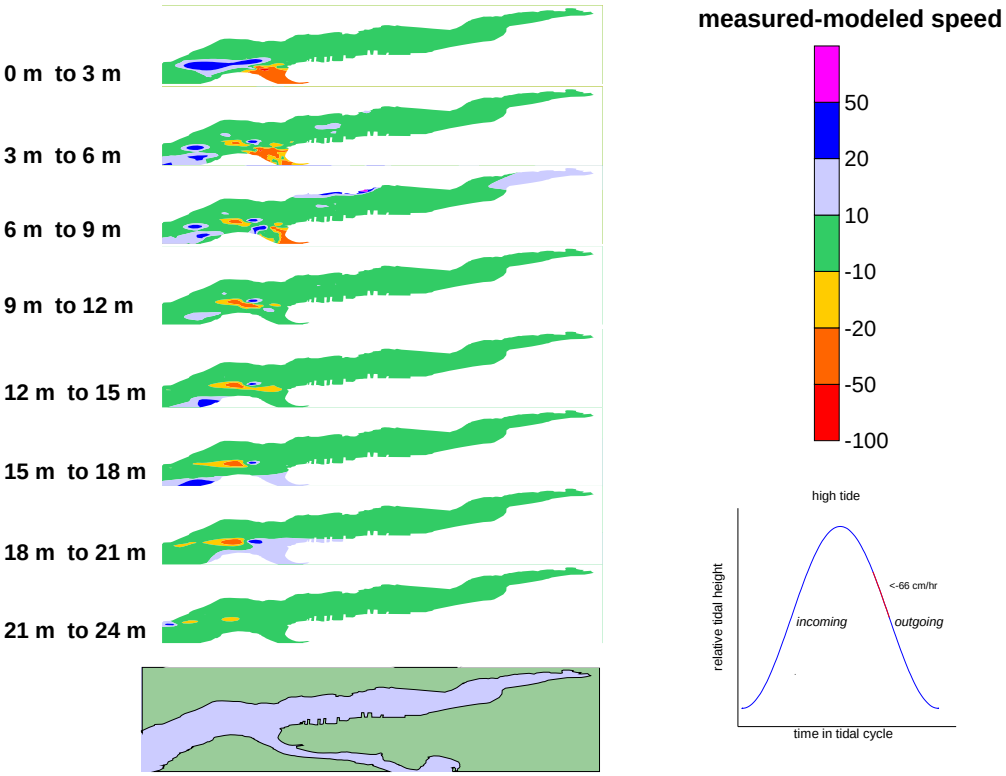

Figure 48: Absolute difference at all depths during tide condition 10

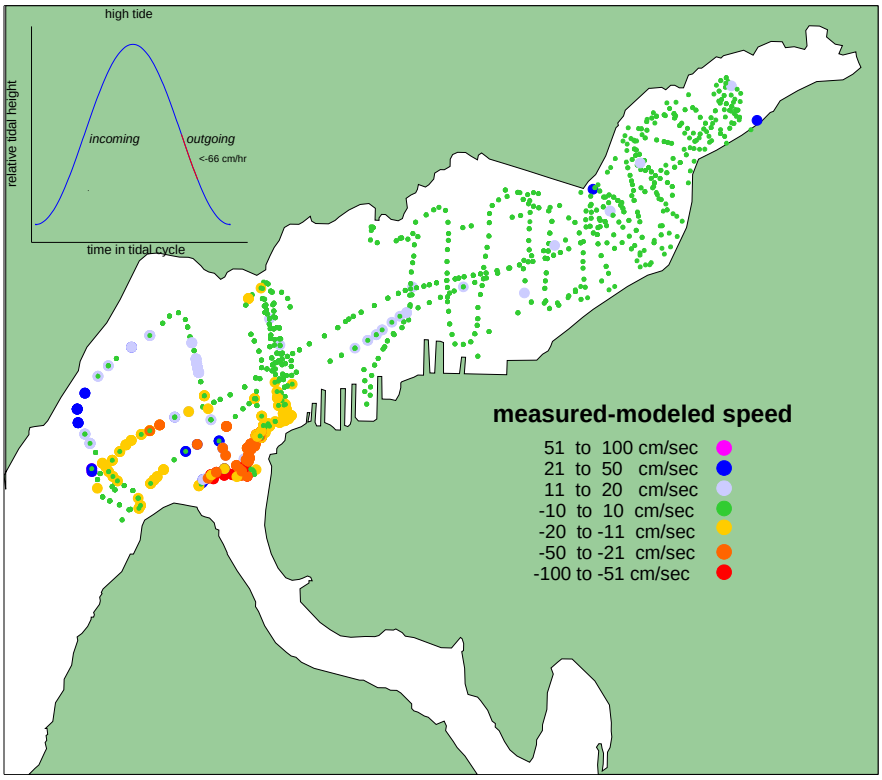

Figure 49: Absolute difference by depth during tide condition 10

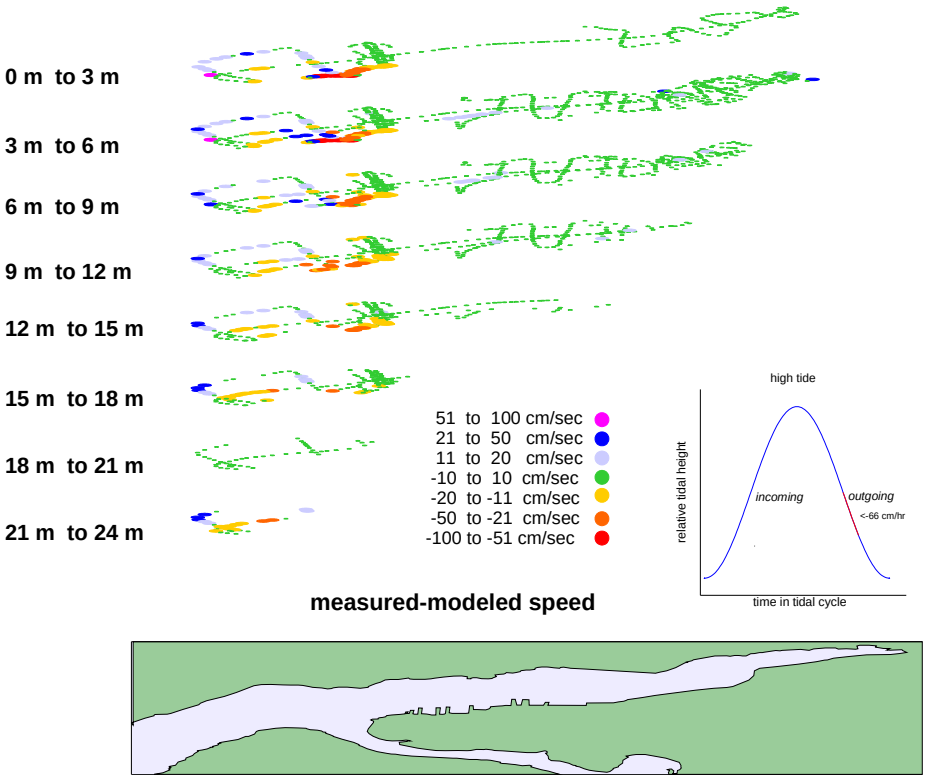

Figure 50: Horizontally smoothed and extrapolated absolute difference by depth during tide condition 10

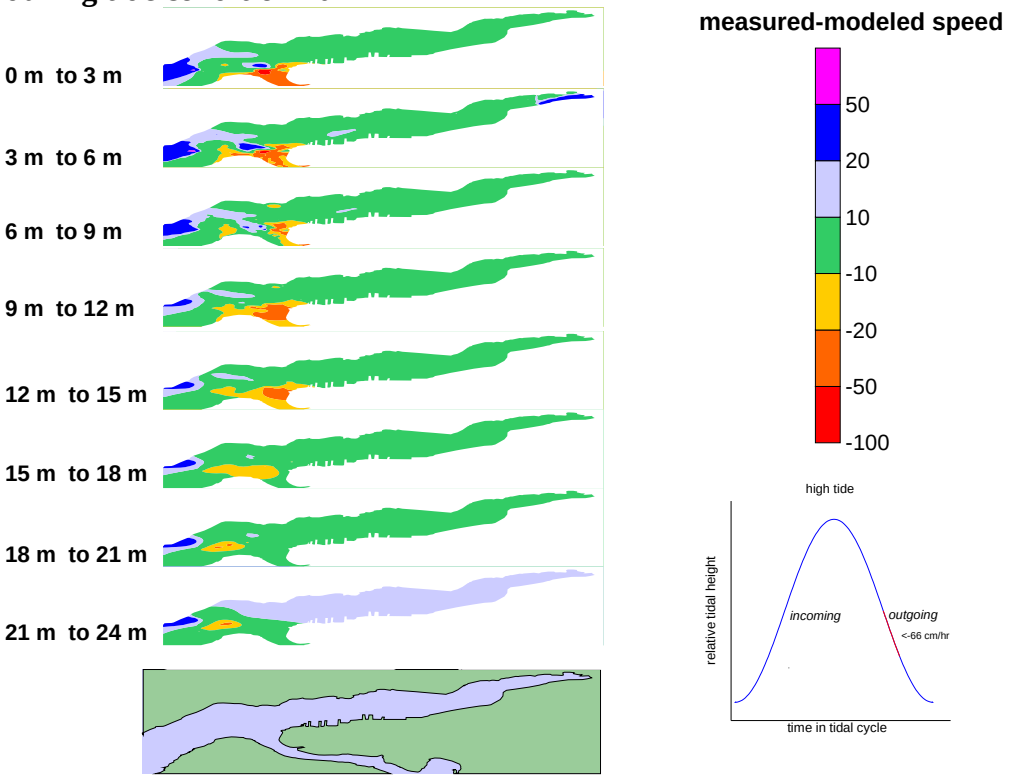

Figure 51: Absolute difference at all depths during tide condition 11

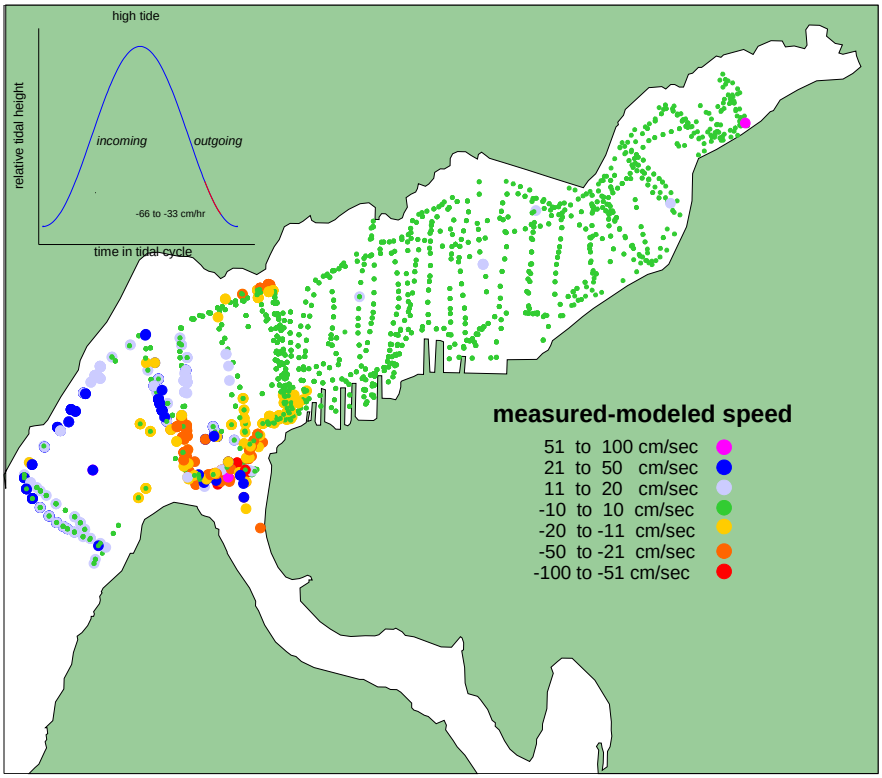

Figure 52: Absolute difference by depth during tide condition 11

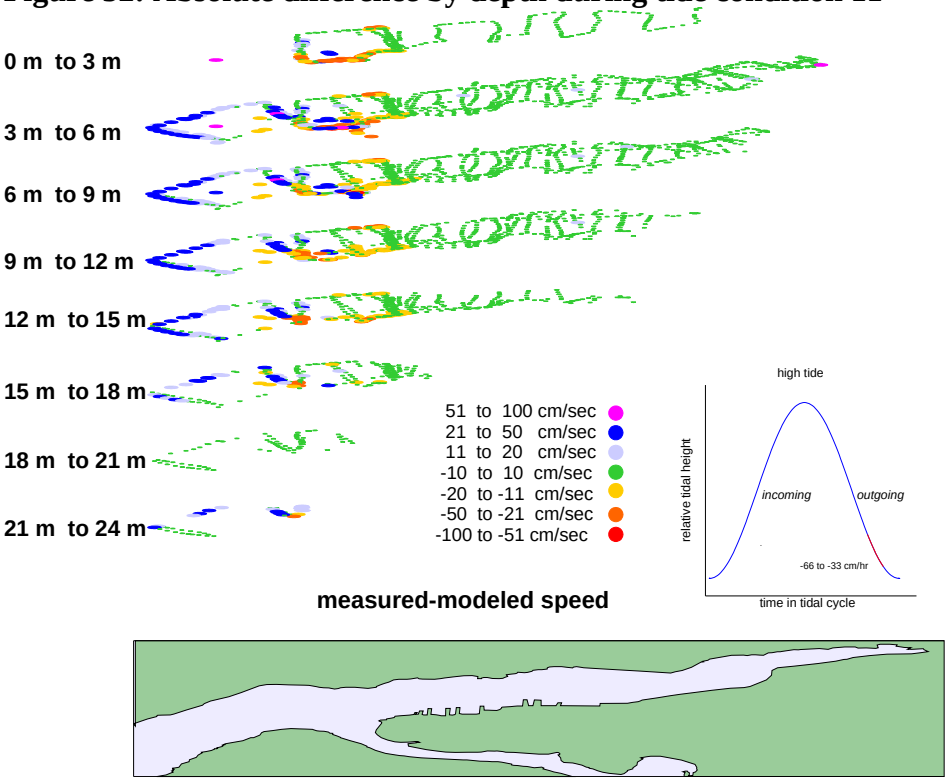

Figure 53: Horizontally smoothed and extrapolated absolute difference by depth during tide condition 11

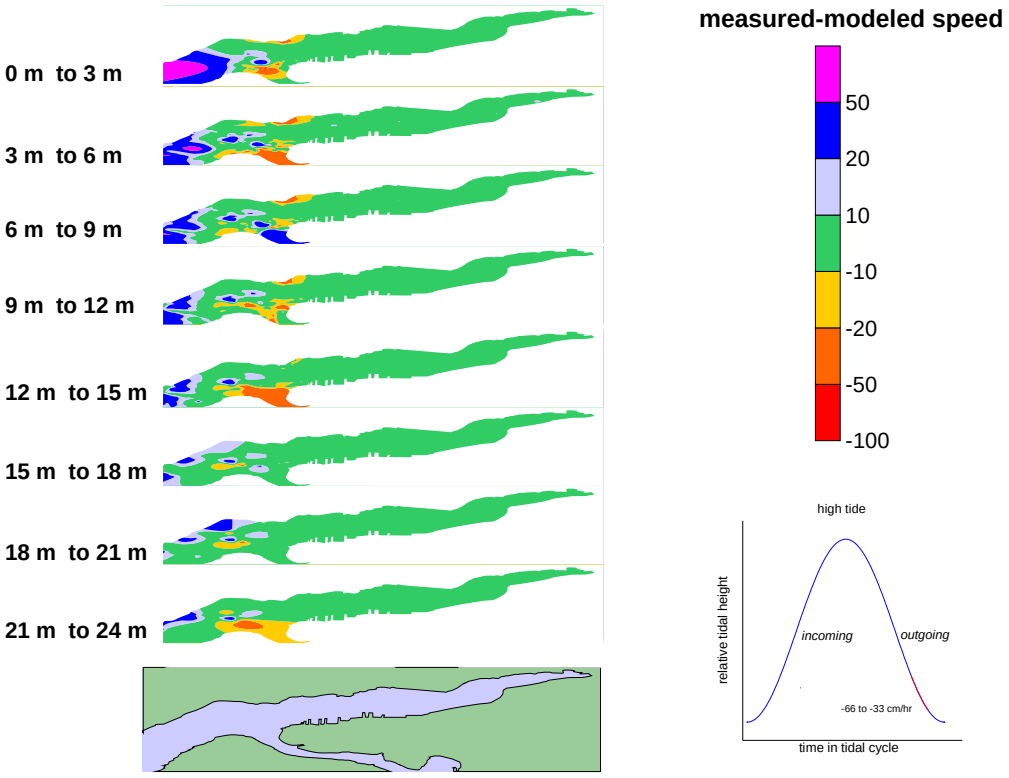

Figure 54: Absolute difference at all depths during tide condition 12

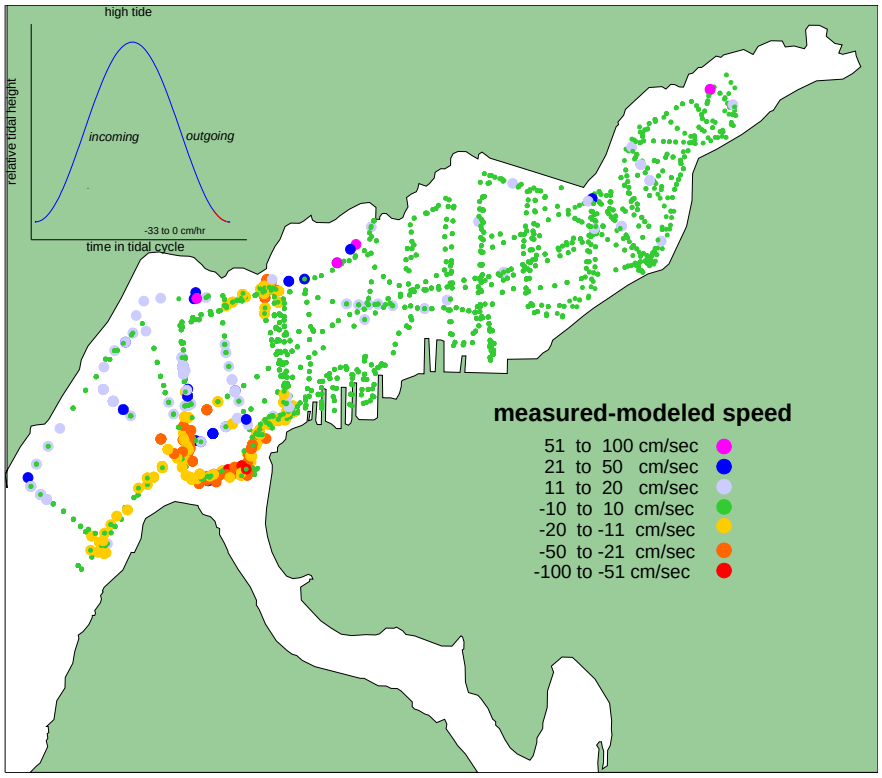

Figure 55: Absolute difference by depth during tide condition 12

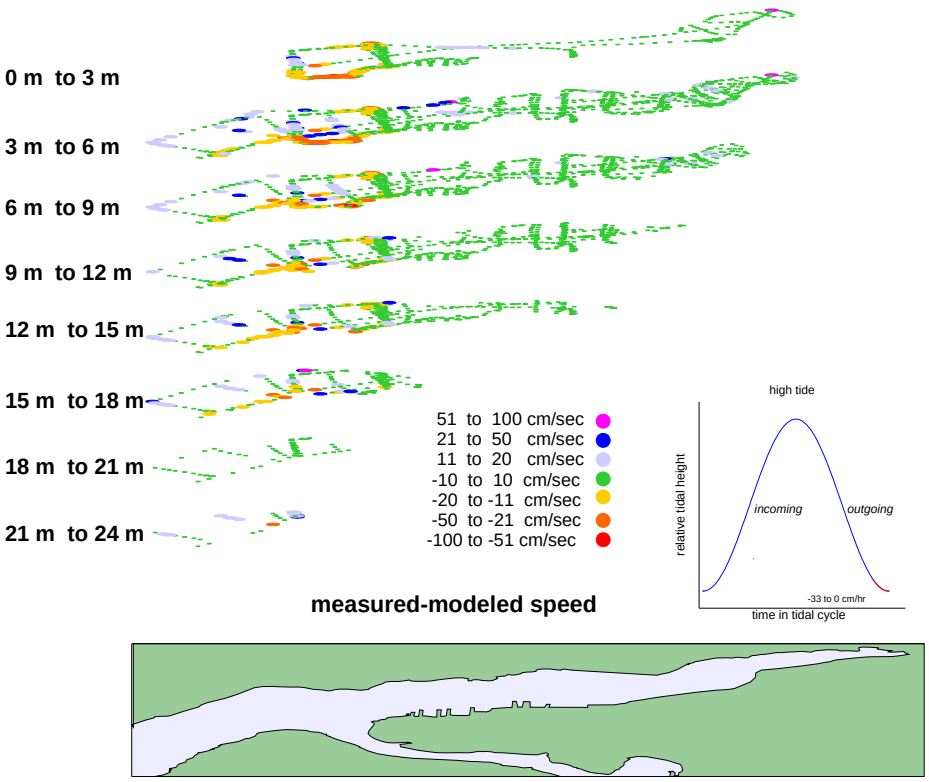

Figure 56: Horizontally smoothed and extrapolated absolute difference by depth during tide condition 12

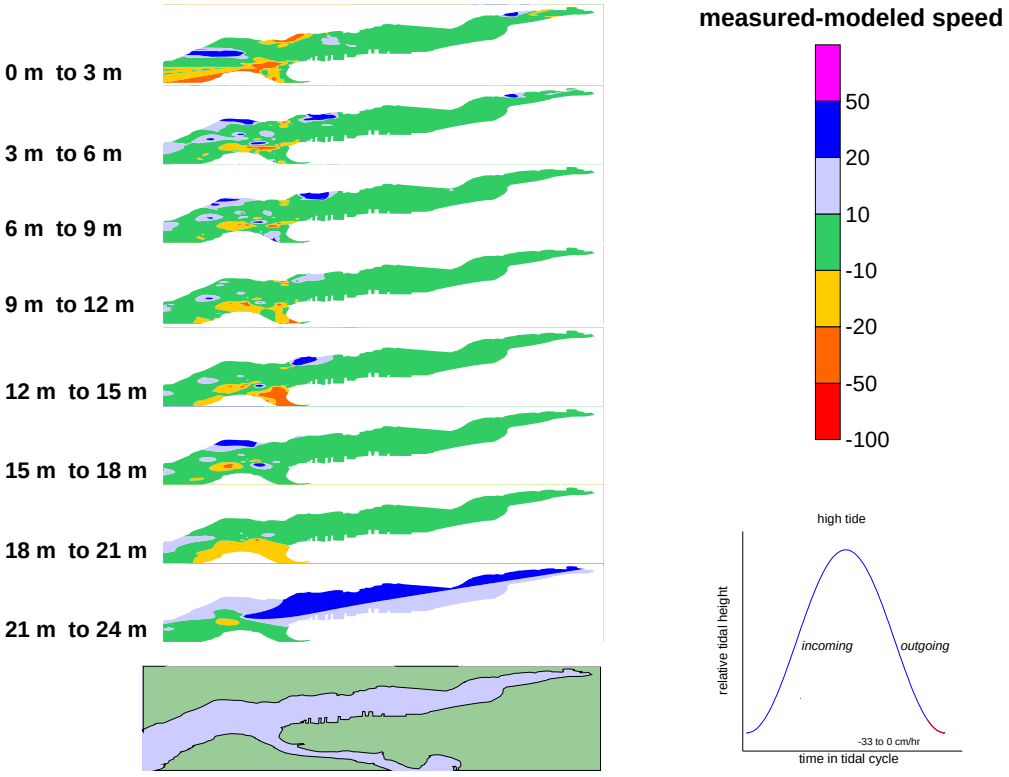

Absolute direction error averaged through the water column: Figure 57 plots root mean square difference between measured and modeled current direction, based on all measurements through the water column. Model results are based on the 9196 grid. Time, node, and depth information are pooled in the error bars. Comparisons can only be made where measurements coincide with model predictions. The biggest errors are seen at periods around slack tide (tidal conditions 1, 6, 7, and 12). Errors decrease during incoming and outgoing tide (tidal conditions 2-5 and 8-11 respectively).

Figure 57: RMS error and std of current direction predictions in Sinclair Inlet

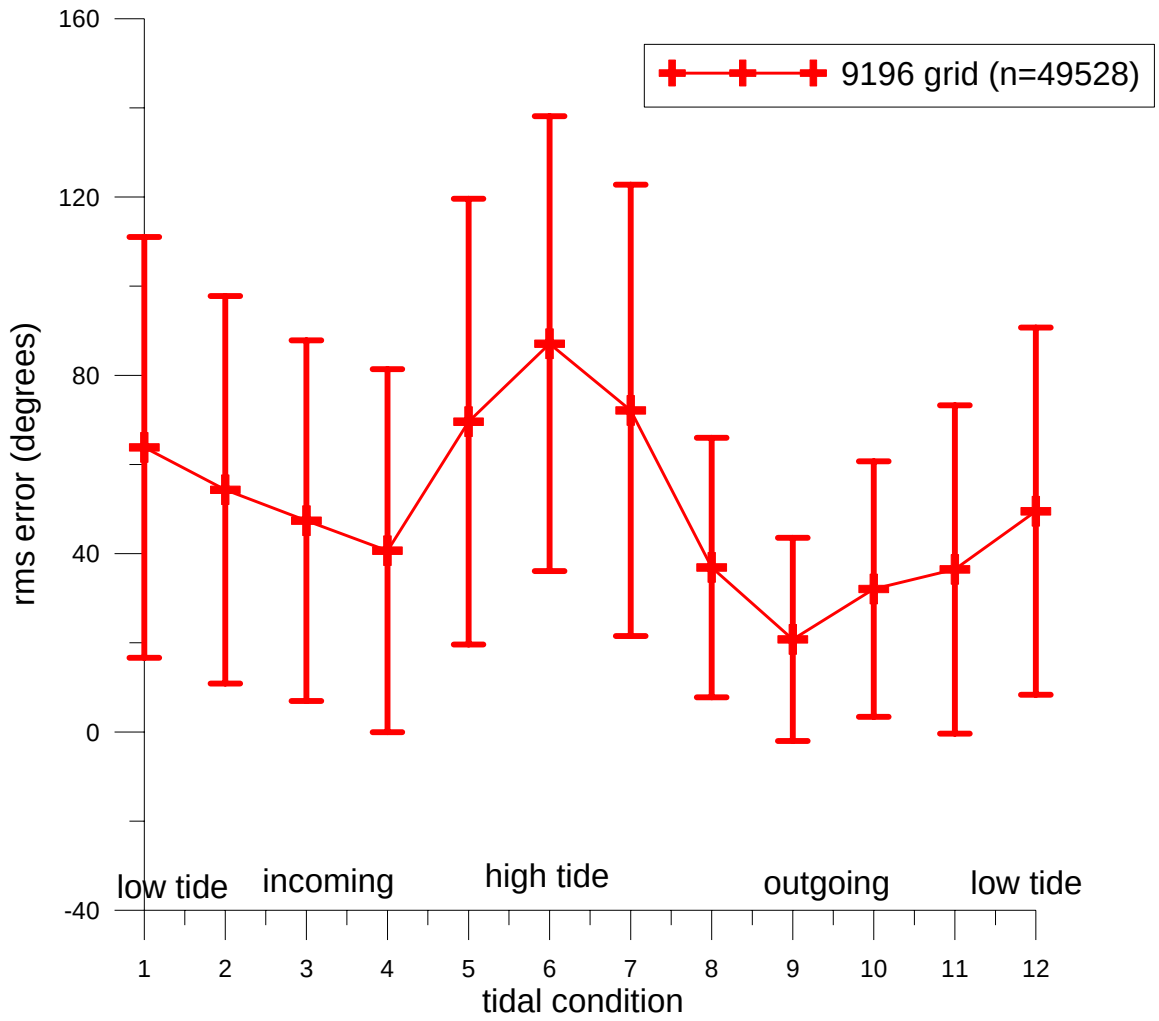

Measured currents were evenly extrapolated over the entire extent of Sinclair Inlet to better compare their pattern to results predicted from the full model grid. The measured currents were broken into u and v (north and east) vectors, independently extrapolated over the Inlet using Surfer© (Surfer, 2004) , and recombined to form speed and direction vectors. Figures 58-69 compare the extrapolated measured vector field (top figure) to the predicted field (bottom figure). Red dots on the measured field indicate where data were collected.

Figure 58: Measured (extrapolated) and modeled current vectors during tidal condition 1

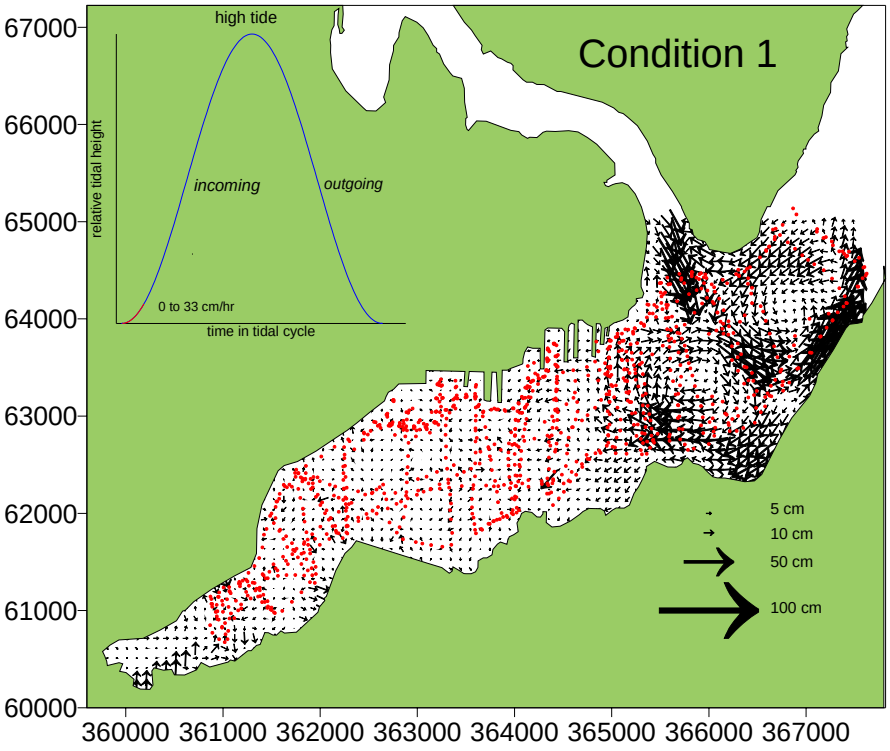

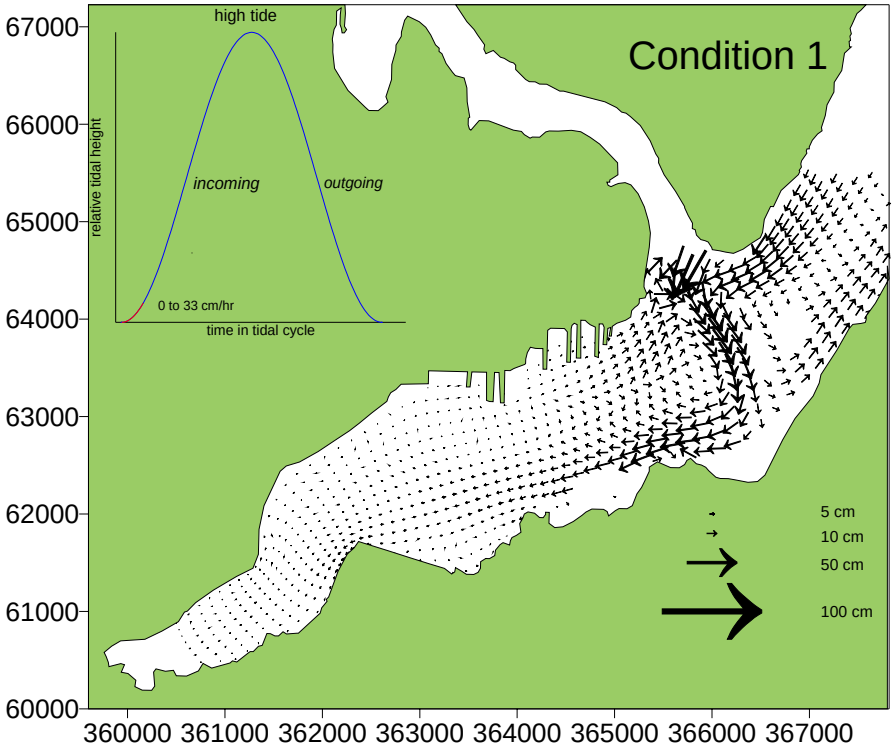

Figure 59: Measured (extrapolated) and modeled current vectors during tidal condition 2

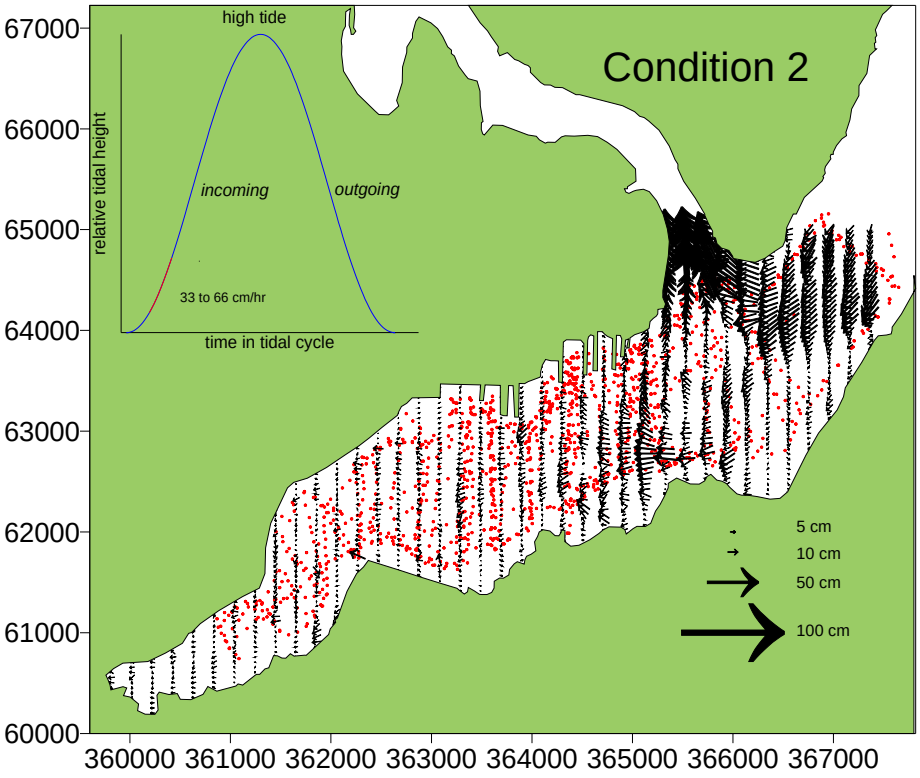

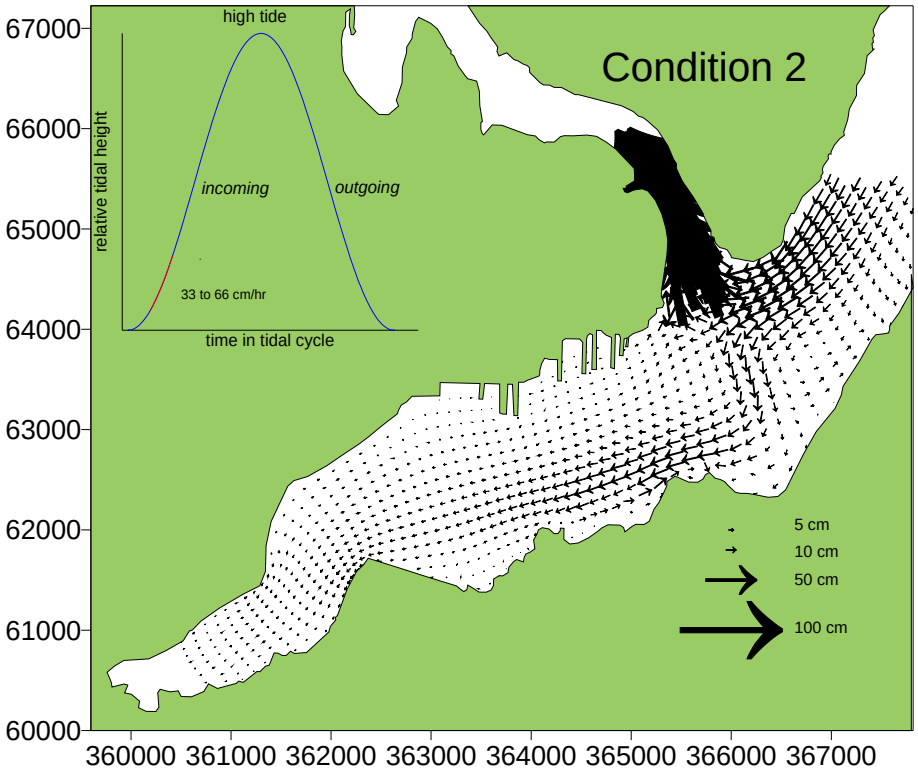

Figure 60: Measured (extrapolated) and modeled current vectors during tidal condition 3

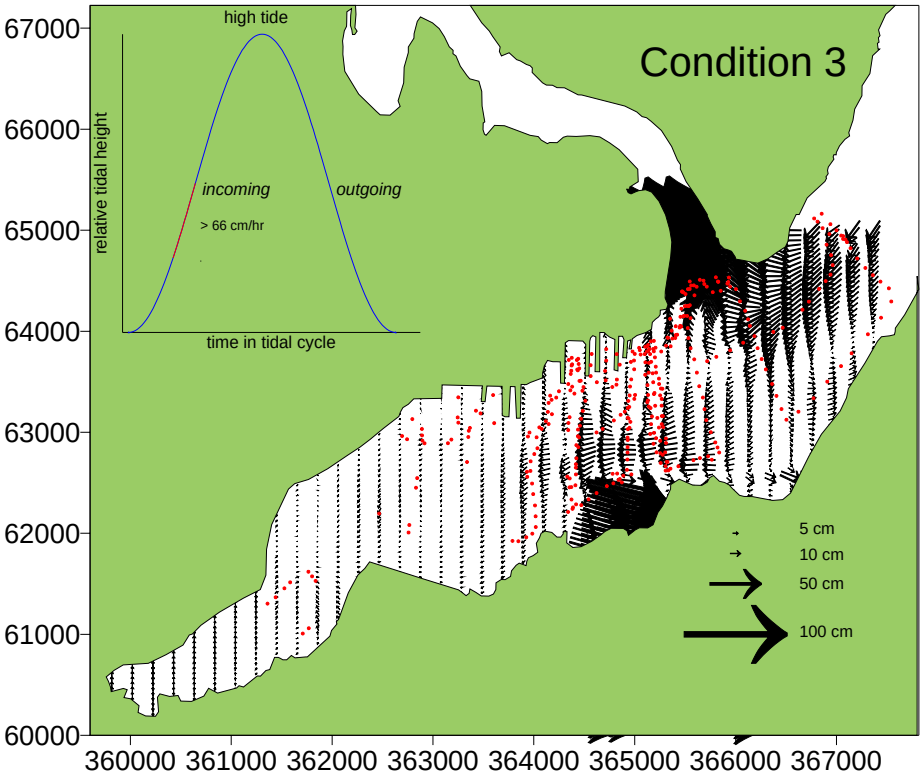

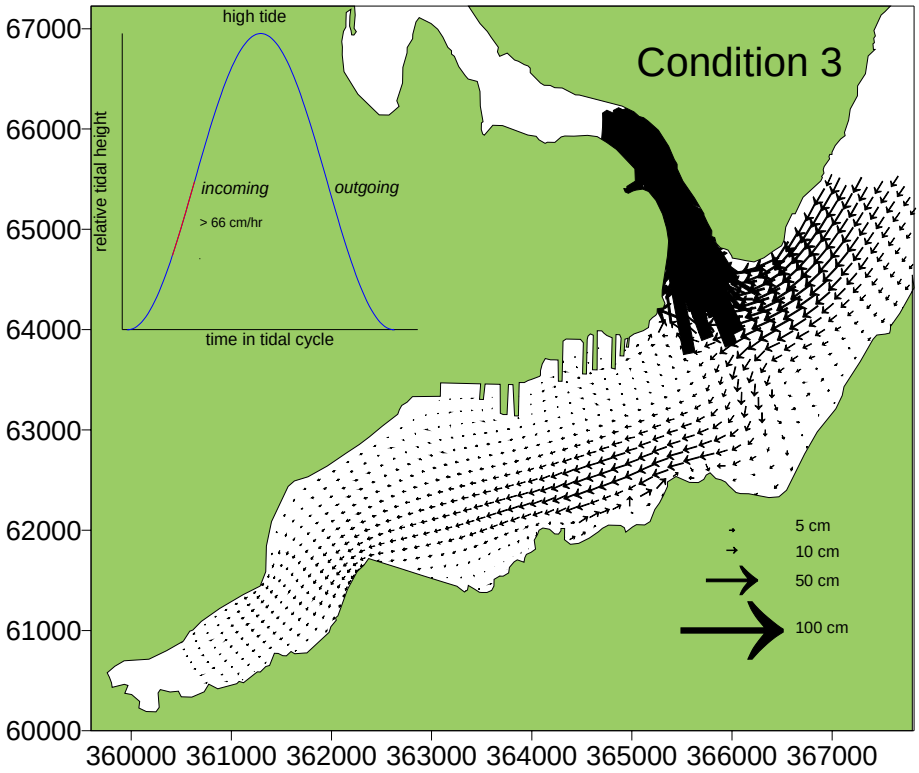

Figure 61: Measured (extrapolated) and modeled current vectors during tidal condition 4

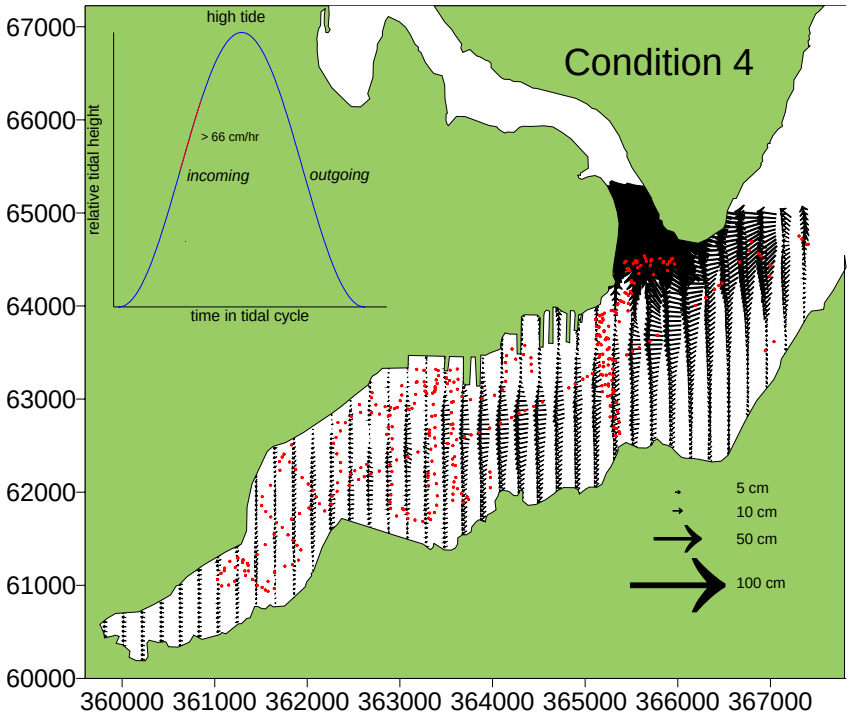

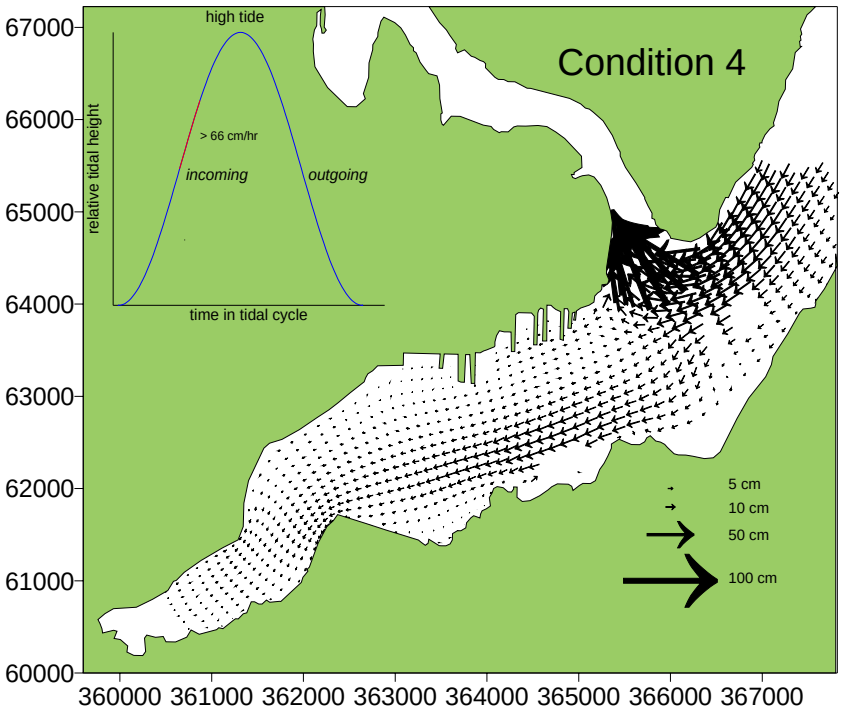

Figure 62: Measured (extrapolated) and modeled current vectors during tidal condition 5

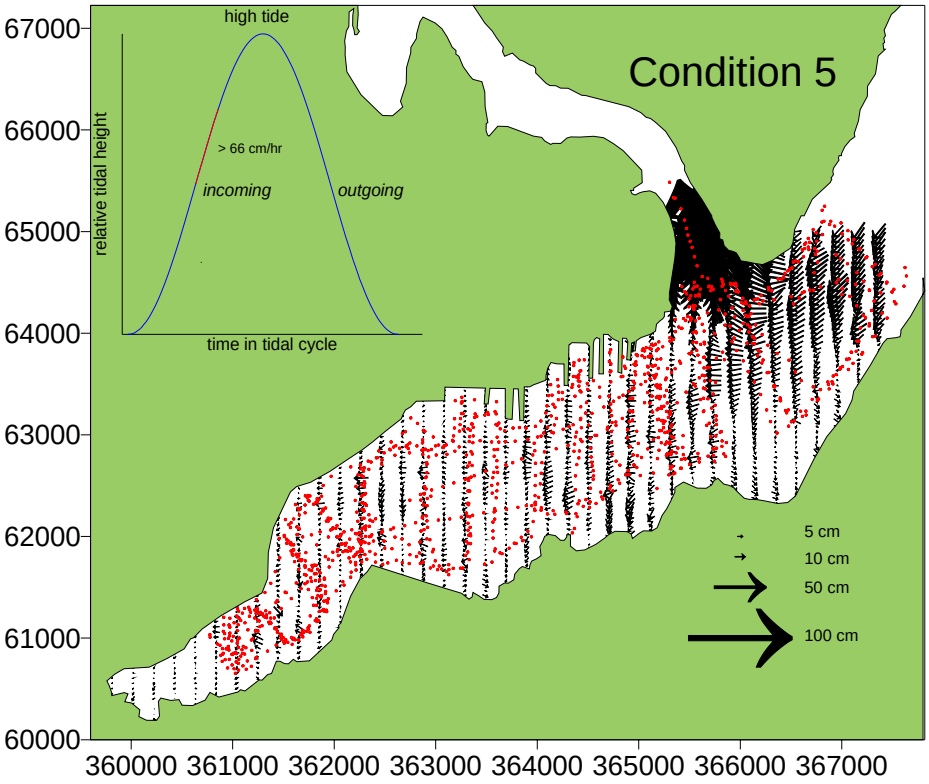

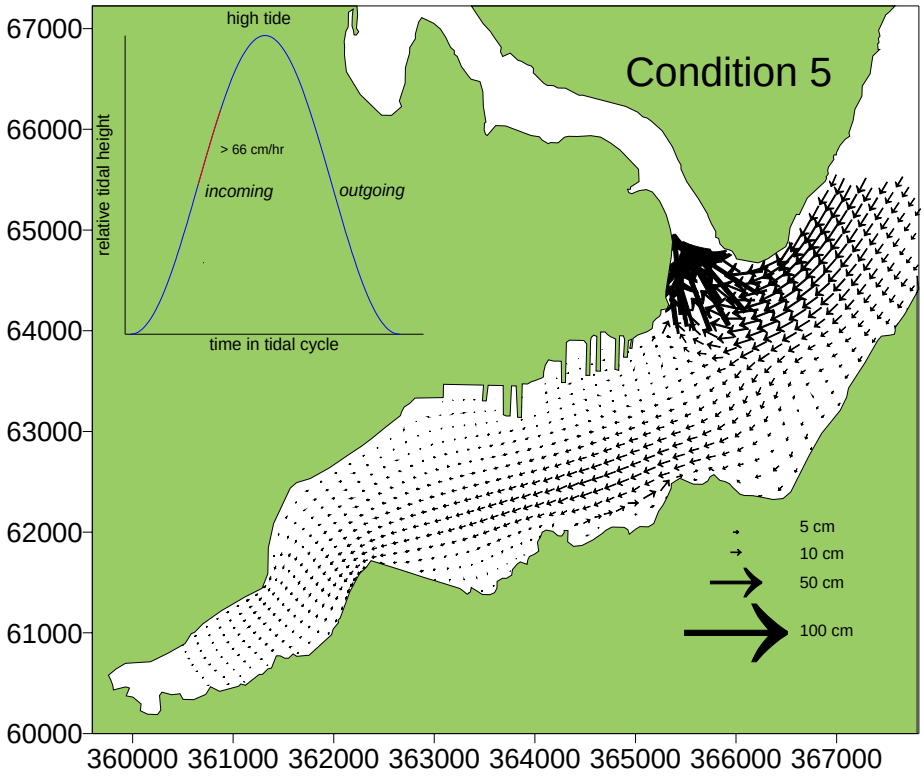

Figure 63: Measured (extrapolated) and modeled current vectors during tidal condition 6

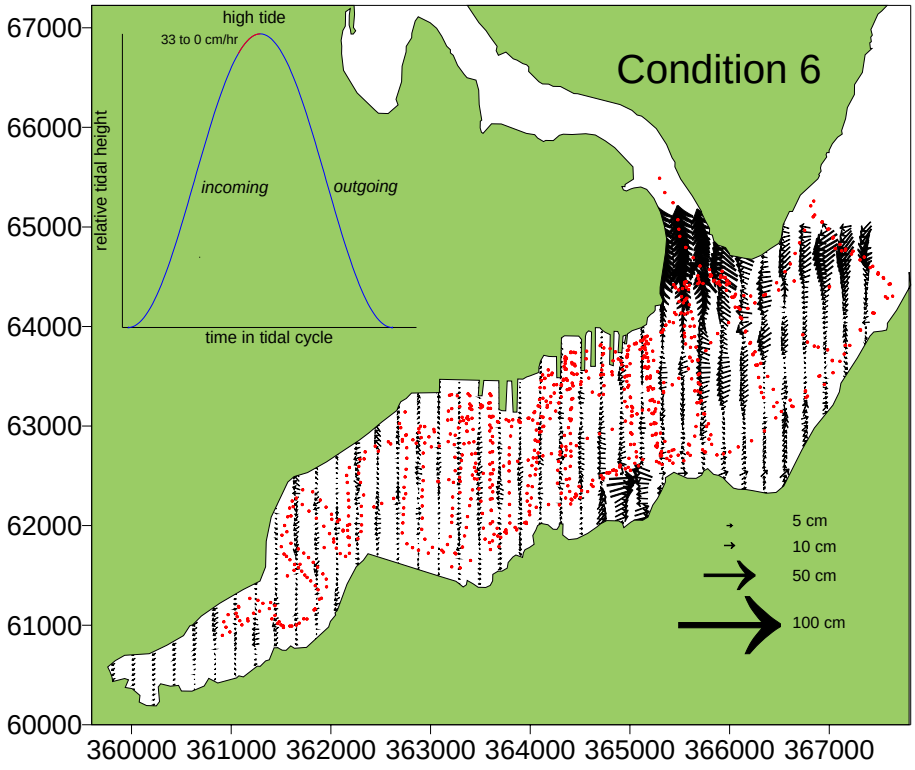

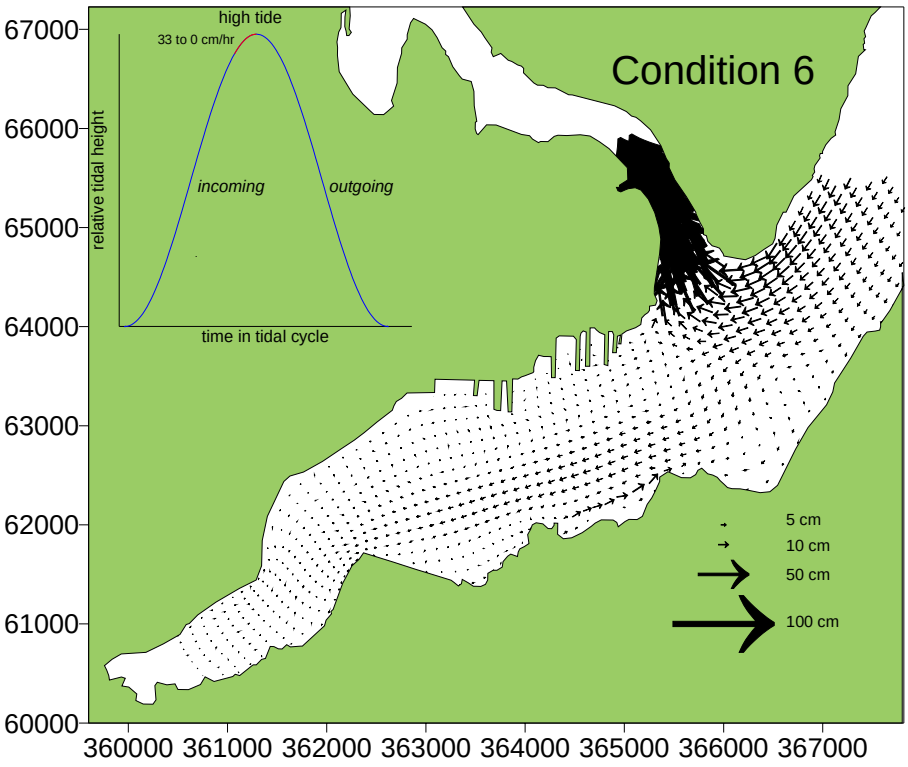

Figure 64: Measured (extrapolated) and modeled current vectors during tidal condition 7

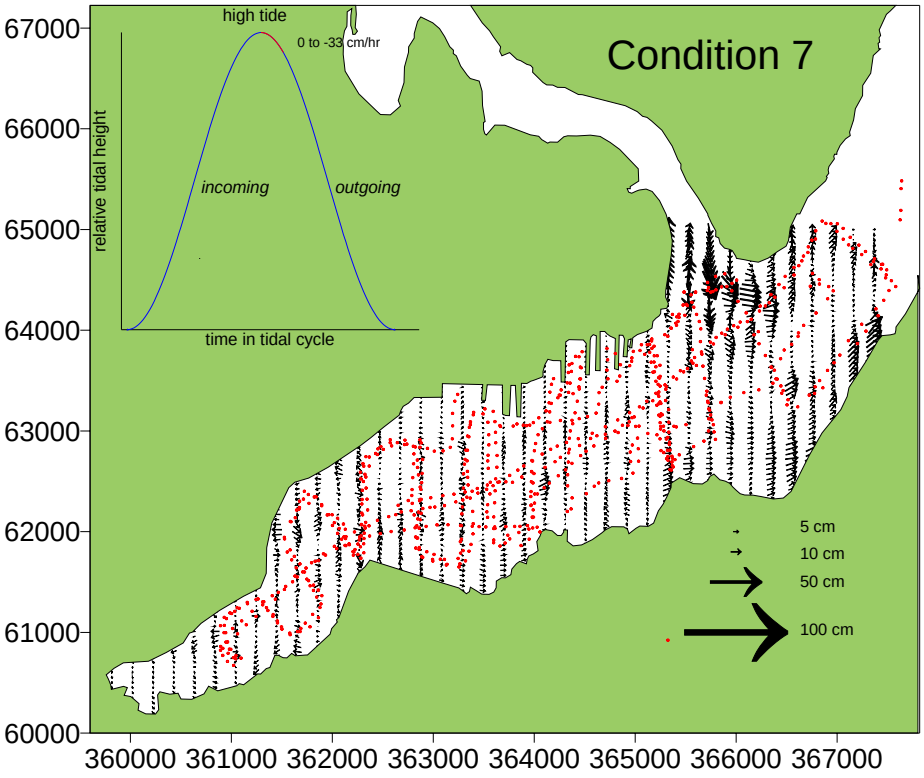

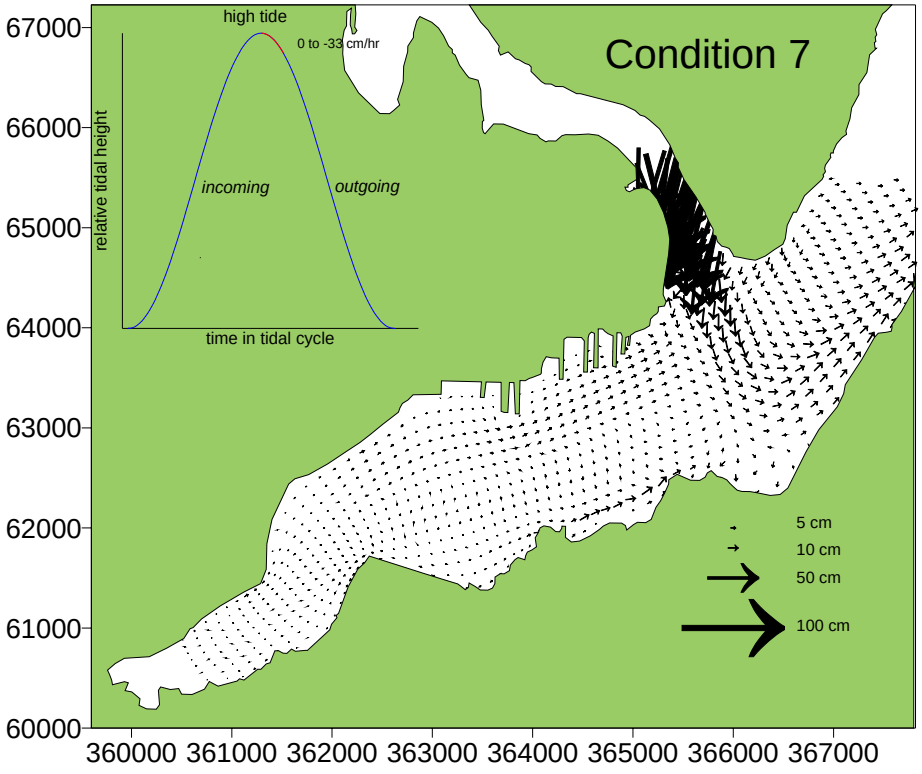

Figure 65: Measured (extrapolated) and modeled current vectors during tidal condition 8

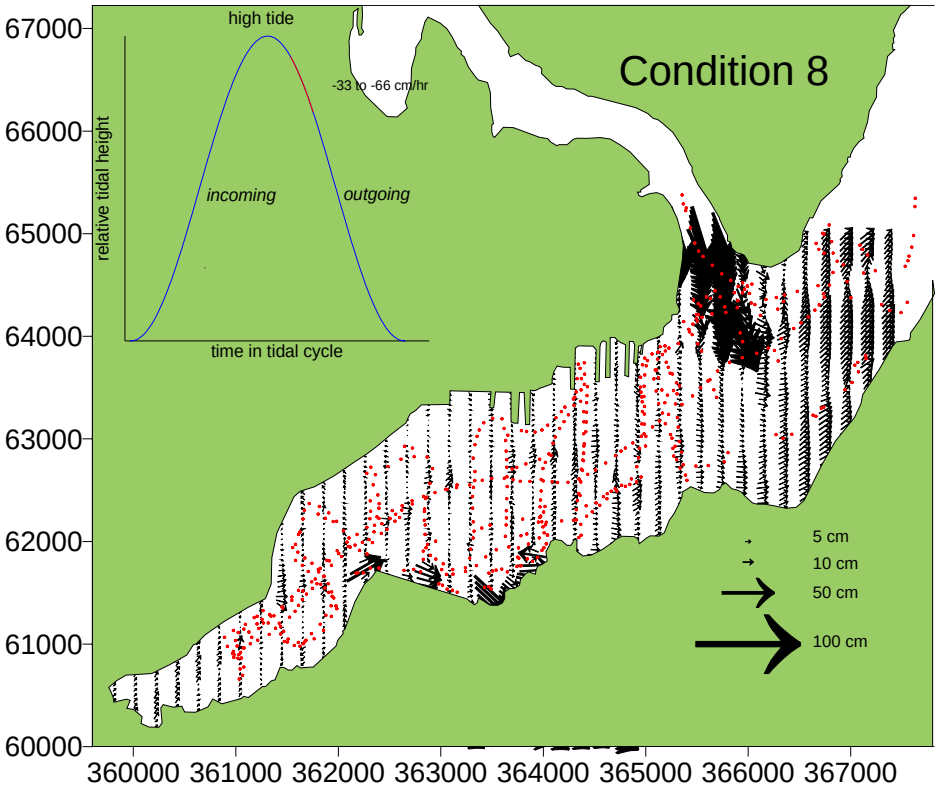

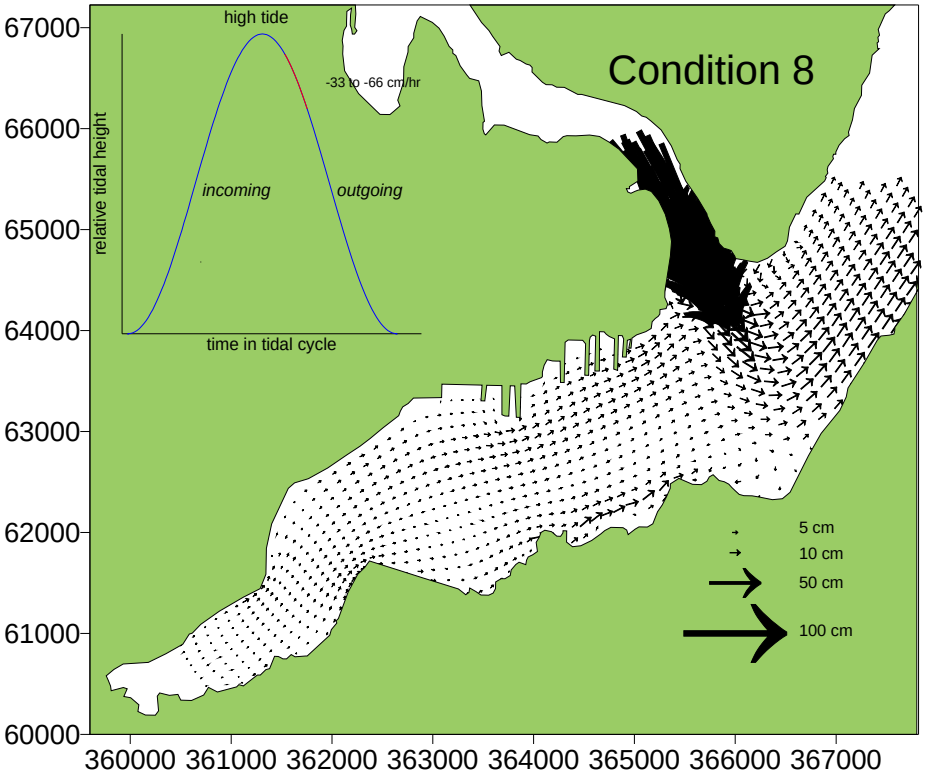

Figure 66: Measured (extrapolated) and modeled current vectors during tidal condition 9

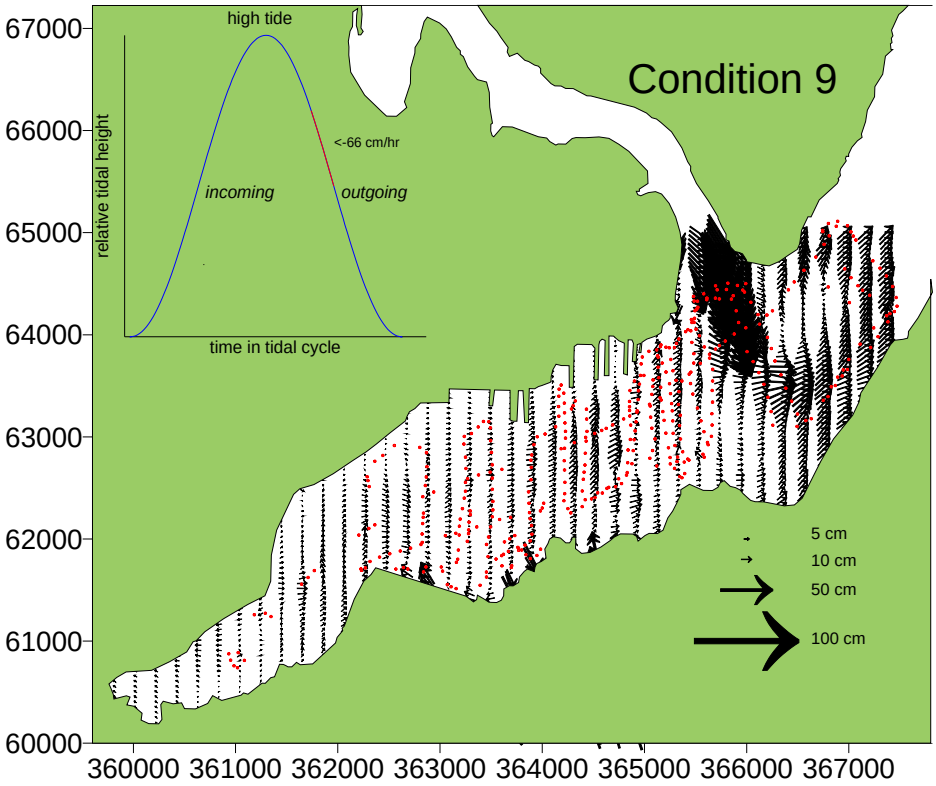

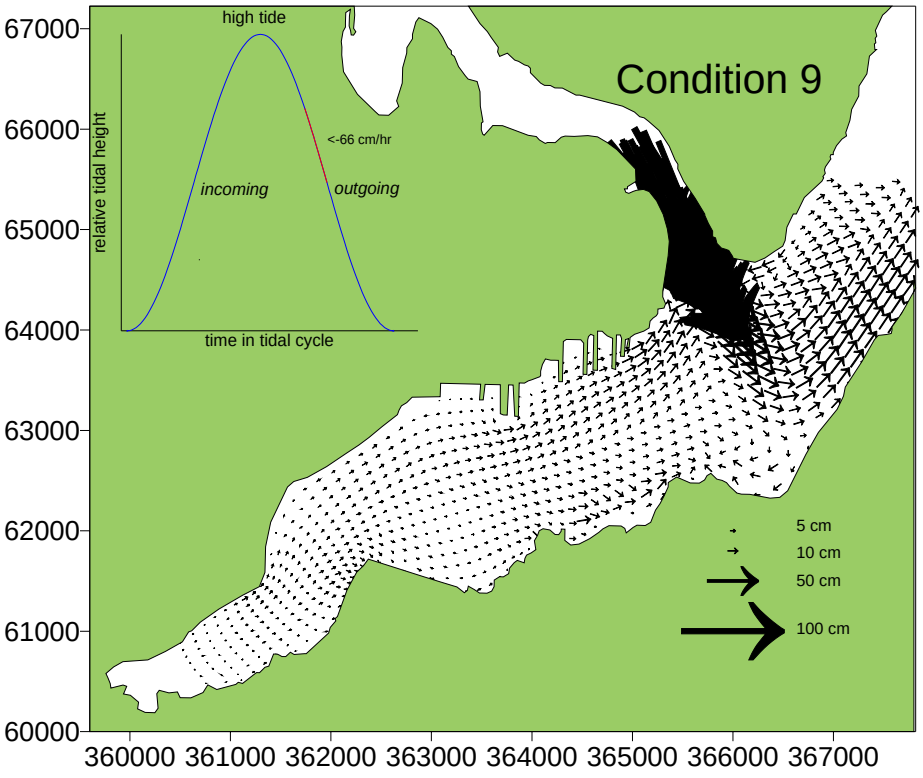

Figure 67: Measured (extrapolated) and modeled current vectors during tidal condition 10

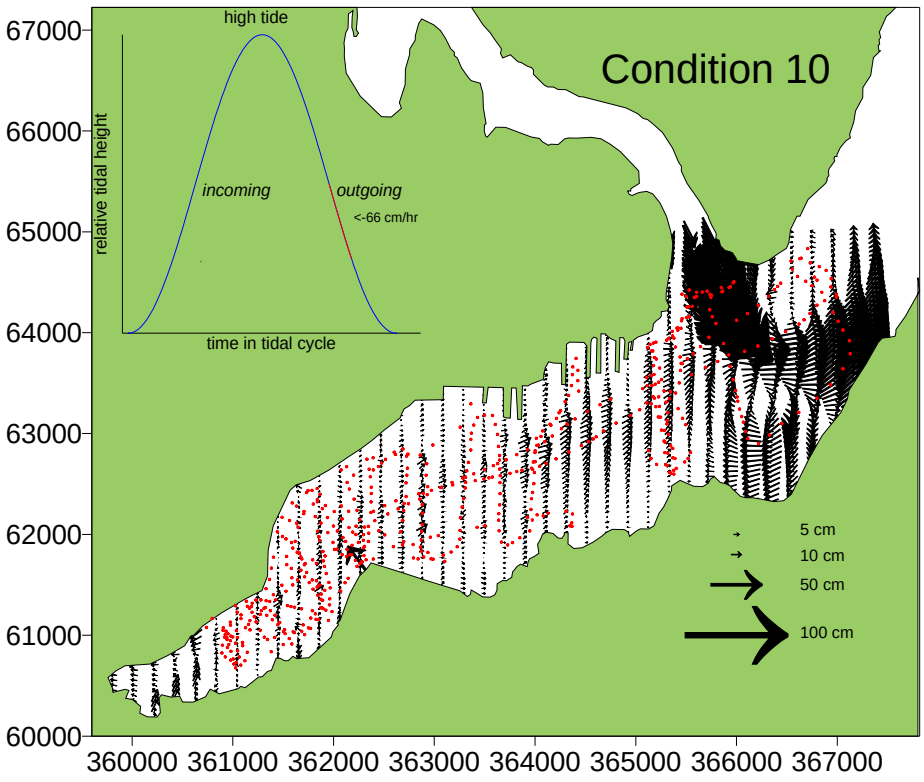

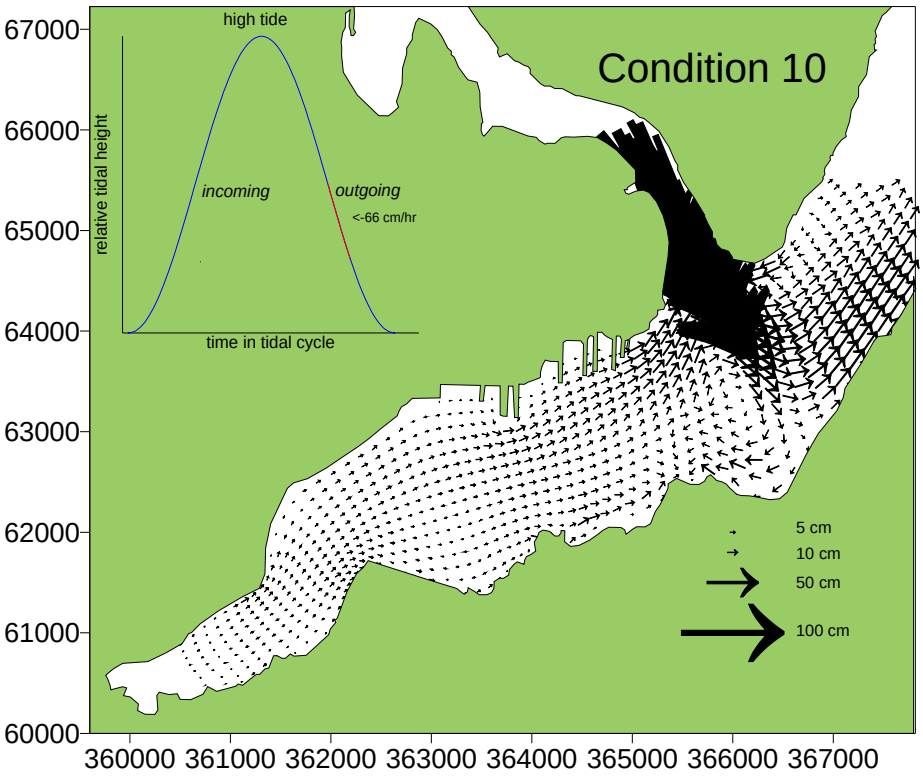

Figure 68: Measured (extrapolated) and modeled current vectors during tidal condition 11

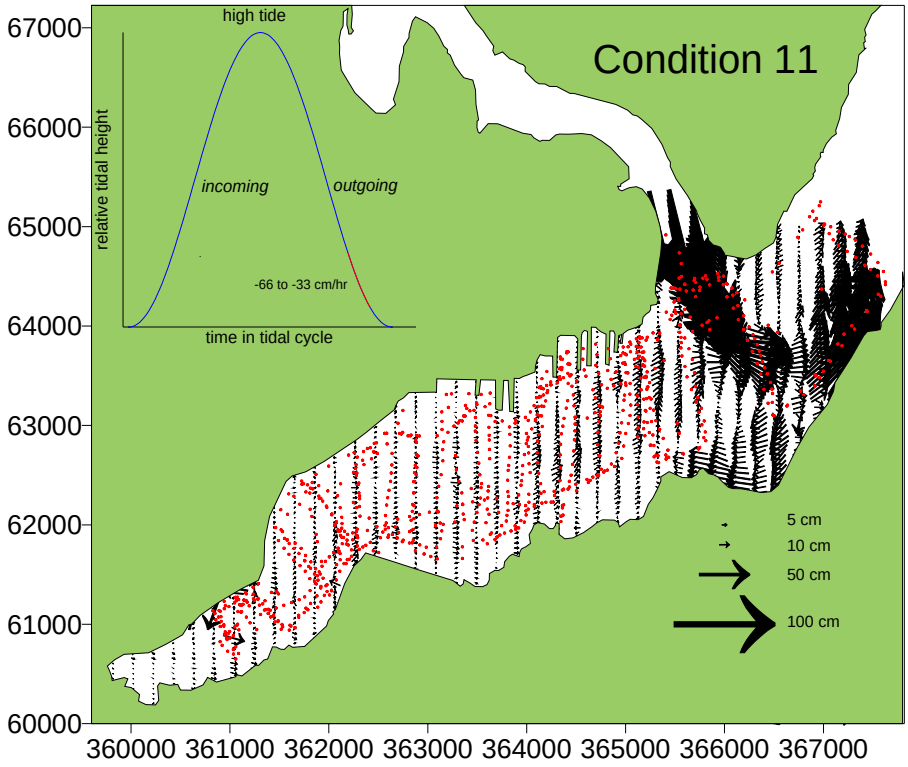

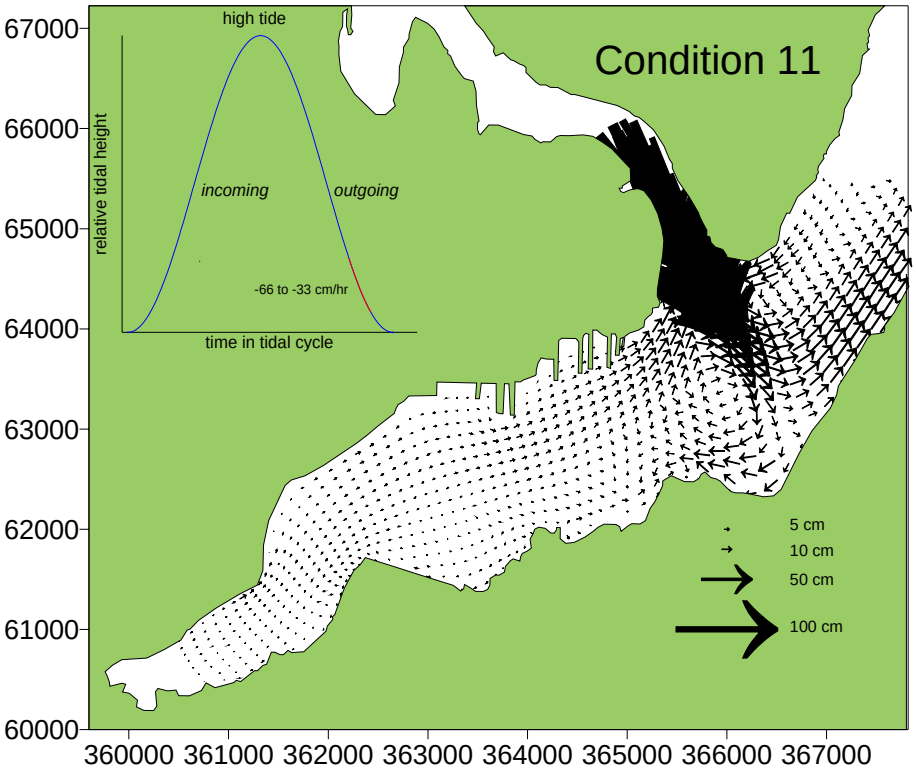

Figure 69: Measured (extrapolated) and modeled current vectors during tidal condition 12

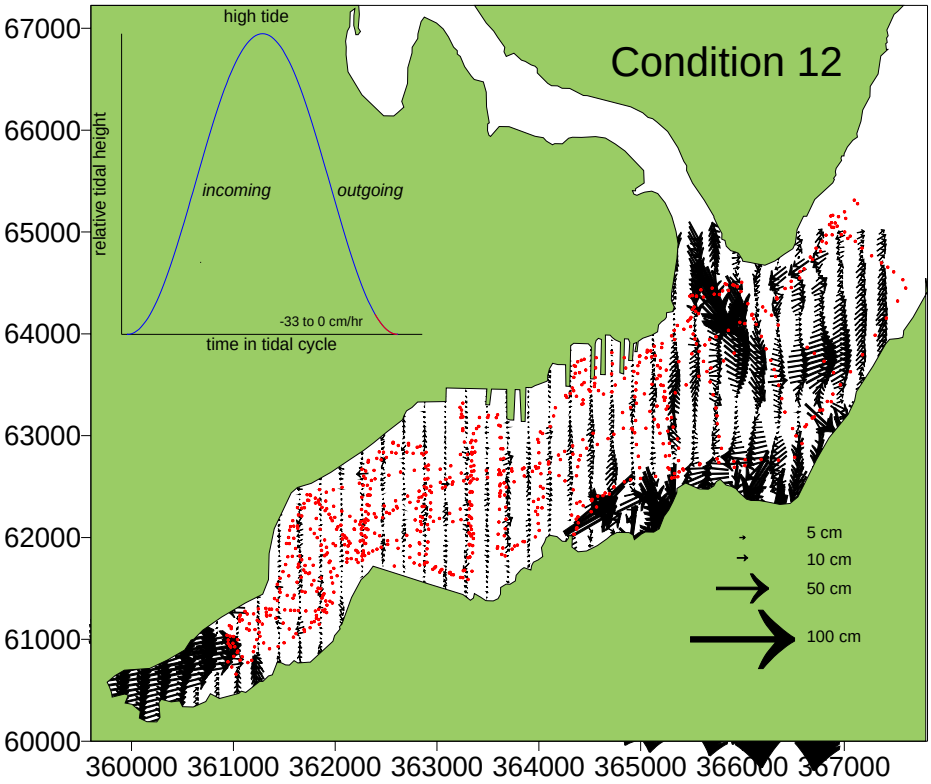

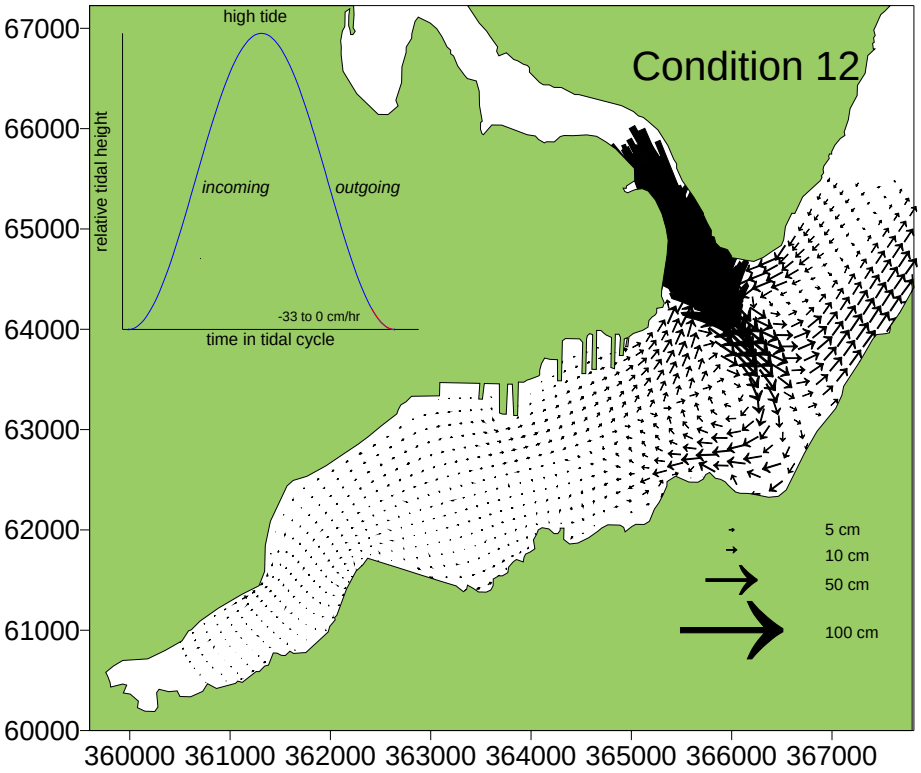

The predicted current vectors appear more continuous and change more gradually than the measured current vectors. This is possibly due to several causes: the measured currents were susceptible to local wind or input stream flows that were not accounted for in the modeling. The ADCP could also have measured residual motion in the wake of the boat, particularly during slack. The extrapolated vector field is also misleading in the above figures and should be viewed with caution, particularly the high velocities near the shore where measurements were not taken. As the boat neared the shore and doubled back across the Inlet, high residual wake currents could have been immediately measured, leading to overly fast currents in random directions and extrapolation of even higher currents to towards the shoreline. The effect of the boat wake would be particularly striking on the normally slow-moving waters along the shore.

Discussion: For the bulk of Sinclair Inlet, away from the shore, CH3D appears to predict currents within 2 cm hr-1 to 5 cm hr-1 of measured values. CH3D over-predicts water speed at the mouth of Washington Narrows and under-predicts water speed near the shore. The latter effect is probably due to wake aliasing from the boat collectiong ADCP data. The predictions of current direction are more regular than measurements. Measurements again could have been aliased by the boat wake, or reflect local wind and input stream conditions. The predicted current speed and direction, without the impact of local weather or boat disturbances may better represent mean current conditions in Sinclair Inlet.

The accuracy of the model in Dyes Inlet remains largely unknown. Long time series of current measurements at a few locations, drogue trajectories and dye dispersal data have not yet been evaluated quantitatively against model predictions. The impact of CH3D hydrodynamic inaccuracies on total maximum daily load calculations is probably best explored by varying tidal forcing to increase model velocities by 50% to 100% (lower plots in Figs 9-20) in a sensitivity analysis. Faster currents will speed short-term contaminant dispersal but will probably have little impact on longer-term residual current transport.

References:

Brown, J. 2001 (ed). User's Guide For A Three-Dimensional Numerical Hydrodynamic, Salinity, And Temperature Model Of Sinclair Inlet. July 2001. Concurrent Technologies Corporation, Contract No: GS-10T-EBD-005, Task Order ID: ABH-170-037, Bremerton, WA

Gilbert, R. O. 1987. Statistical Methods for Environmental Pollution Monitoring. John Wiley and Sons, Inc. New York.

Katz C.N, P.L. Noble, D.B. Chadwick, B. Davidson, and R.D. Gauthier. 2004. Sinclair Inlet Water Quality Assessment: Water Quality Surveys Conducted September 1997, March 1998, and July 1998. Prepared for Puget Sound Naval Shipyard Project ENVVEST. Space and Naval Warfare Systems Center, San Diego, CA, January 2004. https://swdata.spawar.navy.mil/envvest/reports/ECOS_Survey_Rpt.htm

Micronautics, 1997. North America Tide Program . Micronautics Inc. 40-A Bay View Street, PO Box 1428, Camden, ME 04843-1428, Phone: (207) 236-0610

Micronautics, 1998. North America Tide Program . Micronautics Inc. 40-A Bay View Street, PO Box 1428, Camden, ME 04843-1428, Phone: (207) 236-0610

RDI, 1989. Acoustic Doppler Current Profilers Principles of Operation: A Practical Primer. RD Instruments. 9855 Businesspark Avenue, San Diego, CA 92131 Phone (619) 693 1178.

RDI, 1996. Acoustic Doppler Current Profilers Principles of Operation: A Practical Primer, Second Edition for Broadband ADCPs. RD Instruments. 9855 Businesspark Avenue, San Diego, CA 92131 Phone (619) 693 1178.

Surfer, 2004. Surfer Surface Mapping System V8.05, May 11, 2004. Golden Software, Inc. 809 14th St. Golden, CO. http://www.goldensoftware.com/

Wang, P.F and K.E. Richter 1999. A Hydrodynamic Modeling Study Using CH3D for Sinclair Inlet, Draft Report. Space and Naval Warfare Systems Center, San Diego, CA, November 3, 1999.

Wang, P.F. 2001. Dispersion resulting from aggregating hydrodynamic properties in water quality modeling. International Journal of Engineering Science, 39:95-112.